Evaluation of the transport and chemistry of climate-relevant species in the lower stratosphere

Giorgio Salvatore Taverna

Submitted in accordance with the requirements for the degree of
Doctor of Philosophy

The University of Leeds
School of Earth and Environment
2019

Declaration of Authorship

I, Giorgio S. Taverna, hereby declare that this thesis and the work presented in it is entirely my own. Where I have consulted the work of others, this is always clearly stated.

Signed: _____

Date: _____

Abstract

This thesis investigates aspects of the chemistry and transport of the upper troposphere and lower stratosphere (UTLS), with a particular focus on the Asian Summer Monsoon (ASM). The overall aims have been pursued through simulations of the TOMCAT three-dimensional (3-D) chemical transport model in comparison with aircraft, balloon and satellite observations. Scientific motivation for this work has been provided by the EU StratoClim project which conducted flight campaigns in Greece (2016) and Nepal (2017).

Simulations of the transport of chemically active tracers to the UT depend critically on the treatment of convection. In this work I have tested and further developed an improvement to the existing TOMCAT model by using a convection scheme based on mass fluxes from archived meteorological analyses. This leads to more rapid uplift of chemical tracers, which is most apparent for those with short lifetimes (e.g. around 5 days). Both the old and new convection schemes have been evaluated against observations.

The model has then been used to quantify the transport associated with the Asian Summer Monsoon (ASM) circulation, focusing on the interannual variability using decadal simulations forced by ERA-Interim reanalysis. The role of large-scale ascent versus convective transport has been investigated, along with the link between the interannual variability of the transport of surface-emitted CO to the UT to the strength of the ASM.

Model intercomparisons of tropospheric age-of-air when the old (Tiedtke) convection scheme is applied, shows weak transport, in particular at UTLS levels, when compared with other state-of-the-art 3-D models. In contrast the new (archived mass flux) scheme shows faster and stronger transport reflected in a younger age-of-air in the UT. A multidecadal (1989-2017) simulation with idealized tracers show that the alternative convection schemes vastly impact the related confinement of such tracers in the ASM anticyclonic structure at 100 hPa. However, connecting this confinement with common metrics of the dynamical strength of the ASM circulation is not straightforward and does not lead to conclusive results over the time period modelled.

The main chemical observations so far available from the StratoClim campaign are water vapour and CO. Comparison between the in-situ water data from the StratoClim and the ERA-Interim values confirms a negative bias in UTLS in the reanalyses over the Indian Subcontinent region. A full chemistry model simulation is able to capture the observed magnitude and variability of the observed CO well. Analysis of daily model output reveals an interesting tri-modal pattern of elevated CO in the ASM region, which is strongly dependent on convection over the Tibetan Plateau but not entirely due to it.

Injection of brominated species into the stratosphere has been investigated using observations from the more extensive American 2013/14 Airborne Tropical Tropopause Experiment (ATTREX) aircraft campaign in the Eastern Pacific. The model simulations with the new convective scheme agree well with UTLS observations of $CHBr_3$, CH_3Br, CH_2Br_2 and H-1211, confirming the injection of around 6 ppt bromine derived from very short-lived substances (VSLS) into the stratosphere. However, comparisons of observed and modelled BrO show that this cannot account in all cases for the amount of inorganic bromine observed in the lower stratosphere, suggesting direct injection of significant levels (a few ppt) of inorganic bromine into the stratosphere in the Tropics.

Finally, I have investigated the impact of artificial injection of particles into the stratosphere – so-called geoengineering through solar radiation management to counteract climate change. I have assessed the possible impact of the underexplored particulate mineral substance, TiO_2, on stratospheric ozone through enhanced heterogeneous chemistry. Model simulations, based on loadings causing a similar climate impact to the Mt Pinatubo eruption, show the injection of TiO_2 particles in the stratosphere likely has only a small impact on present-day ozone concentrations (decrease of up to 0.06%). With further assumptions about the possible role of TiO_2 on chlorine heterogeneous chemistry, a model simulation to 2049 with recurrent large Pinatubo-like volcanic eruptions shows that the impact with declining stratospheric chlorine loading is not more than a -2.5% change in ozone.

Acknowledgements

I would like to acknowledge the cooperation and support I have received through many persons right from the beginning of my Ph. D programme. First and foremost, I wish to place on record my sincere thanks to Prof. M. Chipperfield, *optimo magistero*, for his unprecedented patience, competence and help shown from the very early stage of my PhD. “Nobody does it alone, Jack. You needed all of them and they needed you”. This sentence from a very famous movie brilliantly describes the in short terms the essence of my PhD path, shaped by the great people I met during my PhD such as Joe McNorton, Tim Keslake, Hannah Mantle, Sandip Dhomse, Leighton Regayre, Andreas Chrysanthou, Matilda Pimlott, Chris Kelly, Chris Wilson, Piers Foster, Adriano Lemos, Marianne Leong, Mohammed, Ryan Hossaini, Ryan Neeley, Emma Bramham, Eric Hintsa and Joachim Fallmann and many others. I wish to express my special gratitude to Richard Pope for his enormous help with IDL coding and Wuhu Feng for his help with code of the TOMCAT model.

A special thank you to all the people I met in the International Student Club during my first two years in Leeds.

I am also thankful to my doctoral administrator Mrs M. Lesnianski.

I thank the EU StratoClim project and the University of Leeds for financial support.

Thank you to Fran for her unconditional help during these five years long journey together.

A great thank you to all my brothers and sisters of Catholic Chaplaincy of the Leeds Universities!

Last but not at least, honour and glory to my Lord Jesus Christ for His grace and mercy for the accomplishment of this thesis.

O quam cito transit gloria mundi.

Contents

"The Earth is blue, how wonderful, it is amazing!"

Yuri A. Gagarin, first human being in space

April 12th, 1961.

List of Figures

List of Tables

Acronyms

ACE-FTS	**A**tmospheric **C**hemistry **E**xperiment-**F**ourier **T**ransform **S**pectrometer
AIRI	**A**ll **I**ndia Summer **R**ainfall **I**ndex
ASM	**A**sian **S**ummer **M**onsoon
ASMA	**A**sian **S**ummer **M**onsoon **A**nticyclone
ATAL	**A**sian **T**ropopause **A**erosol **L**ayer
ATTREX	**A**irborne **T**ropical **T**ropopause **E**xperiment
BOB	**B**ay **o**f **B**engal
CALIOP	**C**loud-**A**erosol **L**idar with **O**rtogonal **P**olarization
CAO	**C**entral **A**reological **O**bservatory
CCM	**C**hemistry **C**limate **M**odel
CDR	**C**arbon **D**ioxide **R**emoval
CEAS	**C**avity **E**nhanced **A**bsorption **S**pectroscopy
CFSR	**C**limate **F**orecast **S**ystem **R**eanalysis
CIMS	**C**hemical **I**onization **M**ass **S**pectroscopy
CLS	**C**onfined **L**ower **S**tratosphere
CNR	**C**entro **N**azionale delle **R**icerche
CPT	**C**old **P**oint **T**ropopause
CTM	**C**hemical **T**ransport **M**odel
DK	**D**hulikhel

DLR	**D**eutsches zentrum für **L**uft- und **R**aumfahrt
DOAS	**D**ifferential **O**ptical **A**bsorption **S**pectroscopy
ECC	**E**lectro-**C**hemical **C**ell
ECD	**E**lectron **C**apture **D**etector
ECMWF	**E**uropean **C**entre for **M**edium-Range **W**eather **F**orecasts
EICMF	**E**ra-**I**nterim **C**onvective **M**ass **F**luxes
EPT	**E**quivalent **P**otential **T**emperaure
ESM	**E**arth **S**ystem **M**odel
EU	**E**uropean **U**nion
FLASH	**F**luorescent **A**irborne **S**tratosphere **H**ygrometer
FZJ	**F**orschungs **Z**entrum **J**ülich
GC	**G**as **C**hromatography
GCM	**G**eneral **C**irculation **M**odel
GHE	**G**lobal **H**awk **E**ye
GWAS	**G**lobal Hawk **W**hole **A**ir **S**ampler
HUPCRS	**H**arvard **U**niversity **P**icarro **C**avity **R**ingdown **S**pectrometer
ICOS	**I**ntegrated **C**avity **O**utput **S**pectroscopy
IPCC	**I**ntergovernmental **P**anel on **C**limate **C**hange
IR	**I**nfra **R**ed
JRA-25	**J**apanese **25**-year **R**eanalysis
JRA-55	**J**apanese **55**-year **R**eanalysis
KAL	**K**alamata
KTM	**K**atmandu
LPR	**L**apse **R**ate **M**inimum
MERRA	**M**odern-**E**ra **R**etrospective **A**nalysis
MIPAS	**M**ichelson **I**nterferometer for **P**assive **A**tmospheric **S**ounding
MLS	**M**icrowave **L**imb **S**ounder
MS	**M**ass **S**pectrometry
NASA	**N**ational **A**eronautics and **S**pace **A**dministration
NCAR	**N**ational **C**enter for **A**tmospheric **R**esearch
NCEP	**N**ational **C**enters for **E**nvironmental **P**rediction
NH	**N**orthern **H**emisphere
NOAA	**N**ational **O**ceanic and **A**tmospheric **A**dministration
NT	**N**ainital
ODS	**O**zone **D**epleting **S**ubstance

OLR	**O**utgiong **L**ongwave **R**adiation
PBL	**P**lanetary **B**oundary **L**ayer
PSC	**P**olar **S**tratospheric **C**loud
PV	**P**otential **V**orticity
QBO	**Q**uasi **B**iennal **O**scillation
SD	**S**pecified **D**ynamics
SH	**S**outhern **H**emisphere
SOM	**S**econd **O**rder **M**oment
SRM	**S**olar **R**adiation **M**anagement
STE	**S**tratospheric **T**ropospheric **E**xchange
TDL	**T**unable **D**iode **L**aser
TIL	**T**ropical **I**nversion **L**ayer
TOC	**T**op **O**f **C**onfinement
TOF	**T**ime **O**f **F**light
TP	**T**ibetan **P**lateau
TTL	**T**ropical **T**ropopause **L**ayer
UCATS	**U**nmanned **A**ircraft **C**hromatography for **A**tmospheric **T**race **S**pecies
UTLS	**U**pper **T**roposphere **L**ower **S**tratosphere
UTS	**U**pper **T**roposphere **S**tratosphere
VSLS	**V**ery **S**hort-**L**ived **S**ubstance
WYI	**W**ebster and **Y**ang **I**ndex
WP	**W**ork **P**ackage

1 Introduction

Since the second half of the 20th century, remarkable importance has been attributed to the mechanism of transport of air from the troposphere to the stratosphere (Charney and Drazin, 1961). Transport from the Upper Troposphere (UT) controls the amount of ozone-depleting substances which can reach the stratosphere and thereby affect the Earth's ozone shield which filters out biologically damaging short wavelength radiation. In this regard, the Upper Troposphere Lower Stratosphere (UTLS) exerts great influence. Generally speaking, the UTLS can be defined as the layer within 5 km of the tropopause, with a clear division between Tropics and Extra-Tropics (Gettelman *et al.*, 2011). The former contains the Tropical Tropopause Layer (TTL), a transition layer between troposphere and stratosphere which has been recognized as the gateway for almost all the air originating from surface to enter the stratosphere, particularly water vapour and very short-lived substances (VSLS). These both have a profound impact on the stratospheric chemical and radiative balance (**Figure 1.1.**) (Gettelman *et al.*, 2011; (Fueglistaler *et al.*, 2009). The Extra-Tropics TTL is characterized by the baroclinic balance and downward propagation of circulation and tracers anomalies (Held, 1982). The complex and not-well-understood interactions between the most important elements of the UTLS, i.e. ozone, aerosol, properties of clouds and water vapour, exert an impact on the temperature structure of the atmosphere and surface climate. For example, ozone anomalies in the stratosphere and consequently in the LS where 90% of ozone is located, have evident consequences in terms of superficial temperature variations in the Southern Hemisphere (Thompson *et al.*, 2011).

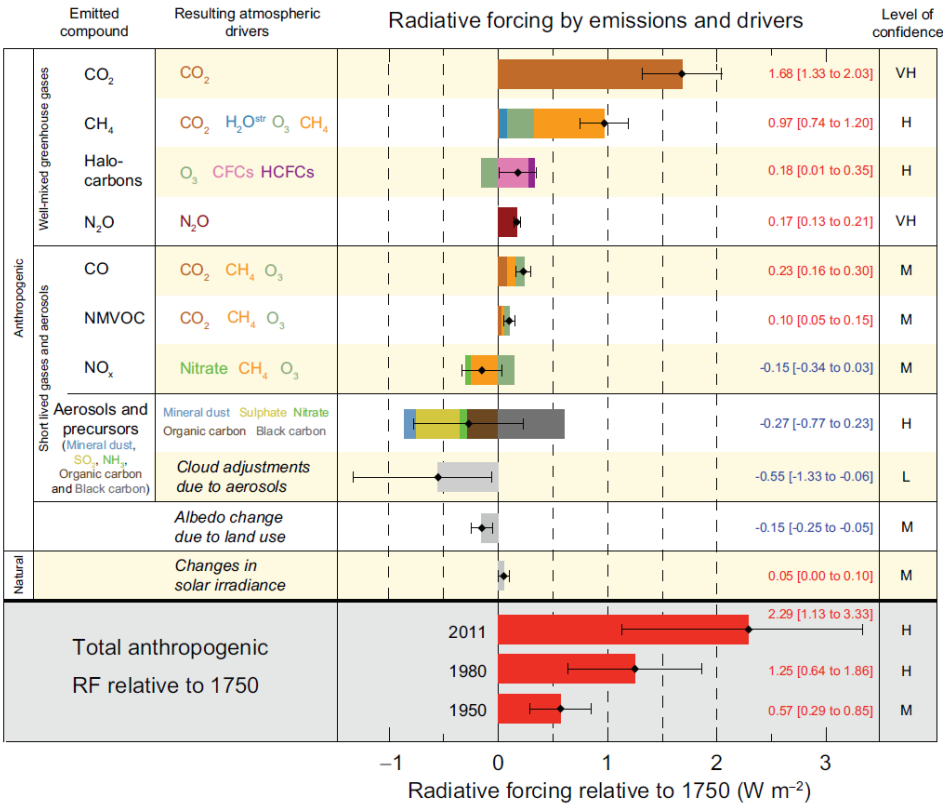

Figure 1.1. Schematic of global average radiative forcing (RF) in 2001 relative to 1750 (Wm^{-2}), divided between emitted compounds. RF values result from the effect of emitted compounds or processes that results in a combination of drivers. Best estimates are shown in black together with corresponding uncertainty. Confidence levels in the net forcing (VH – very high, H – high, M – medium, L – low, VL – very low) are provided on the right. For further details see (IPCC, 2013).

Depletion of stratospheric ozone has been a major scientific and environmental issue of the past few decades. Farman, *et al.*, (1985) first reported the large losses of column ozone over Antarctica. A period of intense research soon revealed that the cause of this depletion was chlorine and bromine which were transported to the stratosphere in the form of long-lived source gases such as chlorofluorocarbons (CFCs) and halons. These source gases decompose in the stratosphere releasing the chlorine and bromine which reside in a range of reservoir and radical species. The radicals can destroy ozone through catalytic cycles. Following action in the Montreal Protocol (and amendments) the production of certain long-lived source gases is now severely limited (or banned completely) and the stratospheric loading of chlorine and bromine is decreasing (WMO, 2014). Hence stratospheric ozone is expected to return to 1980 values during this century and the first

signs have been detected (e.g. , Solomon *et al.*, 2016; Chipperfield *et al.*, 2017)**.** However, there is concern that the transport of naturally emitted or uncontrolled anthropogenic halogenated very short-lived substances (VSLS) might delay the recovery of stratospheric ozone (**Figure 1.2.**). These VSLS, with lifetimes of 6 months or less, may not be expected to reach the stratosphere in large quantities. However, efficient transport mechanisms which allow this have been identified and VSLS source gases have been observed in the lower stratosphere (Hossaini *et al.*, 2017). Among these transport mechanisms, the Asian Summer Monsoon (ASM) is believed to play an important role.

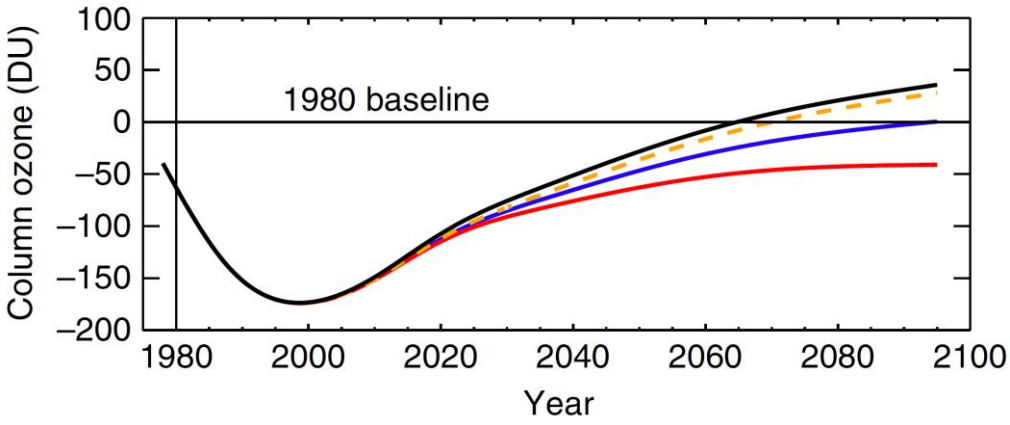

Figure 1.2. SLIMCAT 3-D chemical transport model (see **Chapter 3** for technical details) simulations of mean change in the October column O_3 (DU) in the stratosphere over Antarctica (60–90°S) relative to a 1980 baseline. Simulations were performed according to three different CH_2Cl_2 VSLS different emission scenarios. Scenario 1 (**blue**, surface CH_2Cl_2 continues to increase at the mean rate observed over the 2004–2014 period), scenario 2 (**red**, surface CH_2Cl_2 continues to increase at the mean rate observed over the 2012–2014 period), scenario 3 (**orange**, no future growth) and scenario 4 (**black**, no CH_2Cl_2 emissions). Note, the 1980 baseline is calculated from a model simulation performed with 2012 meteorology, in a similar manner to the forward simulations, to isolate the impact of CH_2Cl_2 growth from inter-annual variability due to meteorology. ERA-Interim meteorological fields availability starts 1979 limiting the simulations to 1980 onwards (1979 is used as spin up year). Figure adapted from Hossaini *et al.*, 2017.

To a first order, Monsoon systems develop when a strong seasonal temperature contrast between land and ocean drastically change the wind circulation in a certain area. Monsoons are present in West Africa, North America, Asia and Australian (Webster and

Fasullo, 2003). The ASM is the strongest monsoon system on the planet and is characterized by the reversal of the surface horizontal winds during the Boreal winter and summer. It is driven, to a first order, by the different physical properties of land (Indian subcontinent) and ocean (Indian Ocean). The associated winds and precipitation over the heated land are organized in cycles lasting between 10 and 30 days, known as "active periods of the Monsoon". The poleward migration of the inter-tropical convergence zone (ITCZ) is another aspect of ASM circulation (**Figure 1.3.)** (Webster and Fasullo, 2003).

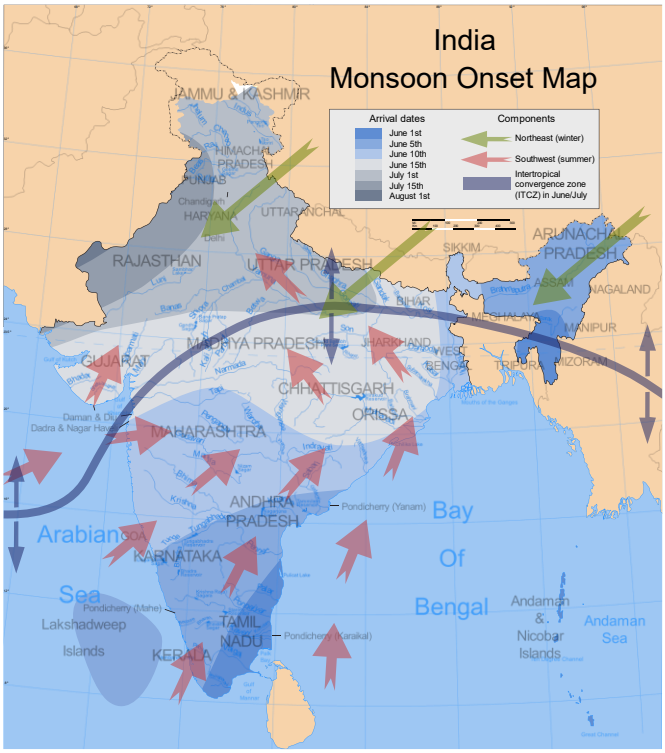

Figure 1.3. India southwest summer monsoon onset map, based on the work of Burroughs, 1999.

The ASM exerts a profound influence on the entire atmosphere and particularly on the UTLS, (Lal *et al.*, 2001; Kripalani *et al.*, 2007) through several spatial and temporal scales, despite its confinement to a relatively small area of the Northern Hemisphere. Distinctive features of this weather system are the associated deep convection (Heath and Fuelberg, 2014; Bergman *et al.*, 2012; Devasthale and Fueglistaler, 2010), and the development of a wide anticyclonic structure (**Figure 1.4.**), extending on average from Egypt to Eastern China in the overlying UTLS (Randel and Park, 2006). Its role in transporting surface-emitted anthropogenic compounds from the surface up to the UT,

and eventually into the stratosphere, has been object of extensive research during the past 20 years and only recently has its effect has been partially understood thanks to in-situ campaigns, satellite observations and modelling results (Dethof *et al.*, 1999; Park *et al.*, 2007, 2008, 2009; Randel *et al.*, 2010).

Given the likely importance of the ASM for the rapid transport of air masses to the stratosphere, the European Union (EU) funded the StratoClim field campaigns in 2016 and 2017. Its aim was to gain a better understanding of the ASM and its role in the climate system. It is well known that climate change can significantly alter the UTLS, e.g. on upward transport in the tropical tropopause region (Gettelman *et al.*, 2010) or in the Asian monsoon circulation (Lal *et al.*, 2001; Kripalani *et al.*, 2007; Turner and Annamalai, 2012), which are key regions for vertical fast transport of species, including VSLS into the stratosphere (Randel *et al.*, 2010). Current understanding of key processes in the role of the upper troposphere and stratosphere (UTS) in climate is limited by the paucity of essential measurements and process studies and their neglect in state-of-the-art climate projections. The StratoClim campaign was conducted in Kalamata (Greece) 2016 and Katmandu (Nepal) 2017 with an unprecedented in-situ aircraft payload for this region and supporting ground stations, designed to perform highly targeted measurements in the ASM region.

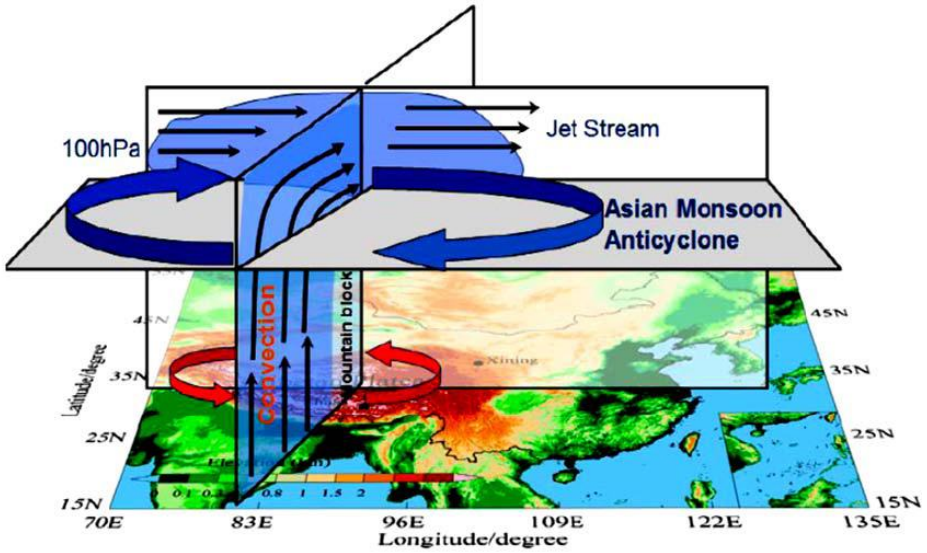

Figure 1.4. The Asian summer monsoon circulation develops a strong anticyclonic vortex in the upper troposphere and lower stratosphere (UTLS, thick blue arrow), spanning from East Asia to the Middle East. The anticyclone is a region of persistent enhanced pollution

in the upper troposphere during boreal summer, linked to rapid vertical transport of surface air from Asia, India and Indonesia in deep convection and confinement by the strong anticyclonic circulation. Figure courtesy of Yong Wang, FZJ Jülich.

Concern over the impact of climate change, and the difficulties in achieving international agreement to limit the emission of greenhouse gases has led to discussion on whether other action could be taken. In August 2006 Nobel Laureate Paul Crutzen published an article which reinvigorated the debate around counter measures against escalating global surface warming, through the intentional manipulation of the environment, so called "geo-engineering" (Crutzen, 2006) . Solar radiation management (SRM) techniques are among proposed geoengineering techniques (**Figure 1.5.**). The aim of implementing these techniques is to enhance the back-scattering of incoming radiation and an option to achieve this is the injection of highly reflective particles at stratospheric levels.

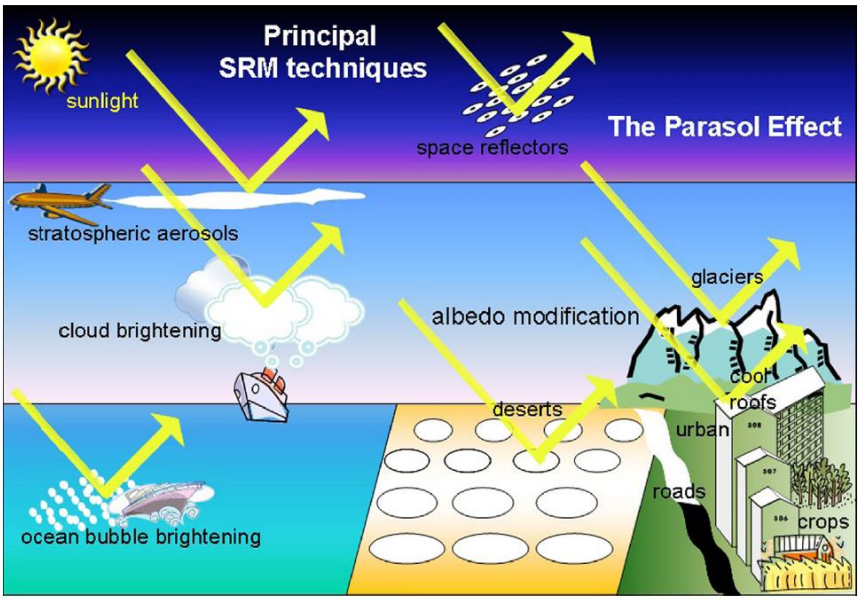

Figure 1.5. Overview of solar radiation measurement (SRM) methods whose main target is to enhance backscattering of the solar radiation into space, thereby reducing surface temperature. Figure taken from Ming *et al.*, 2014.

To date, injection of sulfuric acid particles and other minerals have been proposed as viable candidates for SRM purposes (Pope *et al.*, 2012; Visioni *et al.*, 2017). However, injection of these particles could have important effects on stratospheric chemistry

through enhanced ozone depletion, especially while the atmospheric loading of chlorine and bromine remains high. These particles could potentially provide surfaces which allow the same heterogeneous reactions as occur on polar stratospheric clouds (PSCs) and volcanic aerosol. The heterogeneous reactions which occur on atmospheric sulfuric acid particles has been widely researched and fairly well understood (Ammann *et al.*, 2013; Burkholder *et al.*, 2015) but this is not the case for other mineral particles. Titanium dioxide (TiO_2) has been suggested as an interesting alternative to sulfate aerosols in SRM due to its large refractive index (Pope *et al.*, 2012). Laboratory data is now becoming available for relevant heterogeneous chemical reactions on TiO_2 particles but the atmospheric implications of these measurements needs to be quantified using realistic stratospheric models (Moon *et al.*, 2018).

This thesis aims to investigate a number of issues related to the chemistry and transport of ozone-and climate-relevant species in the UTLS. A particular focus will be on the dynamics of the ASM, especially in relation to new observations from the StratoClim campaign. A further focus will be to assess the behaviour of TiO_2 as a suitable particle for SRM purposes with particular focus on stratospheric impact and ozone depletion through activation of chlorine radicals.

1.1 Aims of this thesis

Although considerable progress has been made in recent years in our understanding of the ASM transport and the impact of intentional injection of particles on the stratospheric composition, important questions still remain. The aims of this thesis are to address some of these open issues, which can be expressed in the following three overarching sets of questions:

Question 1. How rapid and efficient is the transport of surface-emitted species to the UTLS in the ASM? Is there significant interannual variability in this? How well can we represent this in global models?

Extensive scientific research in the past years has improved our understanding of the transport in the UTLS due to deep convection associated with the ASM and elsewhere in the Tropics. However, important aspects are still uncertain and remain unquantified, along with our ability to model this sub-gridscale process in global models. The details

of the mechanisms of the transport, namely fast vertical deep convection versus large-scale ascent, geographical contributions and subsequent uplift in the stratosphere are not well not understood, along with how the importance of these processes varies for tracers of different lifetimes. Also, transport mechanisms from surface to the UTLS due to ASM activity are not yet well understood and corroborated by reliable measurements (Ploeger *et al.*, 2017).

Question 2. What is the chemical composition of air entering the stratosphere via the Asian Summer Monsoon? How well can campaign data characterize this?

A crucial issue is how and to what extent the ozone and the water vapour abundance are changing in the UTLS, as their impact on its radiative balance have been well established (Forster and Shine, 1999, 2002). Net upward flux of water vapour in the tropical tropopause due to the ASM has been pointed out by Gettelman *et al.*, (2004) but related in-situ measurements are so far missing. A direct role of the ASM in transporting halogenated compounds in the stratosphere has been proven only for a limited number of long-lived species (Umezawa *et al.*, 2014) and analogous studies for VSLS are still lacking which is particularly important due to their short lifetime and potential impact on stratospheric ozone. Likewise, in situ detailed measurements of VSLS are inadequate and localized and show wide spatial and temporal variations (Butler *et al.*, 2010). However, transport of anthropogenic and natural compounds into the stratosphere, due to the ASM, remains debated (Bourassa *et al.*, 2012; Fromm *et al.*, 2013; Bourassa *et al.*, 2013). Particular importance needs to be addressed to the transport of halogenated VSLS which are not regulated by the Montreal Protocol and whose negative effect on stratospheric ozone has been recently quantified (Hossaini *et al.*, 2017). The analysis of StratoClim campaign data (and complementary data from the NASA East Pacific Airborne Tropical Tropopause Experiment (ATTREX)) is expected to shed new light on these aspects, validating the model representation of chemical species in the UTLS.

Question 3. What are the potential impacts on stratospheric composition of geoengineering approaches using TiO_2?

Injection of any particle into the stratosphere potentially provides a surface for heterogeneous reactions which can perturb the background chemistry. In particular, heterogeneous reactions can activate stable reservoir species into more chemically active

forms, which in turn can lead to ozone depletion. The impact of known and potential heterogeneous reactions needs to be assessed using detailed models of stratospheric chemistry. Important issues to assess are the extent of ozone depletion that might be caused due to known reactions, and what might be the most important reactions for which laboratory data is not yet available. TiO_2 particles have been proven to be an interesting candidate for SRM purposes, due to their large refractive index which is very close to the ideal H_2SO_4 corresponding value. Also, it has been largely studied and used in the context of submillimetre applications. (Pope *et al.*, 2012). The energy absorbed by such a particle is then ri-emitted in the longwave form, but its thermal effect in the stratosphere is less than the same of sulfuric acid (see **Figure 6.5**). Nevertheless, the evaluation of uptake coefficients of potential ozone-depleting reactions, which involve particles suitable for SRM purposes, is still largely missing. So far, uptake coefficients for reactions triggered by the TiO_2 particles in the stratosphere have been measured only for the hydrolysis of N_2O_5 and $ClONO_2$ (Tang *et al.*, 2014, 2016). Corresponding chemistry-climate model (CCM) results on stratospheric ozone and N_2O_5 abundance show evident discrepancies with similar TOMCAT CTM simulations (Moon *et al.*, 2018), suggesting that further investigations are needed to give a definite answer for the reliability of these particles for the above-mentioned purposes.

1.2 Thesis layout

The thesis is organised as follows. **Chapter 2** contains a literature review and general background covering the characteristics of the UTLS and the details of ASM transport. **Chapter 3** describes the TOMCAT model used in various configurations throughout this study. **Chapter 4** discuss the evaluation of TOMCAT model with improved treatment of convection and studies of tracer transport in the ASM anticyclone. **Chapter 5** presents comparisons of the model with observations obtained during the EU StratoClim field campaigns of 2016 and 2017 and the NASA ATTREX campaign of 2013. **Chapter 6** presents a short review on stratospheric injection of particles for SRM purposes and discusses the results of the TOMCAT simulations to study the effect of TiO_2 particles on the stratospheric ozone concentrations. Finally, **Chapter 7** summarises the result of the thesis, synthesises overall conclusions and gives suggestions for future work.

2 Background

2.1 Introduction

This chapter provides information on the relevant scientific background which forms the basis that motivates results shown in subsequent **Chapters 4**, **5** and **6**. Section 2.2 outlines the structure of the atmosphere, with a particular focus on the upper troposphere and lower stratosphere (UTLS). **Section 2.3** describes the transport characteristics associated with the Asian Summer Monsoon (ASM) circulation, which is central to the aims of much of this work. Finally, **Section 2.4** summarises the 2013-2019 EU StratoClim project which provided scientific support for this thesis. In particular, the StratoClim field campaigns in 2016 and 2017 provided observations on which model comparisons in **Chapter 5** are largely based.

2.2 Vertical structure of the atmosphere

The Earth's atmosphere extends from the surface until about several hundred kilometres altitude. The vast majority of chemical reactions and dynamical effects occur in the homosphere and this layer is what is commonly defined as "Earth's atmosphere" within the scientific community. However, according to the vertical temperature profile and physical-chemical processes which characterize the atmosphere, it is convenient to divide it into the following two macro-layers:

- **Homosphere**: This extends from surface to about 100 km, characterized by fairly constant mixing ratios of the main constituents N_2 (78%), O_2 (21%), Ar (1%) and very long-lived tracers (CO_2), almost independent with height.
- **Heterosphere**: Above 100 km the mean free path (distance between two distinct collisions of a gas molecule) is more than 1 m so that collisions are so rare that any molecular species is then considered as independent. Under these conditions, the concentration of heaviest elements decreases with height more rapidly than lighter ones (H, H_2, He) and consequently are more abundant. In this region, the

temperature profile is no longer used as a criterion to determine atmospheric properties.

The division of the homosphere based on the temperature profile, reveals the presence of four fundamental layers: the **troposphere**, **stratosphere**, **mesosphere** and **thermosphere** (**Figure 2.1.**).

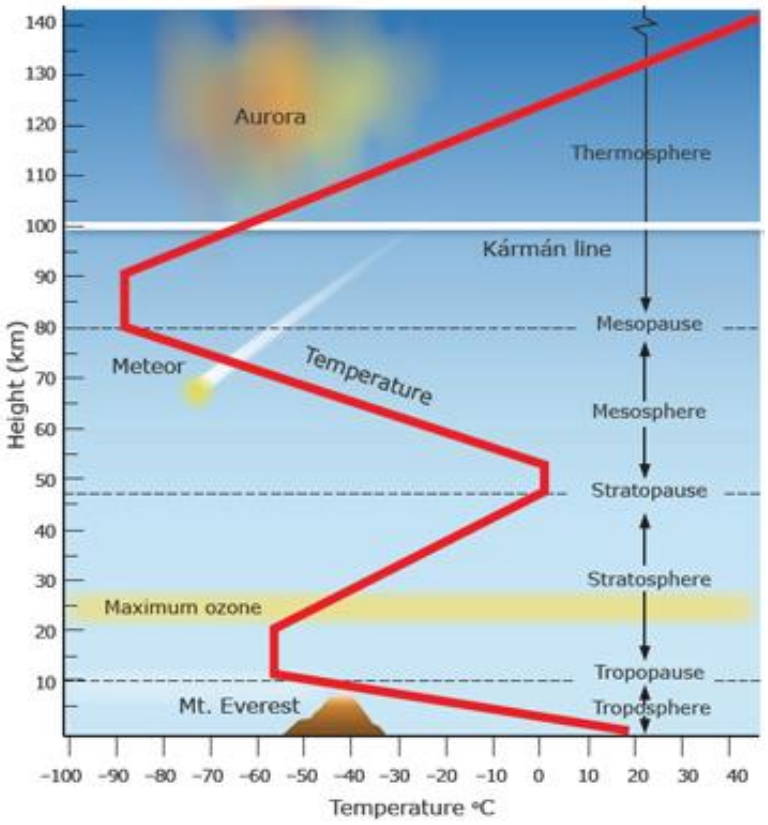

Figure 2.1. Mean vertical structure of the Earth's atmosphere showing temperature from the surface to the thermosphere. The Karman line conventionally defines the limit between the upper atmosphere and the deep space. (© 2014 University of Waikato, www.scienceleanr.org.nz).

2.2.1 Troposphere

The troposphere is the atmospheric layer which extends from surface to about 10-12 km altitude. It is characterized by a fairly constant temperature with altitude decrease whose value is btw the dry and the moist adiabatic lapse rate, -10 °C/km and -6.5 respectively. The reason for this decrease is the adiabatic expansion of an air parcel, caused by the

reduction of pressure with height, which ultimately cools it down. The presence of warm air at lower altitude and colder air above creates vertical instability which mixes the troposphere.

The troposphere contains about 80% of the overall atmospheric mass and nearly all of the atmospheric water vapour. Aerosols in the troposphere have short residence times, of the order of magnitude of weeks, because wet deposition, dry deposition and rain scavenging constantly remove them.

As shown in **Figure 2.2.**, the vertical extent of the troposphere varies strongly with latitude. It reaches 7-8 km above poles, 10-12 km at middle latitudes and 16-18 km in the Tropics, where strong convective activity typical of this region pushes the limit of troposphere (i.e. the tropopause) upward.

The top of the troposphere (so called tropopause) is limited by a temperature inversion which acts as a boundary. This drastically limits the extension of convective vertical motion, although occasional deep convective systems (clouds) can break through in the UTLS (**Section 2.2.4**), in the tropics. However, the mere temperature inversion is not sufficient for a full description of the properties of the tropical tropopause and a complex interplay between ozone, water vapor distribution together with effects of the dynamics and convective/radiative equilibrium better represents the characteristics of this layer (Highwood and Hoskins, 1998, MacKenzie *et al.*, 2006). The ascent of air in the UTLS occurs over the tropics, via a seasonal cycle of temperatures in the tropopause which then regulates the amount of water vapor entering the lower stratosphere. Once in the lower stratosphere, air is uplifted further up showing water vapor values which resemble tilted stripes in a time height cross section (the so-called “atmospheric tape recorder”, Mote *et al.*, 1996). Eventually, once in the UTLS air can ascend further to higher levels of the stratosphere and impact the ozone layer therein present. This phenomenon occurs during ASM and it is one of the foci of the EU StratoClim campaign (**Section 2.4** and **Chapter 5**). The latitudinally varying height of the tropopause (dark solid line, **Figure 2.2.**) is characterized by discontinuity at mid-latitudes.

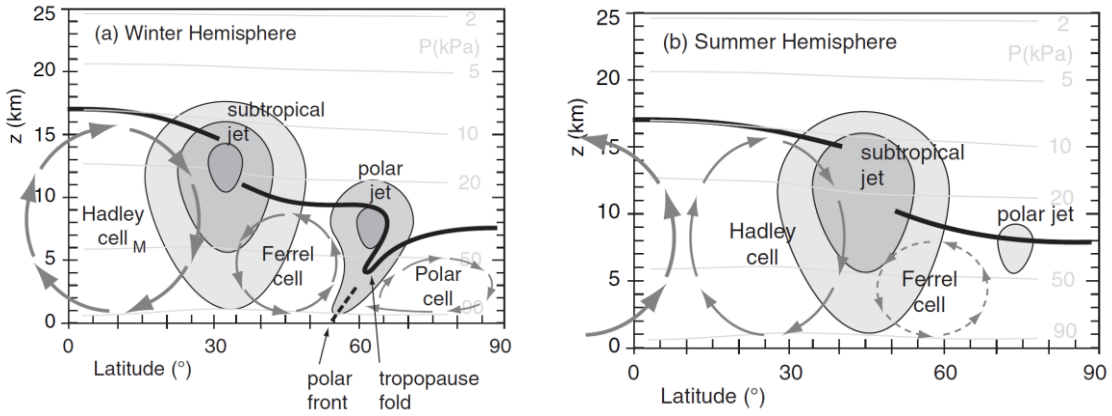

Figure 2.2. Simplified vertical cross section of tropopause (thick solid line) and zonal wind (perpendicular to the page) for **(a)** the winter and **(b)** the summer hemispheres. Darker shading indicates larger windspeed. Image adapted from Stull, 2011.

This tropopause discontinuity corresponds the maximum meridional temperature gradient, which is responsible for the evolution of a "jet stream", which flows from the west and reaches speeds greater than 200 km/h (**Figure 2.2.**).

The troposphere contains the Planetary Boundary Layer (PBL) which extends from the surface to about 2-3 km. It is characterized by an active eddy mixing, due to turbulent transport generated by internal friction and vertical motion generated by heated surface by solar radiation. The height of the PBL shows a strong diurnal cycle and generally increases during daytime (due the action of convection) and reduces at night-time (Garrat, 1994). Within the PBL two sublayers can be identified:

- **Laminar boundary layer**: This is the "closest" layer to surface, usually just a few millimetres thick, characterized by laminar motion.
- **Turbulent surface layer**: This is depicted by maximum turbulence intensity caused by small scale vortices generated by the friction with the surface roughness. The turbulent surface layer extends for 50-100 m during daytime, while it reduces to a few metres during night-time.

The meridional tropospheric circulation can be subdivided in three cells (**Figure 2.3.**):

- **Hadley cell:** This is driven by the strong convection typical of equatorial regions. It transports humid air from the Intertropical Convergence Zone (ITCZ) up to the

tropopause, where it eventually loses almost all of the accumulated moisture, before descending in the Tropics (30ºS - 30ºN). Dry surface air is then re-transported to the equator.

- **Ferrel cell:** In order to explain the presence of westerlies at mid-latitudes, in 1856 Ferrel hypothesized the presence of an indirect cell, where warm "remaining" air from the Hadley cell flows poleward accompanied by equatorward transport of cold air from the subpolar jet at higher levels. The Ferrel cell is less stable than the other cells described here and contributes to the establishment of perturbations at mid latitude.

- **Polar cell:** Poleward of 60° latitude, warm and cold air masses are fairly well separated. Closer to the poles the flux of cold polar air prevails over any other air flow and builds up a convective cell with warm air rising at 60° and extremely cold air subsiding at the poles. Very low temperatures and humidity make the weather system stable and very dry. Also, as the tropospheric column above the poles is just 8 km deep, compared to 18 km above Tropics, a stable low pressure system persists and is called the polar vortex.

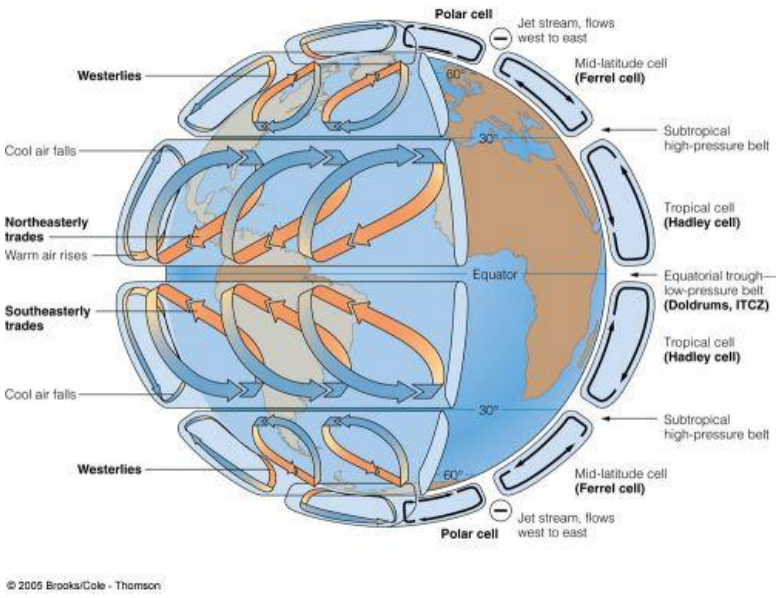

Figure 2.3. Representation of the Earth's mean atmospheric circulation. Blue arrows denote cold air, red denote warm air. Copyright Brooks/ Cole Thomson, www.meteoportaleitalia.it.

2.2.2 Stratosphere

The stratosphere extends from the tropopause (**Figure 2.1.**) to the stratopause at about 50km and can be divided in two sub-layers. The former extends in a region where the temperature remains approximately constant (see **Figure 2.1.**) and correspond to the UTLS (**Section 2.2.4**), whose tropical part will be described in detail in **Section 2.3**. The latter extends for about 25-30 km where temperature increases with altitude and for which vertical mixing is strongly inhibited.

The stratosphere contains most of the atmospheric ozone (about 90%) which reaches its maximum concentration between 15-35 km altitude. Ozone (O_3) absorbs the solar ultraviolet (UV) radiation consequently heating the stratosphere and causing the temperature inversion (**Figure 2.2.**). The absorption of the UV radiation by the ozone is fundamental to maintain life on Earth and via reactions involving O_3, O_2 and O:

$$O_2 + h\nu \rightarrow O + O \qquad (\lambda < 242 \text{ nm})$$

$$O_2 + O + M \rightarrow O_3 + M$$

$$O_3 + h\nu \rightarrow O_2 + O \quad (290\text{nm} < \lambda < 310 \text{ nm})$$

where $h\nu$ is a photon energy and *M* represents an inert atmospheric gas such as N_2 and O_2 which absorbs the excess of kinetic energy generated by the collision between molecular and atomic oxygen (Matsumi *et al.,* 2002).

Brewer, (1949) and Dobson, (1956) first hypothesized a single poleward cell to drive the stratospheric circulation, in order to explain the observed ozone stratospheric distribution. This circulation is the so-called Brewer-Dobson circulation or BDC (Butchart, 2014). Tropospheric air rises in the Tropics and is transported to the winter pole, causing large ozone columns there (**Figure 2.4.**). Unlike the Hadley cell, the BDC is not generated by convection but is forced by large-scale atmospheric waves. It shows large seasonal variability and it is predicted to accelerate under current and future climate change (Butchart, 2014).

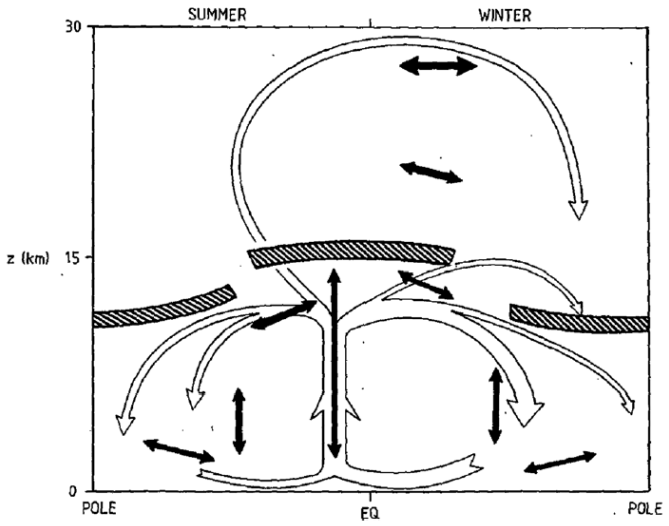

Figure 2.4. Simplified representation of the mean meridional tropospheric and stratospheric circulation of a general circulation model (GCM) at the solstices. Broad arrows show advective transport, while thin double headed arrows shows locations and directions of diffusive transport (figure adapted from Butchart, 2014).

2.2.3 Mesosphere and thermosphere

The highest temperatures in the stratosphere are reached at stratopause levels (**Figure 2.1.**), above which the mesosphere, which literally means "middle atmosphere", begins. The mesosphere extends till about 80 km and is the final layer of the homosphere. In this region temperature drops with altitude, to its minimum (-130°C) at the mesopause. Consequently, vertical mixing due to resulting convection is frequent.

The thermosphere is several hundreds of kilometres deep and is characterized by large diurnal temperature variations. Note that temperature in the thermosphere is strictly linked to the intensity of the solar radiation (UV and *x-rays*) and its increase with altitude is due to the absorption of solar radiation by the photo-dissociation of molecular species such as N_2 and O_2. Above 100 km altitude, cosmic radiation produces the ionization of atoms releasing electrons.

2.2.4 Upper Troposphere Lower Stratosphere

This section focusses on the UTLS, which is the vertical domain relevant to the results presented in **Chapters 4**, **5** and **6**. The UTLS can be roughly defined as the layer ±5 km around the tropopause (Gettelman *et al.*, 2011); this definition developed through time starting from the pioneering work of De Bort, (1902). An historical review of the development of the concept of tropopause can be found in (Gettelman *et al.*, 2011). As a transitional layer, mechanisms which operate in this region can play a role in dynamical, radiative and chemical processes which occur in the surrounding troposphere and stratosphere. For instance, the stratosphere-troposphere exchange (STE) is an important two-way process which alters the chemistry of both the troposphere and stratosphere (Holton *et al.*, 1995). Nevertheless, the UTLS is important for reasons far beyond mere chemical aspects. It is the region where the Cold Point Tropopause (CPT) lies (**Figure 2.7.**). It is defined as the minimum temperature value below the Karman line, apart from the minimum reached at mesopause altitudes (**Figure 2.1.**). Unlike the latter, the CPT regulates the amount of water vapour transported into the stratosphere thereby playing a large role in the radiative balance of the entire atmosphere (Forster and Shine, 1999). In the Tropics, the dynamics of the UTLS is influenced by the Quasi Biennial Oscillation (QBO), which is the periodic variation (~28 months) of the direction of the zonal wind between 16-50 km, subsequently defined as the Upper Troposphere and Stratosphere (UTS), (Baldwin *et al.*, 2001). The QBO acts on the tropospheric dynamics modifying planetary waves in the UTLS (Garfinkel and Hartmann, 2010). Notably, the QBO is evolving in the context of a warming climate, thus stressing the overall atmospheric chemical and radiative atmospheric interactions.

It is convenient to divide the UTLS into two separate regions, depending on the latitude (**Figure 2.5.**):

- **Tropical UTLS**: This region is characterized by radiative-convective balance and contains the Tropical Tropopause Layer (TTL) (Fueglistaler *et al.*, 2009). The top of the TTL is an extremely important level because the flux of tropical air to higher latitudes is prominent (Tuck *et al.*, 1997, Rosenlof *et al.*, 1997). Analysis of **Figure 2.7.** (below) shows that the ASM anticyclone is located within the TTL, thus being an effective transport route for air therein comprised to spread at stratospheric heights.

- **Extratropical UTLS**: Unlike its tropical counterpart, the extratropical UTLS is characterized by different controlling physical processes. Baroclinic wave dynamics, reflected in the different tropopause height (≈17 km in the Tropics, ≈10 km in the extra-Tropics) is dominant here (Held, 1982).

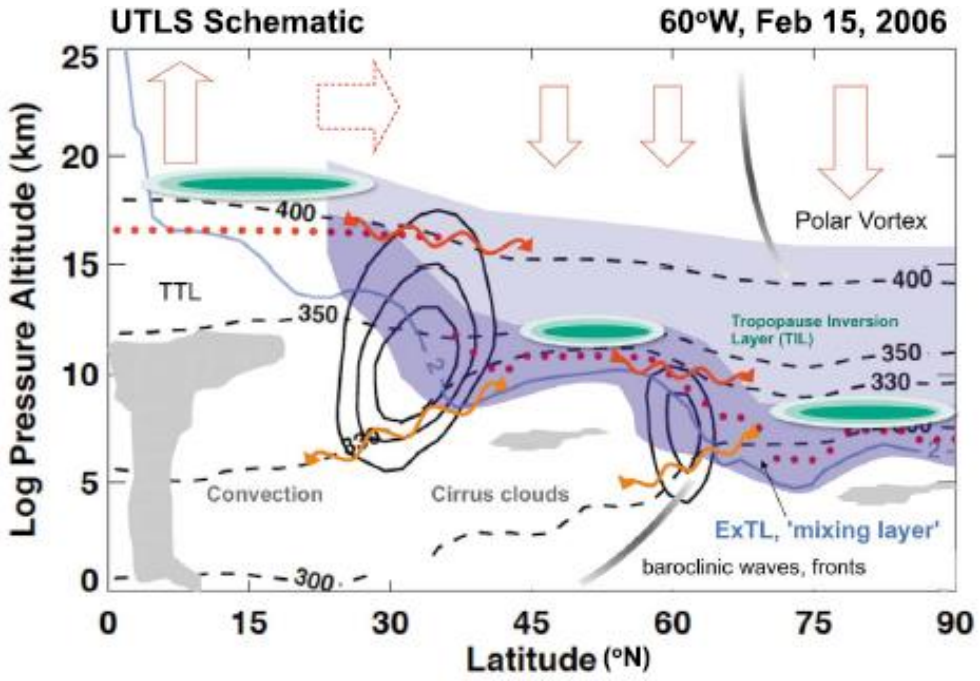

Figure 2.5. Snapshot of the UTLS latitude-height structure along 60°W, on 15 February 2006. Solid black lines show wind contours (10 ms^{-1} internal), potential temperature surface (dashed black lines), thermal tropopause (red dots), PV surface (2 PVU, light blue solid line). Extratropical layer in dark blue shading. Clouds and synoptic weather systems in grey shading. Static stability contours in tropopause inversion layer (TIL) are shown in green shading. Quasi-isentropic exchange (red wavy arrows), cross-isentropic exchange (orange wavy arrows). BDC is shown in deep, red solid outline, shallow dotted solid outline. Figure adapted from Gettelman *et al.*, 2011.

2.3 ASM transport

The ASM is one of most prominent atmospheric phenomena, involving a large portion of the terrestrial surface in the northern hemisphere, and affecting the lives and economic

resources of more than a billion people. In the last two decades, extensive research has been conducted to try to better understand the role of the ASM in transporting climate-relevant species from the surface to the UTLS and related confinement in the corresponding Asian Summer Monsoon Anticyclone (ASMA). This section presents the basic concepts which defines the ASM transport via its circulation (**Section 2.3.1**) and confinement in the ASMA (**Section 2.3.2**).

2.3.1 ASM circulation

Historically, the term “monsoon” derives from Arabic word "mawsim" (مس وم , season) that was used to describe a weather system that shows a winter-summer shift of the horizontal wind field. However, the word monsoon has gradually come to refer to regions where there is a drastic change in rainfall intensity between winter (dry season) and summer (rainy season) (Webster, 1987). Monsoon systems have a profound impact on local, regional, and global scales of the tropical climate. The most prominent monsoon systems are the Asian Summer, West African and Australia Summer Monsoon (**Figure 2.6.)**. Precipitation is considered the most important meteorological element to characterize monsoon activities and these three monsoons have roughly these same mean precipitation rate (10 mm/day, Hung *et al.*, 2004 and Janicot *et al.*, 2011). While the West African and Asian Summer Monsoon are dynamically linked on several time scales, showing temporal fluctuations in the corresponding rainfalls (Janicot, 2009), the Australian Summer Monsoon rainfalls are not strongly correlated with succeeding Asian Summer Monsoon rainfalls (Hung *et al.*, 2004). A comprehensive study (Uma *et al.*, (2004) shows that Monsoon in both Northern and Southern Hemispheres have a significant, although variable, impact on the water vapor distribution in the UTLS, a key factor in the overall radiative balance of the overall atmosphere (Forster and Shine, 1999, 2002).

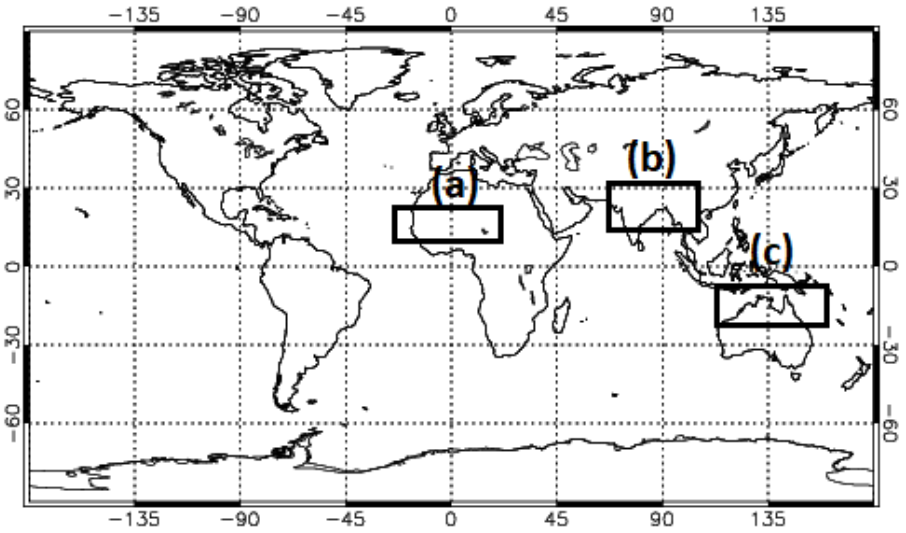

Figure 2.6. Schematic geographical position of the West African **(a)**, Asian Summer **(b)** and Australian Summer Monsoon **(c)**.

In order to observe a monsoon structure a drastic temperature contrast between land-ocean is needed, generated by the solar heating. The ASM is probably the most important seasonal meteorological phenomenon in the Northern Hemisphere. During boreal summer the Indian subcontinent is much warmer than the neighbouring Indian Ocean, the heat capacity of the latter being about four times greater than the former (4281 $Jkg^{-1}K^{-1}$ for water and 1300 $Jkg^{-1}K^{-1}$ for dry land). However, wet soil can have about a 30% higher heat capacity than dry land (Webster and Fasullo, 2003). This temperature distinction generates a pressure gradient between the Indian Subcontinent and the Indian Ocean which in turn develops a flow of oceanic moisture-rich air. This is the flow which brings abundant rainfall over the Indian Subcontinent and develops the so-called the Asian Summer Monsoon (ASM) (**Figures 2.7.** and **2.8.**). During autumn, the maximum solar heating peaks equatorward, transporting water vapour-depleted air to the Indian Ocean. This is the so-called dry phase of the Asian Monsoon. Monsoon precipitation shows variability from subseasonal (Parthasarathy *et al.*, 1994) to interannual time scales (Turner and Annamalai, 2012).

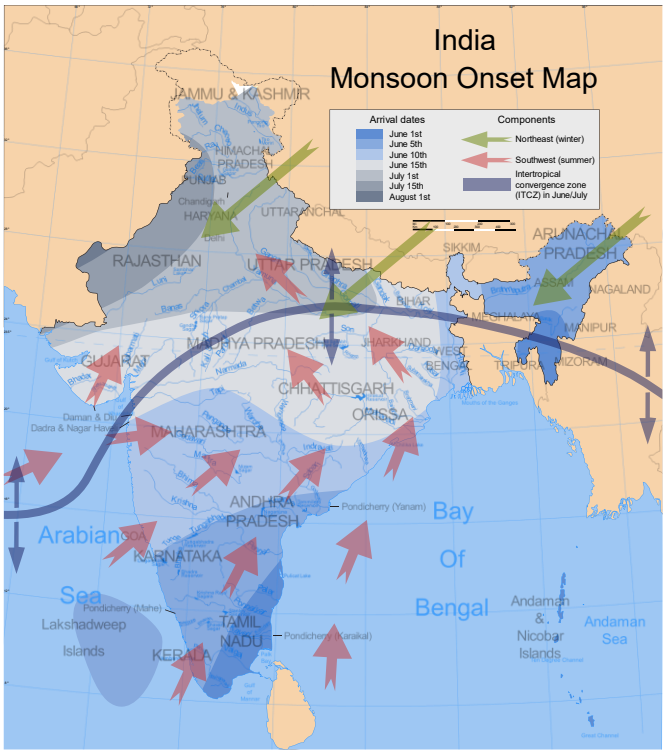

Figure 2.7. Map representing the passage of the ASM over India. Red arrows refer to the summer wind, while green arrows refer to the winter wind direction. The blue line illustrates the position and displacement of the ITCZ (figure from Burroughs, 1999).

Distinctive features of this weather system are the associated deep convection (Devasthale and Fueglistaler, 2010; Bergman *et al.*, 2012; Heath and Fuelberg, 2014) and the development of a wide anticyclonic structure, extending on average from Egypt to Eastern China in the overlying UTLS (**Section 2.2.4**) (Randel and Park, 2006). This atmospheric layer extends from 12 km (~183 hPa) to 22 km (~45 hPa) and includes the TTL (Fueglistaler *et al.*, 2009). Coupling effects between the troposphere and stratosphere occur in this region, controlling dynamics, physics and chemistry of radiatively relevant species such as water vapour, ozone aerosols and cirrus (Gettelman *et al.*, 2011). Processes in the UTLS can therefore modify both the troposphere and the stratosphere.

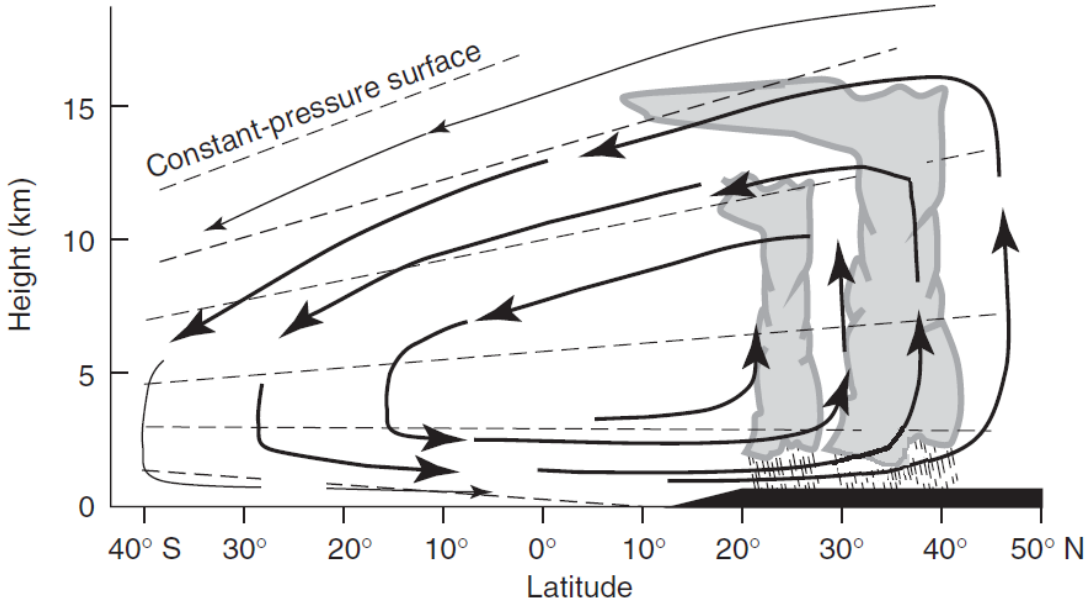

Figure 2.8. Mechanistic representation of the development of the meridional circulation associated with the ASM. Air coming from lower latitudes is water vapour-rich and eventually drawn over the land. Note the extension of the cumulus which can reach heights up to 15 km, corresponding to tropopause levels (not shown) (figure adapted from Webster and Fasullo, 2003).

2.3.2 ASM anticyclone

The previous section described how the ASM circulation develops and brings abundant rainfall to the Indian subcontinent, impacting the life of a population of more than a billion individuals. Together with the prominent horizontal wind, a related vertical transport associated with the ASM couples to surface emissions impacting regional air-quality and the chemical-radiative balance of the overlying UTLS (Wang, 2006). The uplift of several pollutants, water vapour and anthropogenic emission, due to the action of the ASM has been evidenced by recent studies starting from the seminal work of Dethof *et al.*, (1999). Once uplifted to UTLS levels, species at tropospheric heights are eventually "confined" into a specific circulatory structure called the Asian Summer Monsoon Anticyclone (ASMA) (Brunamonti *et al.*, 2018) (**Figure 2.9.**). The air within the ASMA is fairly isolated from the surroundings, acting as an active barrier for the tracers therein comprised. The ASMA develops roughly from the Middle East to East China and is far from being static and constant in space and time. Rather, it shows

bimodality (Nützel, *et al.*, 2016; Pan *et al.*, 2016) (**Figure 2.10.**) east-westward displacement (Nützel, *et al.*, 2016) and eddy shedding (Popovic and Plumb, 2001; Vogel *et al.*, 2014). However, an unequivocal definition of the ASM anticyclone itself has not yet been found. An approach based on PV-gradient maxima on the 380K level highlighted the existence of a barrier to separate low PV air, typical of the ASM circulation, from the surroundings (Ploeger *et al.*, 2015). Low PV air has been identified as a proxy for the existence of an anticyclonic structure (Garny and Randel, 2013) while an empirical method based on the maximum of geopotential positive height to define the centre of the anticyclone has been recently developed (Pan *et al.*, 2016).

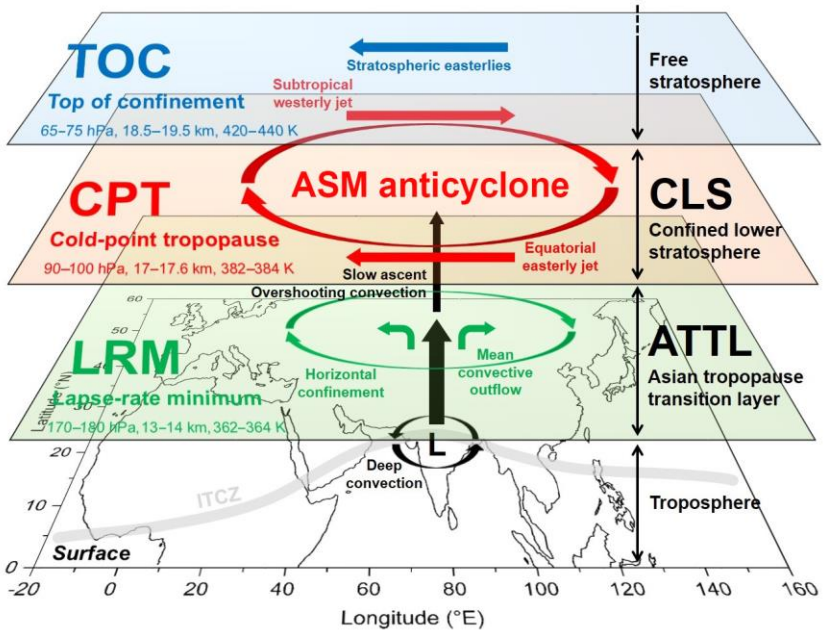

Figure 2.9. Illustration of the ASMA together with the highest (Top of Confinement, TOC) and lowest levels (Lapse Rate Minimum, LRP). The ASMA forms within these levels. Approximate pressure, altitude, potential temperature and dynamical features of the ASM area indicated. Description of the features CLS, LRM and ATTL are given in Brunamonti et al., 2018. Figure adapted from Brunamonti et al., 2018.

In addition to a purely dynamical portrait of the ASMA, it has been recently observed that species such as CO and O_3 (Park *et al.*, 2007, 2008, 2009) HCN (Randel *et al.*, 2010), CH_3Cl (Umezawa *et al.*, 2014), CH_2Cl_2 (Leedham Elvidge *et al.*, 2015), NH_3 (Höpfner *et al.*, 2016), water vapour (Rolf *et al.*, 2018) and aerosols (Vernier *et al.*, 2015). are transported from the troposphere to the ASMA levels via transport mechanisms which

are related to three dynamical regimes of the ASM: convection over the Bay of Bengal, via the Tibetan plateau and large-scale ascent from the Pacific pool (**Figure 2.11.**, Fu *et al.*, 2006; Park *et al.*, 2009; Chen *et al.*, 2012) .

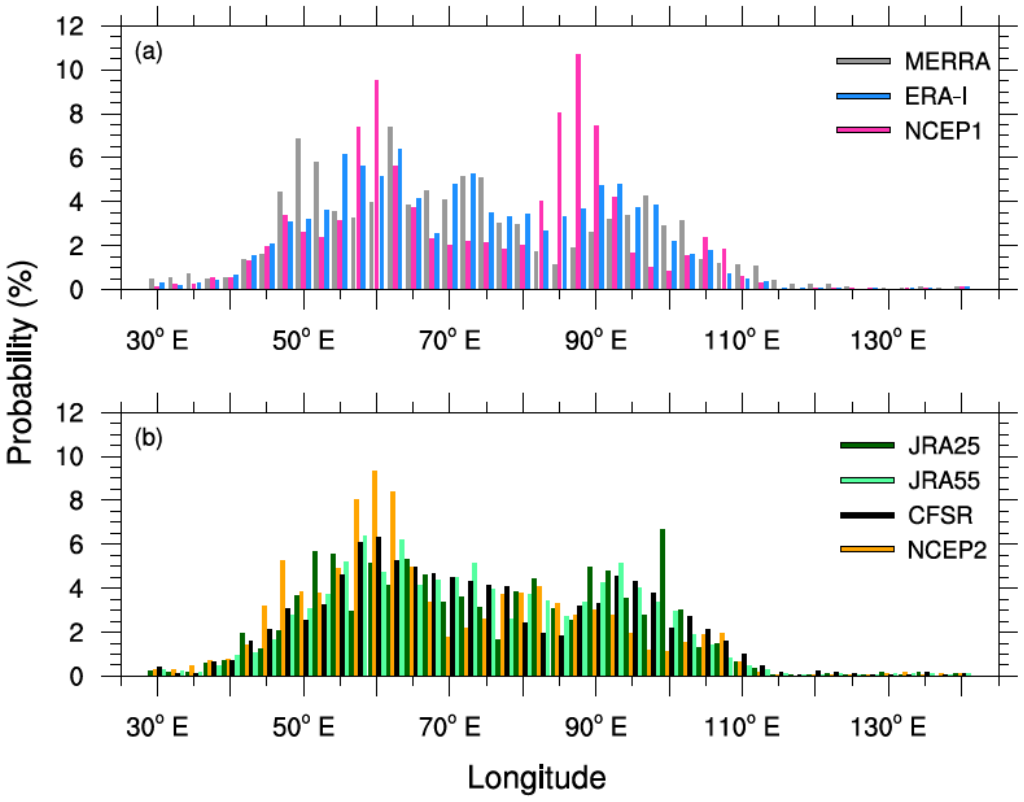

Figure 2.10. Distribution of the locations of the ASMA centre determined using daily geopotential height at 100 hPa during JJA in various reanalyses (roughly 30 years of data have been used): **(a)** Modern-Era Retrospective Analysis (MERRA), ERA-Interim (ERA-I), National Centers for Environmental Prediction/National Center for Atmospheric Research 1 (NCEP 1), **(b)** Japanese 25-year reanalysis (JRA25), Japanese 55-year reanalysis (JRA55), Climate Forecast System Reanalysis (CFSR), NCEP/Department of Energy (NECP 2). Figure taken from Nützel, *et al.*, 2016.

The contribution of each of these regions to the overall vertical transport is not clear, although a recent work (Pan *et al.*, 2016) seems to identify the Tibetan plateau as a preferred boundary source region. The analysis of the ASM transport regimes and timescales is significant not only in terms of composition, dynamical and radiative characteristics of UTLS but also in the complex interactions between aerosols and clouds (Bollasina *et al,.* 2011). Furthermore, tracers from the UTLS can ascend to the free

stratosphere and interact with ozone and water vapour, whose radiative effect is substantial (Forster and Shine, 2002) (**Figure 2.9.**). However, in addition to the direct radiative effects of these forcings, growing evidence supports the idea that changes in the chemical composition of the UTLS affects surface climate, via radiative and dynamical mechanisms (Eyring, *et al.*, 2010).

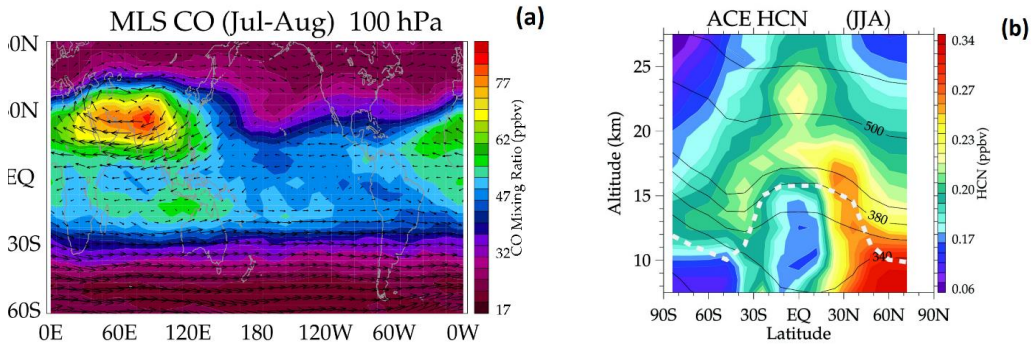

Figure 2.11. (a) Map of Microwave Limb Sounder (MLS) CO mixing ratio at 100 hPa in the Eastern Hemisphere. Black arrows denote the horizontal wind direction and strength. Figure from (Park *et al.*, 2007). **(b)** Aura Atmospheric Chemistry Experiment- Fourier Transform Spectrometer (ACE-FTS) latitude vs altitude plot of HCN JJA zonal mean average. HCN is a chemical constituent of biomass burning and wildfires and is denoted by a strong oceanic sink. White dashed line shows the tropopause, while solid black lines denote isentropic levels. Figure taken from Randel *et al.*, 2010.

2.4 StratoClim project

The importance of the UTLS for impacting the radiative balance of the atmosphere, through the redistribution of aerosol, ozone-depleting substances (ODSs), water vapour and properties of clouds has been discussed in **Section 2.2.4.** Subsequent transport in the "free stratosphere" (**Figure 2.9.**) is still an ongoing debated topic and conclusive results are still lacking (Ploeger *et al.*, 2017). In order to have a clearer picture of the chemical and dynamical processes that determine the composition of the UTLS, the production, transport, loss and redistribution of ozone, aerosols, water vapour and clouds need to be better understood. Accordingly, detailed observations in the source areas of transport are needed.

The uplift of air to UTLS heights is nevertheless not longitudinally symmetric. A key pathway has been identified in the ASM circulation, by Randel *et al.*, (2010). For these reasons, the EU funded the project Stratospheric and Upper Tropospheric Processes for Better Climate Predictions (StratoClim, www.stratoclim.org) from 2013 to 2019. StratoClim was coordinated by Prof. Markus Rex at the Alfred Wegener Institute, Bremen, Germany and had components of observations and modelling. In particular, StratoClim had a significant field campaign, which took place 2016 and 2017 in Greece and in the Indian subcontinent. Overall StratoClim aimed to provide the scientific community with information to answer the following questions (www.stratoclim.org):

- What are the processes which regulate the flux of aerosols and its precursors, water and very short-lived substances (VSLS) and where are they able to break into the stratosphere?
- What is the impact of changing in stratospheric ozone and how does climate change affect surface climate and tropospheric composition and how does climate change affect the ozone layer?
- What is the impact of changes in the concentration, nature and physical characteristics of the stratospheric aerosols on global climate and how does climate change impact the stratospheric aerosol?
- What are the processes which link the aerosols in the UTS (roughly defined as the layer between 10-50 km, **Sections 2.2.1** and **2.2.2**) with cloud properties and how will these evolve under climate change conditions?
- What is the interconnection between climate change and alterations in the stratospheric circulation?
- How does tropospheric weather variability interact with the UTS and vice versa?
- How does the tropical and extratropical efficiency evolve under climate change?
- What is the effect of both natural and anthropogenic emissions of sulfur containing species on UTS aerosols and clouds?
- What is the impact of change in the UTS on societies and their economic activities?

The scientific conclusions of the StratoClim project will be used to include the role of the UTS in the state-of-the-art Earth System Models (ESMs) and Chemistry-Climate Models (CCMs), to produce new and better climate projections. In order to achieve these goals,

the StratoClim project was divided in nine work packages (WPs), as shown in **Figure 2.12.**

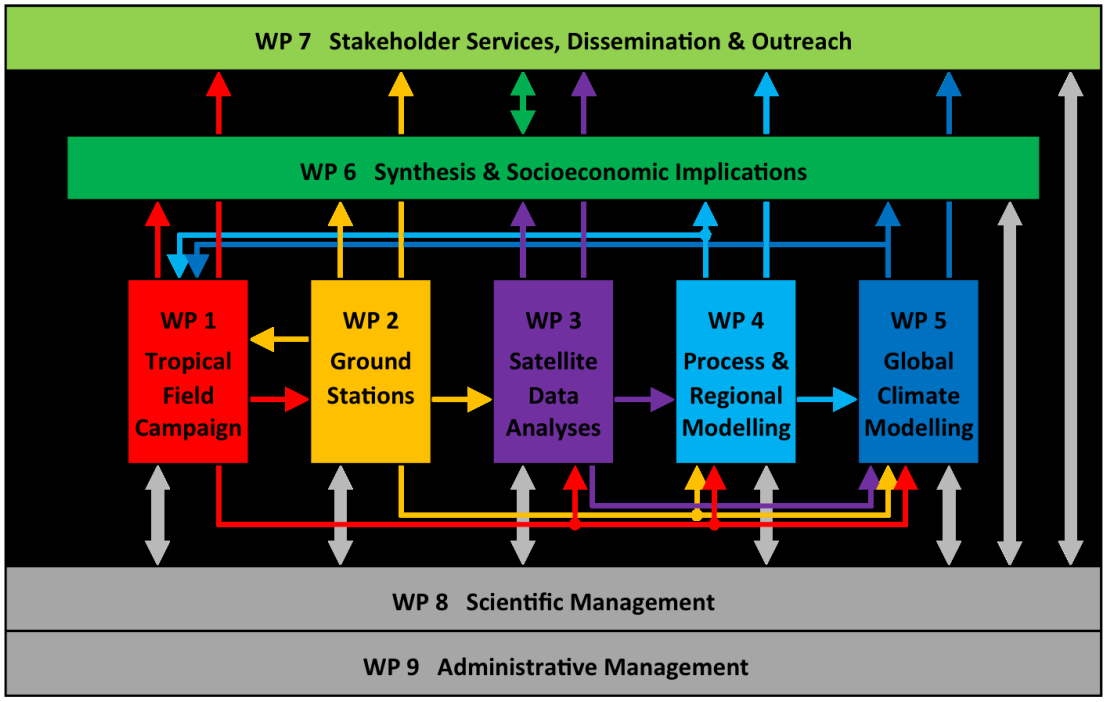

Figure 2.12. Organizational chart of the EU-StratoClim project. Courtesy of Fred Ströh, Juelich, Germany.

WP1: Tropical field campaign. To understand the processes which lead to the interaction between ODSs and other pollutants, in-situ observations are needed to obtain the required spatial and temporal resolution. During the tropical field campaign, which took place 2016 (Greece) and 2017 (Nepal), the former Soviet Union spy aircraft M55 Geophysica was used (Stefanutti *et al.*, 1999) (**Figure 2.13.**).

Between 1996-2010 the M55 Geophysica has been successfully deployed in many other scientific campaigns such as APE-THESEO (Stefanutti *et al.*, 2004) and SCOUT O_3 (Vaughan, *et al.*, 2008) .

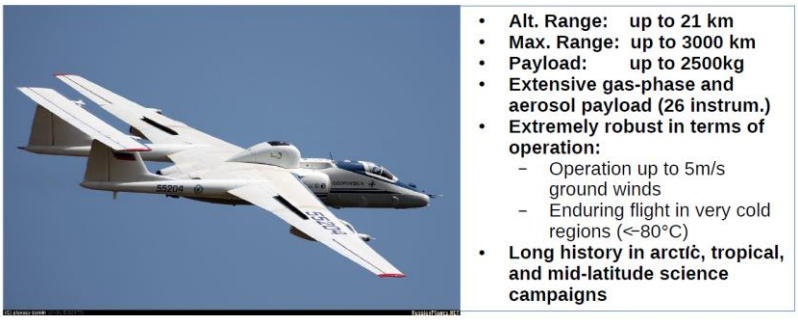

Figure 2.13. Technical specifications of M55 Geophysica aircraft, used during StratoClim tropical campaigns in 2016 and 2017. Courtesy of Fred Ströh.

With a maximum operational altitude of 21,000 metres and a range of 3,000 km, M55 Geophysica provides unique in-situ measurements in barely accessible regions. The aircraft campaign has been conducted in Kalamata, Greece, in summer 2016 and in Katmandu, Nepal in 2017. The "Greek" campaign can be considered as a test for the proper tropical campaign in Katmandu 2017. Locations of the 11 flights are shown in **Figures 2.14.** and **2.15.**

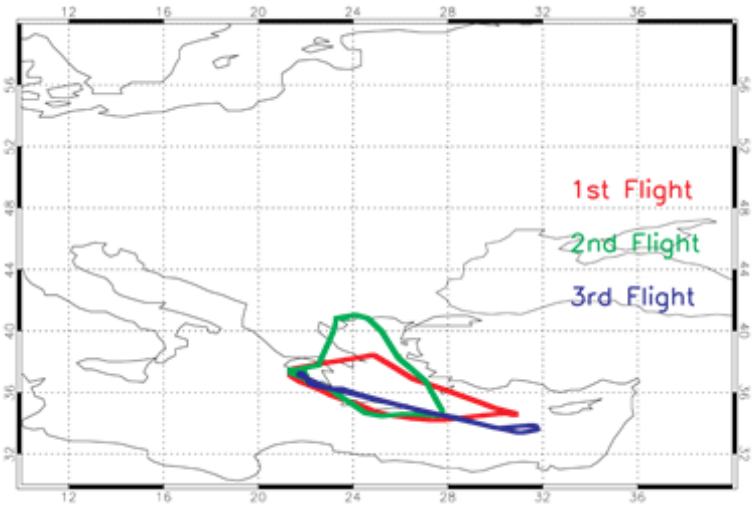

Figure 2.14. Geographical location of the M55 Geophysica during the StratoClim tropical campaign, Grece 2016.

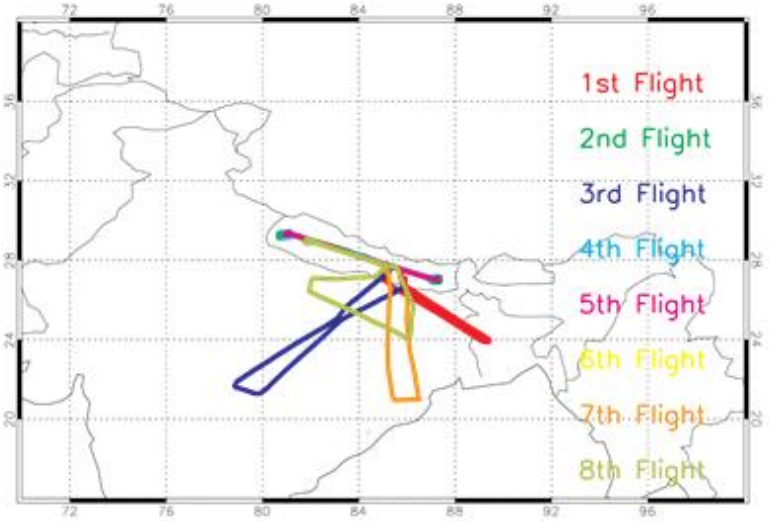

Figure 2.15. Same as **Figure 2.14.** but for the Nepal campaign, based in Katmandu in 2017.

To pursue the scientific goals of the project, the aircraft was equipped with an unprecedented payload which included remote sensing, particle and gas-phase instruments. **Table 2.1.** summarizes the characteristics of the latter.

Instrument	Parameter	P.I.	Technique	References
		IN SITU INSTRUMENTS, GAS PHASE		
FOZAN	O_3	Ulanovsky, CAO	Dye chemiluminescence+ECC	(Ulanovsky et al., 2001; Yushkov et al., 1999)
FISH	H_2O (total)	Krämer, JUELICH	Lyman-a	(Zöger et al., 1999)
FLASH	H_2O (gas phase)	Khaykin, CAO	Lyman-a	(Sitnikov et al., 2007)
SIOUX	NO, Noy, Particle Noy	Schlager, DLR	Chemiluminescence, Au converter, subsonic inlet	(Voigt et al., 2005)
HAGAR	N2O, CFC12, CFC11, CH4, H2, SF6, Halon1211, CO2	Volk, BUW	GC with ECD IR absorption	(Homan et al., 2010)
WAS	Long lived trace gases and isotopologues	Röckmann, UTRECHT	Whole air sampling with lab GC and MS analysis	(Kaiser et al., 2006)
COLD	CO	Viciani, CNR	TDL	(Viciani et al.. 2018)
STRATOMAS	H2SO4 / SO2	Schlager, DLR	CIMS	
AMICA	OCS, CO, CO_2, HCN (t.b.d.)	von Hobe, JUELICH	ICOS	
CHIWIS	H_2O / HDO ratio	Moyer, Univ. Chicago	CEAS	
FUNMASS	HCl, HNO3, BrO, SO2, ... (switchable)	Stroh, FZJ	CIMS-TOF-Mass Spectrometer	

Table 2.1. Summary of the gas-phase instrumentation on board M55 Geophysica during the Tropical field campaign (WP1). Acronyms used are as follows: Central Aerological Observatory (CAO), Electro-Chemical Cell (ECC), Deutsches zentrum für Luft- und Raumfahrt (DLR), Bergische Universität Wuppertal (BUW), Gas Chromatography (GC), Electron Capture Detector (ECD), Infra Red (IR), Mass Spectrometry (MS), Centro

Nazionale delle Ricerche (CNR), Tunable Diode Laser (TDL), Chemical Ionization Mass Spectroscopy (CIMS), Integrated Cavity Output Spectroscopy (ICOS), Cavity Enhanced Absorption Spectroscopy (CEAS), Forschungs Zentrum Jülich (FZJ) and Time Of Flight (TOF).

In addition to detailed in-situ flight observations, the tropical campaign was complemented with observations provided by ground stations located in the following key areas: Island state of Palau (7.34°N, 134.47°E) and Bhola Island, Bangladesh, (22.41°N, 90.76°E) (**Figure 2.16.**).

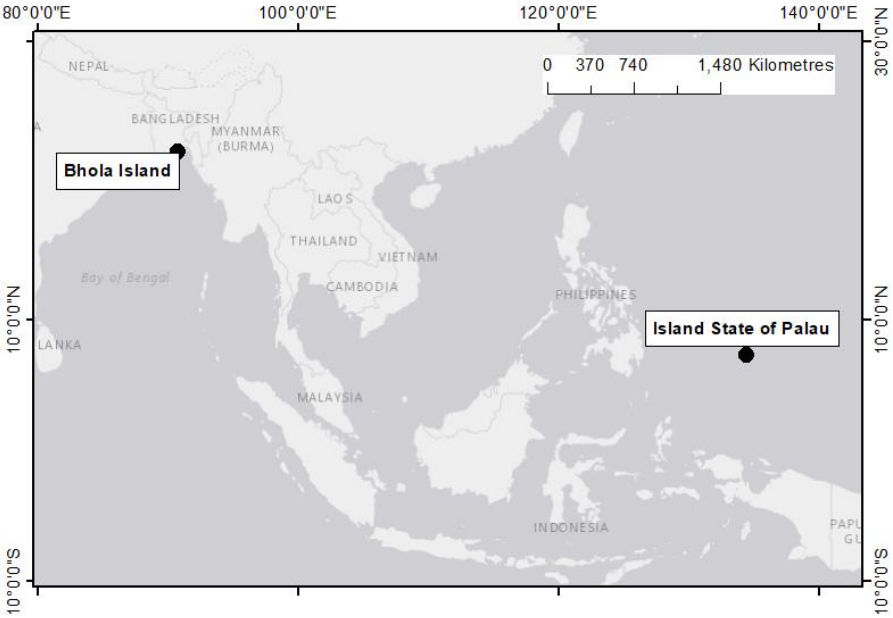

Figure 2.16. Map of ground stations of the StratoClim campaign.

WP2 is based on the analysis of data derived by the instrumentation on these two stations. These stations are designed to study the TTL above the West Pacific warm pool, which is an important source of air which feeds the stratosphere (Chen *et al.*, 2012). Vertical profiles of SO_2 and CO_2, collected in the Bhola Island, have been compared with corresponding measurements in Palau. In combination with these, water vapour and ozone profiles have also been collected in summer 2016 in Nainital, India (29.35°N, 79.46°E) and Dhulikhel, Nepal (27.62°N, 85.54°E). These measurements evidence that vertical transport can occur well above the CPT (**Figure 2.17.**).

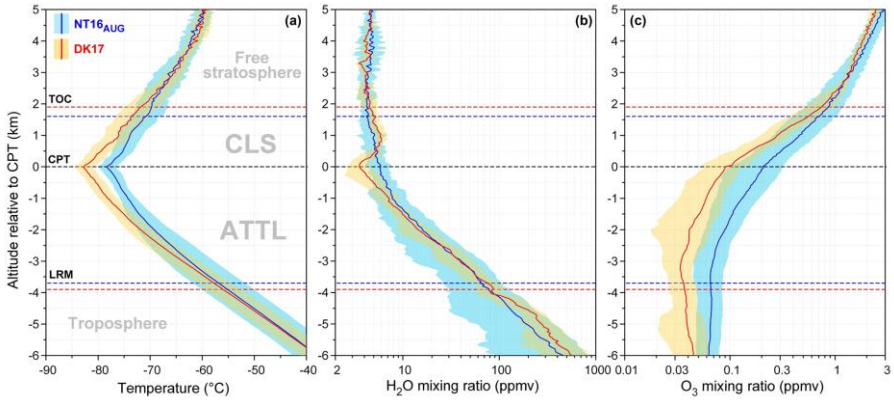

Figure 2.17. Mean profiles (solid lines) and standard deviations (coloured shading) of **(a)** temperature, **(b)** the H_2O mixing ratio and **(c)** the O_3 mixing ratio as a function of altitude relative to the CPT. NT16AUG (blue) refers to the balloon campaign in Nainital, August 2016. DK17 (red) refers to similar campaign in Dhulikhel in July-August 2017. Dashed lines show the average CPT (black) and the average LRM and TOC levels (**Section 2.3.2**) for NT16 and DK17. Figure adapted from Brunamonti *et al.*, 2018.

WP3 focused on the analysis of satellites SO_2, OCS UTS data, combined with analogous CCM and CTM simulations. In particular, observations of these species during the Michelson Interferometer for Passive Atmospheric Sounding (MIPAS)/ENVISAT era (2002-2012) (Fischer *et al.*, 2008) together with measurements from the aircraft campaign have been fed into CTMs to determine budget and variations of stratospheric sulfur loading.

WP4 and **WP5** were devoted to the understanding of the upward transport mechanisms, for climate relevant tracers to break into in the stratosphere, crossing the tropopause. The findings of this analysis will form the basis on which modules to be included in CCMs and ESMs will be developed.

WP6 explored the socio-economic implications of the results of the previous WPs. For instance, impact on the Asian Monsoon rainfall is a crucial part of the work of WP6. However, due to the enormous potential of the conclusions of WP6, policy makers and economic stakeholders are their natural recipients.

WP7 is then focused on the way how the results of WP6 are communicated to wider, politically and economically influenced audiences. WP8 and WP9 aimed to ensure an

efficient organization of all the WPs, through a primary management structure consisting of a coordinator, executive group and an external advisory board (**Figure 2.10.**).

At the time of writing StratoClim has recently finished as a project, but analysis of the observations will continue in various scientific groups. The work presented in this thesis is, in part, a contribution to the results of StratoClim. I make use of new observations that became available after the 2016 and 2017 campaigns and I perform model studies which address some aspects of the wider aims of StratoClim.

3 The TOMCAT 3-D Model

3.1 Introduction

Numerical models are essential tools for understanding chemistry and transport in the atmosphere. These models are a mathematical representation of our current understanding of relevant processes. Comparison of model simulations with observations allow us to test our understanding. Discrepancies point to a failure of our theories (and/or model) which then need to be investigated. Once a model has been successfully developed it can be used for predictions and to explore different possible scenarios.

A range of atmospheric chemistry models exist and there a number of different possible classifications which distinguish them. A primary classification relates to the domain size and dimensionality of the model. Models range from global, three-dimensional (3-D) models, through regional 3-D models, to simple 'box' models (Seinfeld and Pandis, 2016) which simulate chemistry at just a single point. Clearly, box models are a lot cheaper computationally and will therefore allow a lot more chemical complexity.

Models can also be classified as Eulerian or Lagrangian. Eulerian models divide their domain up into an array of fixed grid boxes. Tracers are then transported between the grid boxes. These models have the advantage of equal coverage of the whole domain and offer a more direct way of analysing global budgets. Lagrangian models follow the movement of air parcels, e.g. a trajectory box model. These models are good for understanding chemistry transformations of air parcels under specific transport regimes but are not so well suited as Eulerian models for global studies.

A final important classification for global 3-D atmospheric chemistry models relates to the treatment of dynamics. 'Off-line' chemical transport models (CTMs) use external winds and temperatures to specify the model meteorology. This makes the models relatively cheap as there is no overhead for the dynamical and radiative calculations. Moreover, by using analysed meteorology, the models are excellent tools for comparing simulations with specific observations. However, as there is no coupling between the

chemistry and dynamics these models cannot be used for coupled feedback studies. Simulations of the future need to use repeating 'past' meteorology. In contrast, coupled chemistry-climate models (CCMs, Eyring, *et al.,* 2010) are based on a general circulation model (GCM) coupled to detailed chemistry These models are needed for coupled predictions of future climate change and the feedbacks with atmospheric chemistry. However, they are very computationally expensive and comparison with past observations is generally done in a climatologically way, although 'nudging' to analysed meteorology can be done (Morgenstern *et al.,* 2009; Connor *et al.,* 2014).

The remainder of this chapter describes the TOMCAT CTM which is used in this study. **Sections 3.1**, **3.2** and **3.3** summarise the basic formulation of the model and its treatment of advection of boundary layer mixing. **Section 3.4** describes the treatment of convection in the model, including the existing Tiedtke scheme and the new scheme based on archived convective mass fluxes which has been developed, tested and used in this work. **Section 3.5** describes the various chemistry schemes which have been used in the simulations subsequently presented in this thesis.

3.2 The TOMCAT model

The TOMCAT 3-D CTM belongs to the wide class of Eulerian models, where fixed grid boxes encompass the Earth the size of which depend on the horizontal resolution and the availability of vertical levels. Tracers are transported through the boxes due to the action of large-scale winds and parameterized mixing, e.g. from convection. Originally separated in a tropospheric (TOMCAT) and stratospheric (SLIMCAT) "versions", the TOMCAT/SLIMCAT model has been firstly used in the early 1990s in the context of evaluating the relevant chemistry of the Arctic winter polar stratosphere (Chipperfield *et al.,* 1993). However, from 1993 the model has undergone continual updates and has been validated by several tropospheric and stratospheric studies due to its comprehensive and detailed implemented chemistry scheme (Chipperfield, 1999, 2006). The dynamical variables (wind, pressure and temperature) needed to force the model are not calculated in a specific internal routine but are downloaded from the European Centre for Medium-Range Weather Forecasts (ECMWF). The model is written in FORTRAN (originally F77 and later F90) and divided in segments and consequently the modules (advective, convective, chemical and radiative) therein incorporated are performed in a 'process split'

sequence. The lack of interaction between dynamical and chemical segments in the model, drastically reduces the computational resources required to run the simulations, compared, for example to coupled chemistry-climate models.

3.3 Model grid

The model uses a Gaussian grid (slightly irregular in latitude, Eliasen, *et al.*, 1970) which encircles the globe latitudinally, longitudinally and vertically, and the resolution of which can be chosen depending on the problem to be studied. In this thesis, simulations with horizontal resolution 5.6° lat × 5.6° lon, 2.8° lat × 2.8° lon and 1.1° lat × 1.1° lon have been performed. These values correspond to the Gaussian grids associated with the T21, T42 and T106 spectral resolutions, respectively, a typical format used by the ECMWF (Dee *et al.*, 2011). The large-scale analyses are input to the model as spherical harmonics are then converted in grid points on Earth with the desired vertical levels. The vertical resolutions used here are 60 vertical levels from the surface to 0.1 hPa, and 31 levels from the surface to 10 hPa. The TOMCAT model uses hybrid $\boldsymbol{\sigma/p}$ vertical levels to follow topography at low height while being purely pressure levels $\boldsymbol{p}$ in the free atmosphere. The pressure at model vertical grid box interface $\boldsymbol{p_{k+\frac{1}{2}}}$ is given by

$$\boldsymbol{p_{k+\frac{1}{2}} = Ap_0 + Bp_s}$$

where p_s is the surface pressure, p_0 is a reference pressure of 1000 hPa, while A and B are two constants for each level. However, levels in UTLS and above are normally characterized by isentropic transport regime and therefore the model has the option ('SLIMCAT') to use $\boldsymbol{\sigma/\theta}$ (potential temperature) as vertical variables. Above a level θ_0 the model uses pure isentropic levels according to the formula

$$\boldsymbol{\theta_{k+\frac{1}{2}} = C\theta_0}$$

with $\mathbf{C \geq 1}$ and $\boldsymbol{\theta_0 \approx 350\ K}$ (Chipperfield, 2006). Between the interface level θ_0 and the surface the pressure of the model half levels is

$$p_{k+\frac{1}{2}} = Cp_{\theta 0} + (1 - C)p_s \qquad with\ C < 1\ ,$$

where $p_{\theta 0}$ refers to the pressure at lowest purely isentropic half level. On the other hand, the temporal resolution (timestep) cannot be chosen arbitrarily, but must obey the Courant-Friedrich-Lewy (CFL) condition, which ensures that the numerical solution of a certain partial differential equation maintains an acceptable stability:

$$\frac{u_i \Delta t}{\Delta x_i} \leq C_1$$

where u_i is the wind speed in the ith direction (*x*,*y*,*z*) and Δx_i is the corresponding resolution. C_1 is a constant which changes according to the partial differential equation considered. Obviously, the CFL condition must hold for all the three spatial components. Consequently, it is apparent that increasing the spatial resolution must result in a reciprocal increase of temporal resolution. The choice of special resolution values is then a compromise between accuracy and computational speed, depending on the available computer resources. It is usually the east-west size of the grid boxes near the pole that poses the strongest CFL constrain in a global CTM. To overcome this TOMCAT uses extended polar zones (EPZ, Prather *et al.*,1987; Rind, 1987) to group grid boxes in the east-west direction at the pole.

3.4 Advection and Planetary Boundary Layer schemes

Apart from negligible molecular diffusion, atmospheric tracers move from the emission point to other parts of the atmosphere, under the action of winds. The TOMCAT off-line CTM does not have a 'dynamical core', meaning that the meteorological fields (winds, temperature, pressure) need to be read-in from an external source. Typically, ERA-Interim reanalyses (Dee *et al.*, 2011) are used but coupling with an external GCM is also possible (Chipperfield, 2006b). Nevertheless, only the horizontal wind components are read into the model. The reason for this lies behind the fact that when archived vertical winds are adapted to the model grid both vertically and horizontally, the corresponding interpolation might bring undesirable inconsistency between horizontal and vertical winds. These are intrinsic problems of off-line models as described by Jöckel, e*t al.*, (2001) and Rotman *et al.*, (2004). To overcome this problem, TOMCAT calculates the vertical component of the winds from horizontal mass fluxes using the continuity

equation. However, the model has the 'SLIMCAT' option to calculate the vertical wind component from heating rates which are derived from a radiation scheme described in Chipperfield, (2006).

To precisely describe the advection of atmospheric tracers, an advection scheme is needed to preserve mass concentration (0^{th} moment order distribution), spatial gradient (1^{st} order moment distribution) and eventually the curvature (2^{nd} order moment distribution, SOM). The computational effort required to operate the scheme largely depends on the amount of moments conserved, with 10 variables for every grid box, tracer and timestep stored if the SOM is conserved. The SOM tracer advection scheme implemented in the model for this study is based on the work of Prather (1986).

The transport from Planetary Boundary Layer (PBL) towards the free atmosphere is parametrized in a corresponding scheme. The model has two options over the choice of a PBL scheme. A local first-order diffusion scheme (Louis, 1979) calculates the eddy-diffusion coefficients in the PBL using the Richardson number which in turn depends on the local wind field gradient and potential temperature. Nevertheless, when the Louis, 1979 scheme is implemented the TOMCAT model shows weak vertical transport and considerable superficial tracer concentrations, as pointed out by Stockwell and Chipperfield, (1999). Another option is using a non-local scheme developed by Holtslag and Boville, (1993). This scheme shows stronger transport out of the PBL (Wang *et al.*, 1999) and then into the free atmosphere, and consequently has been used in this study.

3.5 Convection schemes

The study of the transport of species emitted at surface to ASM anticyclone levels requires that the effect of convection in the TOMCAT model is represented in a realistic way. This thesis has compared two convection schemes: the existing default Tiedtke scheme, which calculates convection in the model based on large-scale analyses which are read in, and a new scheme which directly uses archived convective mass fluxes from the same source as the large-scale analyses.

3.5.1 Existing Tiedtke scheme

The default convection scheme in the TOMCAT model, based on the work of Tiedtke, (1989), makes use of mass fluxes which reproduce the cloud properties to evaluate the

budget of heat and moisture due to convective-driven transport. This scheme has been used in TOMCAT since the work of Stockwell and Chipperfield (1999). Large-scale meteorological variables within ERA-Interim reanalyses (winds, temperature, humidity) are used in this scheme to calculate entrainment, detrainment and cumulus downdrafts (Stockwell and Chipperfield, 1999). **Figure 3.1.** shows the vertical structure of the variables used in the Tiedtke scheme to calculate the convective contribution to the transport of tracers. Cloud is at *k* level with entrainment and detrainment rates (units of $1/s^3$) at the top of the cloud indicated by E_u^k and D_u^k , respectively. $M_{d,u}^k$ is the fraction of tracer mass from down (up) and then transferred through model interface *k* due to all sub-gridscale processes. The scheme tests the presence of a cloud via the calculation of the relative humidity, which must be at supersaturation level (*RH >100*). Once a cloud is "found", buoyancy of the air parcel is tested and a criterion on the horizontal convergence of moisture below the cloud base discerns between shallow and deep convection according to the formula

$$\int_{surface}^{cloud\ base} \boldsymbol{v} \cdot \boldsymbol{\nabla}\rho_w \, dz = \int_{surface}^{cloud\ base} \{\rho_w \, \boldsymbol{\nabla} \cdot \boldsymbol{v} - \boldsymbol{\nabla}(\rho_w \boldsymbol{v})\} \, dz$$

where $\boldsymbol{v}$ is the horizontal wind, ρ_w is the water density (kg(water)m^{-3}) and *z* is the vertical coordinate. If the integral on the right side is positive, the grid column is convectively unstable and deep convection is initiated. It is worth remembering that the water mixing ratio together with the wind fields are taken from the ECMWF reanalyses, from fields which have already been subject to convection.

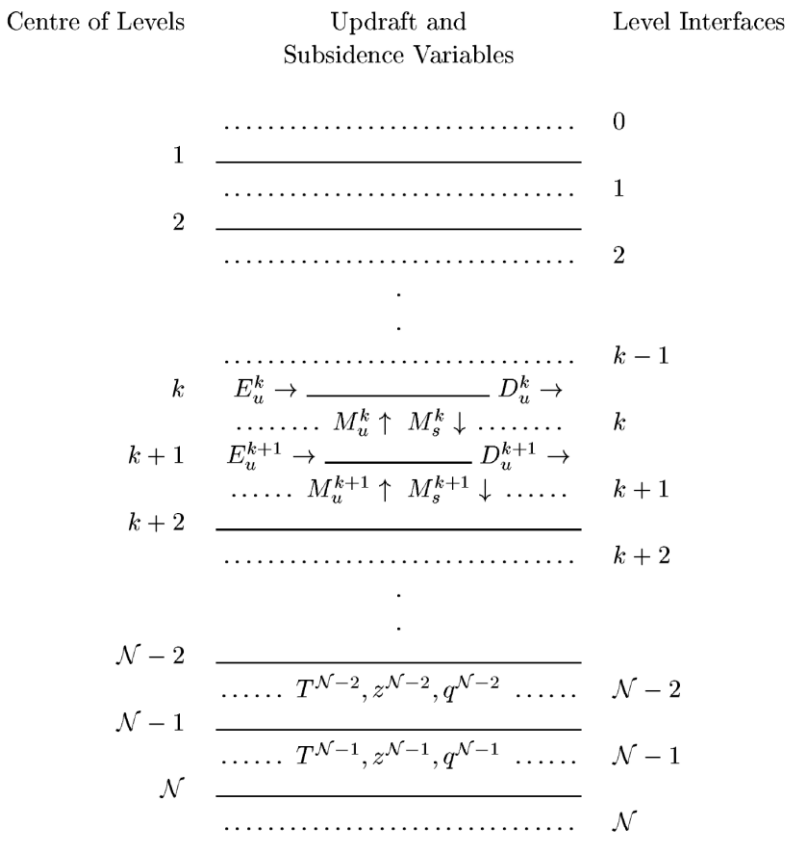

Figure 3.1. Convective variables for the Tiedtke shown on TOMCAT vertical levels. Taken from Chipperfield, (2006a).

The Tiedtke scheme has been used in several studies focused on the transport of VSLS up to UTLS heights (see Hossaini *et al.*, (2012) and references therein).

3.5.2 Archived Convective Mass Fluxes

An alternative to the 'online' (or diagnosed) Tiedtke scheme which is explored in this thesis is the use of ERA-Interim archived convective mass fluxes. An early version of this approach was tested by Feng *et al.*, 2011 who examined the vertical extent of convection by this method, compared to the existing Tiedtke scheme. Their results show that the former can reach higher altitudes (≈100 hPa) compared to the latter (≈200 hPa). However, a previous study by Hossaini *et al.*, (2010) pointed out that when the default Tiedtke scheme is implemented, the model overestimates the rapidly uplifted concentration of CH_2Br_2 (≈7 days lifetime) and $CHBr_3$ (≈2 days lifetime). Subsequently, a general improvement of the model and the implementation of the ERA-Interim archived mass fluxes (Hossaini *et al.*, 2012) seem to produce results which better adhere to observations.

In this new approach the 6-hourly accumulated (forecast) fields of vertical convective mass flux (*M*, **Figure 3.1.**) and detrainment rates (*D*) for both updrafts and downdrafts are read in from ERA-Interim reanalyses at $1^o \times 1^o$ resolution. These fields are then averaged onto the current model horizontal and vertical grids being used in the particular simulation. The third component of tracer transport by convection, the entrainment rate (*E*) at each model level, is derived in order to conserve tracer mass balance. Once these three components are derived, the same convective tracer transport routines as used for the online Tiedtke scheme are used, i.e. the model calculated values of *E*, *D* and *M* for both updrafts and downdrafts in **Figure 3.1.** are replaced by the archived values.

The use of archived convective tracer fluxes from the same source as the large-scale meteorology appears attractive and self-consistent. It should have the advantage that the CTM should be able to reproduce the extent of convection produced in the high resolution system that produces the analyses. However, it should be noted that the archived convection fields are not available for all meteorological analyses. In the case of ECMWF, the reanalyses supply them but they are not available for the regular operational analyses due to the computational and storage costs involved. A further likely advantage of the new method is that as the large-scale analyses will have already been subject to the effects of convection it is likely that the online Tiedtke approach will underestimate convection. This was shown in the original analysis by Feng *et al.*, (2011) and is illustrated in **Figure 3.2**.

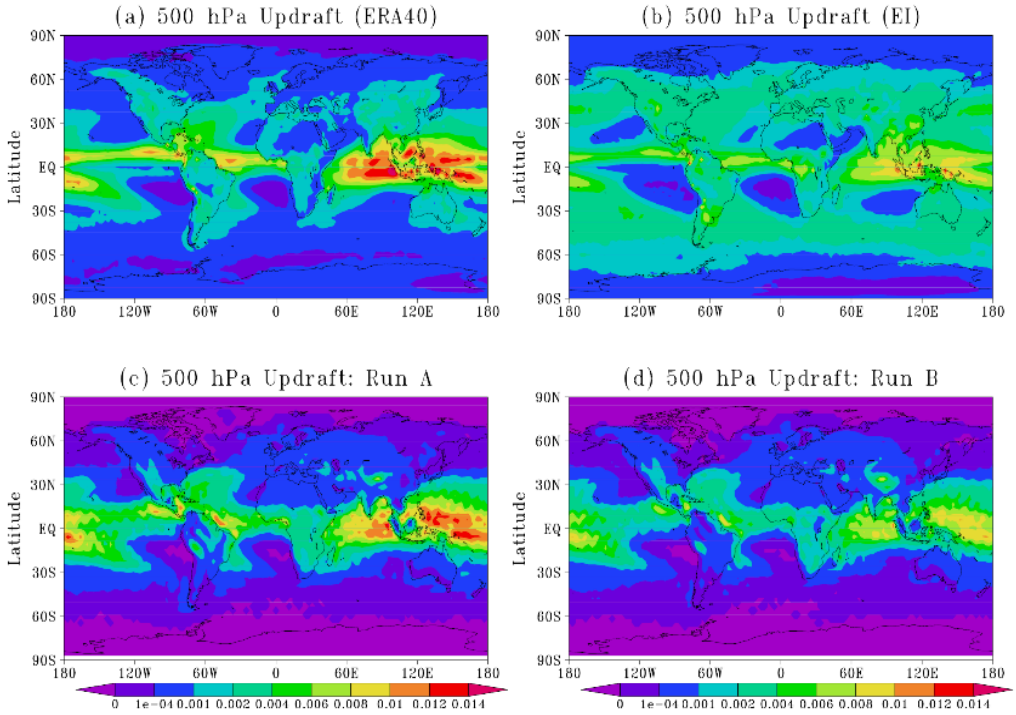

Figure 3.2. (a) Convective updraft mass fluxes (kg m^{-2} s^{-1}) at 500 hPa averaged over time period 1989-2001, using ERA40 Reanalyses. **(b)** Same as **(a)**, but using ERA-Interim reanalyses, averaged over 1989-2005. **(c)** Convective updraft mass flux from results of TOMCAT T42 simulation with ERA40 Reanalyses (operational analyses after 2001), averaged over 1989-2005. **(d)** Same as **(c)** but using ERA-Interim reanalyses. Details of the simulation setups are available in Feng *et al.*, 2011. The different average time periods depend on the corresponding data availability. Figure adapted from Feng *et al.*, 2011.

Compared to the early testing of the scheme by Feng *et al.* (2011), the work in this thesis has developed the scheme into a robust parameterisation suitable for long, multidecadal studies (by ensuring exact mass conservation within the convective transport) and tested it for a wide range of tracers. As extensively shown in **Chapter 4**, this new version of the convection scheme is consistent with fast deep convective activity typical of tropical regions, which are the key regions of this study.

3.6 Chemistry schemes

The TOMCAT model allows the inclusion of several chemistry schemes to reproduce at best the conditions of the experiment. These can be either be detailed 'full' chemistry

schemes for tropospheric/stratospheric studies or a specific simplified scheme for idealised tracers. In this way the model can used as tracer transport model, with or without coupled full chemistry. In either case a standard chemistry scheme called *CHIMIE* is the basic tracer subroutine implemented within the model.

3.6.1 Simplified approach

The simplified approach makes use of artificial, idealized tracers and processes which can be used to gain insight into a particular problem. It is characterized by generally a small number of specific tracers (typically 10 or fewer) and a simplified chemistry scheme, to reduce the computational cost and complexity. Due to this relatively low computational cost, this approach can be used for multiannual simulations, which would be prohibitive with 'full' chemistry. In this study, this approach has been used in **Chapter 4** to study the interannual variability of artificial and idealized tracers in and around the ASM. In this case a bespoke *CHIMIE* subroutine has then been modified to include the tracers specifically created for this kind of simulation: surface emitted species with specified atmospheric loss. The decay of a tracer mixing ratio mr in this simplified approach then depends exclusively on the lifetime of the tracers according to the formula

$$\boldsymbol{mr_{i+1} = mr_i \exp\left(-\frac{\Delta t}{\tau}\right)}$$

where i is the timestep label and $\boldsymbol{\Delta t}$ timestep. In this study, two idealized tracers CO25 and CO50 with lifetimes of 25 and 50 days, respectively, have been used corresponding to CO lifetimes in the range typical of the tropical regions (Novelli *et al*., 1998; Petrenko *et al.*, 2013). These CO tracers used realistic surface emissions of CO, which vary with location in response to industrial and fire activity. The main source ignored in these kinds of runs are the secondary chemical source from oxidation of other hydrocarbons in the atmosphere. In terms of direct emissions the main two are included (anthropogenic and biomass burning) although there is also a small direct biogenic source (see **Table 3** in Zheng *et al.*, 2019). Further artificial tracers TR5 and TR50, with 5- and 50-day lifetimes, were also used. These tracers have the boundary conditions of an arbitrary 100 ppbv mixing ratio, zonally homogenous. The TR50 tracer therefore provides a contrast with CO50 in terms of its simpler surface distribution. Tracer TR5 is very short-lived and provides information on very rapid vertical transport which is not revealed by CO25.

3.6.2 Full chemistry approach

The TOMCAT model has two ‘full’ chemistry schemes, both of which are used in this thesis. The first scheme is a flexible ‘tropospheric’ scheme, most recently described by Monks *et al.,* (2017). The second scheme is based on the original ‘stratospheric’ scheme described by Chipperfield (1999). The stratospheric scheme is less flexible but well tested and more computationally efficient for studies related to stratospheric ozone.

The ‘tropospheric’ full chemistry approach provides the required chemical details needed to represent the complexity of the chemical and radiative mechanisms which govern the UTLS. The full chemistry scheme is based on the work of Carver *et al.,* (1997) who developed the *ASAD* package which incorporates reactions for 79 species, including O_3, CO, CH_4 , C_2-C_3 hydrocarbons, H_2O, H_2O_2, H_2SO_4, N_2O_5, NO_x, HNO_3. This version of the model is also coupled to the GLOMAP aerosol module. Surface emissions are specified from standard inventories (Monks *et al.,* 2017). This scheme has been used for the detailed chemistry simulations in **Chapter 5**. These simulations are very costly in terms of time and computational resources and therefore they have been run only for the years of the StratoClim campaign (2016 and 2017).

The ‘stratospheric’ scheme is used in **Chapter 6** for the model simulations for the therein described geo-engineering study. The scheme includes a description of the chemistry of the main families which affect stratospheric ozone, namely HO_x, NO_y, Cl_y, and Br_y along with the major source gases such as halocarbons, CH_4 and N_2O. The scheme includes gas-phase chemistry as well as a treatment of heterogeneous chemistry on sulfate aerosols and polar stratospheric clouds (PSCs). For the work described in **Chapter 6** the subroutine *CHIMIE* was modified to include a treatment of heterogeneous chemistry on TiO_2 particles.

4 Modelling the interannual variability of tracer transport via the Asian Summer Monsoon

4.1 Introduction

The vertical transport of air masses associated with the Asian Summer Monsson (ASM) circulation is of undoubted primary importance due to its influence on the composition of the upper troposphere / lower stratosphere (UTLS) (see **Chapter 2**). The evaluation of this transport requires detailed in-situ observations in remote areas which often have poor operational access. Although, this observational "gap" has to some extent been addressed by the StratoClim campaigns in 2016 and 2017 (see **Chapter 5**) complementary modelling studies are also essential in order to understand the underlying mechanisms of this transport.

Convective transport is a key component of rapid vertical motion in the troposphere, but it is challenging to represent as a subgrid process in a large-scale model. The first part of this chapter describes TOMCAT 3-D CTM simulations of tropospheric age-of-air (AoA) used as a diagnostic for transport times, when the default Tiedtke convection scheme is replaced with a new one based on archived ERA-Interim updrafts (**Chapter 3**). The validation of this new scheme is further motivated by a recent study which showed that the default (Tiedtke) scheme is not consistent with the deep intense convection-driven transport typical of the Tropics. This new version of the model forms the basis for the results shown in the second part of the chapter, where simulations conducted using artificial tracers and idealized CO tracers with specified lifetimes ranging from 5-50 days are used to test the ability of the model to quantify the transport from surface to ASM anticyclonic levels.

The chapter is structured as follows: **Section 4.2** evaluates the results of TOMCAT simulations when a new convection scheme (ERA-Interim updrafts) is used. **Section 4.3** is devoted to the study of TOMCAT-simulated artificial and idealized tracers when the two convection schemes are compared, along with simulations when convection is

switched off, with particular attention on the ASM region. **Section 4.3** summarizes the results presented here.

4.2 Test of ERA-INTERIM updraft convection scheme

The terrestrial surface is the source of almost all pollutants and climate-relevant species which reach the stratosphere, and the ASM is believed to play an important role in the global vertical transport (see **Chapter 2**). To assess this transport quantitatively, and to study the related mechanisms, modelling studies require that convective parameterisations therein incorporated should be tested against observations. A typical metric used to determine this kind of transport is the "Age of Air" (AoA), a concept first used for the investigation of the stratospheric transport timescales (Hall and Plumb, 1994). In this context it is defined as mean of the "age spectrum of the time distribution since the fluid elements constituting a given stratospheric air parcel lost contact with the troposphere" (Holzer and Hall, 2000), i.e. the mean time since an air parcel entered the stratosphere at the tropical tropopause.

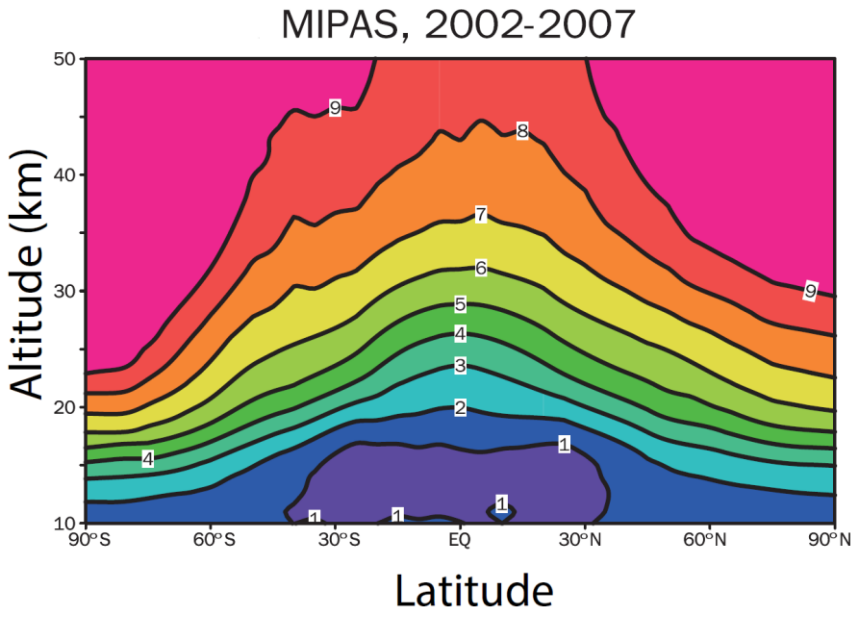

Figure 4.1. Annual mean stratospheric Age of Air (AoA) (years) for the period 2002-2007 calculated from SF_6 Michelson Interferometer for Passive Atmospheric Sounding (MIPAS) measurements. Figure adapted from Kovács *et al.*, (2017).

AoA is not a directly observable quantity so it needs to be estimated from appropriate real tracers, e.g. SF_6, which is particularly suitable as it displays a near-linear growth in its tropospheric mixing ratio due to its near-constant emissions and long lifetime (1278 years, Kovács *et al.*, 2017). **Figure 4.1.** shows zonal mean plot of stratospheric AoA which follows to the presence of well-known pathways from the surface to the stratosphere, with the tropical upwelling areas characterized by "young" AoA, while at higher latitudes the stratospheric AoA may reach values of up to ten years. Following the idea of developing an analogous tropospheric version of AoA (Waugh *et al.*, 2013; Holzer and Waugh, 2015), Krol *et al.*, (2018) studied the performance of six global models (CTMs and GCMs), including TOMCAT, for their ability to convectively redistribute tracers in the troposphere and transport to stratospheric levels, from Northern Hemisphere (NH) to Southern Hemisphere (SH) and vice versa. This is a crucial aspect of tropospheric transport to be quantified, when large dynamical systems which involve deep convective activity, such as the ASM, are involved. However, as shown below, the standard TOMCAT model persistently showed slow and weak transport throughout the troposphere to stratospheric levels, when compared to observations and other models (Krol *et al.*, 2018). To compare different model results, which have different advective, convective and meteorological parametrisations, in a clear and robust way a protocol with appropriate boundary conditions which can be implemented in all the models is necessary. The protocol used to develop the simulations for this chapter is taken from Krol *et al.*, (2018) and presented in **Section 4.2.1**.

4.2.1 Age of Air tracer protocol

The modelled AoA is calculated from the mixing ratio of five artificial tracers emitted at specific locations (forcing volumes): surface, NH or SH (see **Table 4.1**). The mixing ratios of these tracers are then evaluated at every grid box of the model. The mixing ratio G in the forcing volume (surface, NH surface or SH surface) grows linearly with time according to the formula $G = ft$, where t is the elapsed time in seconds since 1st January 1988 and $f = 10^{-15}\ mol\ mol^{-1}s^{-1}$ is a forcing constant. At the end of the simulation, on the 31st of December 2014, $G \approx 852\ nmol\ mol^{-1}$. The mixing ratios of these tracers are set to zero on the 1st of January 1988, with the mixing ratio of AoA tracer defined at

every time step in its forcing volume (see Table 4.1) to the *G* value. The AoA of an air parcel, with mixing ratio *M* is calculated as $AoA = t - \frac{M}{f}$ in seconds. It can easily be verified that the mixing ratio *M* in close proximity with the boundary will be $M = ft$ and then $AoA = 0$. The longer since the atmospheric air was in the boundary forcing volume, the lower its mixing ratio will be and the older its age. A main aim is to classify models according to their transport characteristics. The boundary conditions used to calculate AoA in the troposphere and are indicated in **Table 4.1**.

AoA tracer	**Forcing volume**
Surface	Surface <100 m
NH surface	NH surface <100 m
SH surface	SH surface <100 m

Table 4.1. Simulated AoA tracers used in the TOMCAT simulations. Table adapted from the work of Krol *et al.*, 2018.

The five models used for comparison with TOMCAT (see **Chapter 3**) are two CTMs, namely NIES (Belikov *et al.*, 2013) and ACTM (Numaguti, Takahashi and Nakajima, 1997), and three GCMs namely LMDZ (Hourdin *et al.*, 2006, 2013), TM5 (Krol *et al.*, 2005) and EMAC (Jöckel, *et al.*, 2006). **Table 4.2** shows the main technical features of the models used.

Model simulations	**Base model**	**Resolution (lon × lat)**	**Vertical levels**	**Meteorological driver data**
LSCE_LMDZ5A	LMDZ	3.75°×1.875°	39 hybrid σ-pressure	Nudged to ERA-Interim
ACTM_T42L67	ACTM	≈2.81°×2.81°	67* σ up to 90km	Nudged to JRA-25
TM5_3X2	TM5	3°×2°	60 hybrid σ-pressure	ERA-Interim
NIES	NIES	2.5°×2.5°	32 hybrid σ-Θ up to 5 hPa	JRA-25
EMAC_T63	EMAC	≈1.875°×1.875°	90 hybrid σ-pressure	Nudged to ERA-Interim
TOMCAT	TOMCAT	≈2.81°×2.81°	60 hybrid σ-pressure	ERA-Interim

Table 4.2. Summary of models used for comparison AoA simulations, adapted from Krol *et al.*, 2018.

4.2.2 Intercomparison of AoA results

Results from Krol *et al.*, 2018 are presented in **Figures 4.2.** and **4.3.** A latitude-pressure cross section of AoA for the surface tracer, averaged over 2000-2011 is shown in **Figure 4.3.** The 6 models generally show the same latitude-vertical patterns, with younger air in the Tropics, where it is rapidly uplifted and older air at the mid-latitudes where stratospheric air is mixed into the troposphere (Holton *et al.*, 1995). However, it is clear that the NIES and TOMCAT show slower transport throughout the troposphere, especially in the tropical upper troposphere with ages around 40 days in TOMCAT compared to around 20 days in other models. TOMCAT and NIES share the same convection parametrization based on Tiedtke (1989) (see **Chapter 3**), which has been shown previously to exhibit weak transport to upper tropospheric levels (Feng *et al.*, 2011).

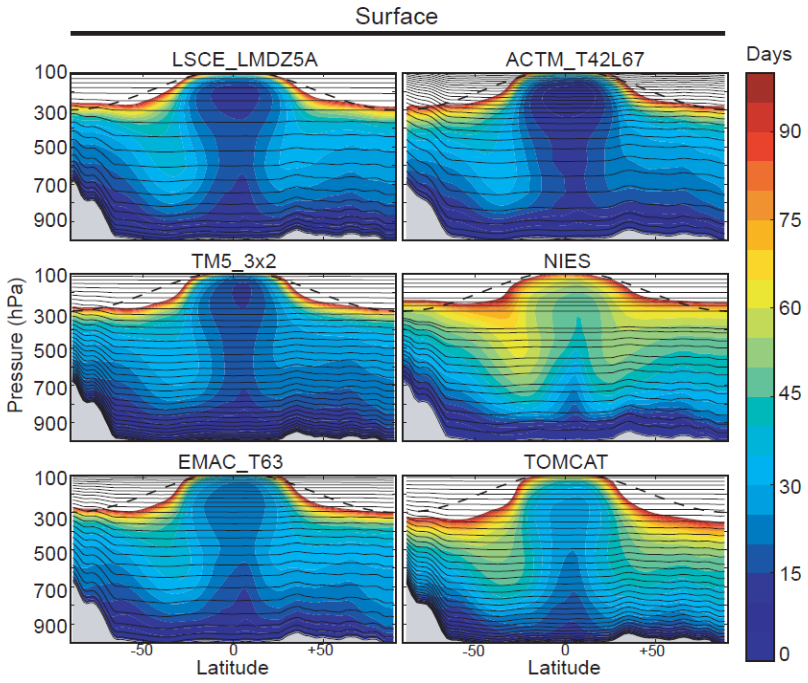

Figure 4.2. Summary of AoA tracer "Surface" zonal mean distributions (days), for 2000-2010 time period. The thin black lines denotes average vertical levels of the models. The dashed black lines show the climatological tropopause. White areas refer to air older than 100 days. From Krol *et al.*, (2018).

The interhemispheric transport plots shown in **Figure 4.3.** using the NH and SH tracers, also highlight some interesting features. In particular, it is clear all models agree that

transport is faster from the NH to the SH than vice-versa, probably due to the asymmetric distribution of land and ocean between in the NH and SH with consequently stronger convection occurring in the former. Moreover, a preferred pathway for the transport seems to be the level around 200 hPa at equatorial latitudes (Prather *et al.*, 1987). As for the surface tracer, TOMCAT and NIES are the models with oldest air in both hemispheres. It is interesting that although TOMCAT and TM5 (see **Table 4.2**) share the same ERA-Interim meteorological datasets, the corresponding AoA (**Figures 4.2** and **4.3**) are radically different, suggesting that the nature of the convection scheme implemented in the model plays a crucial role. Nevertheless, the modelling of the transport of any tracer in the atmosphere is the result of a complex interplay between advection, convection schemes, boundary layer mixing and meteorological dataset used.

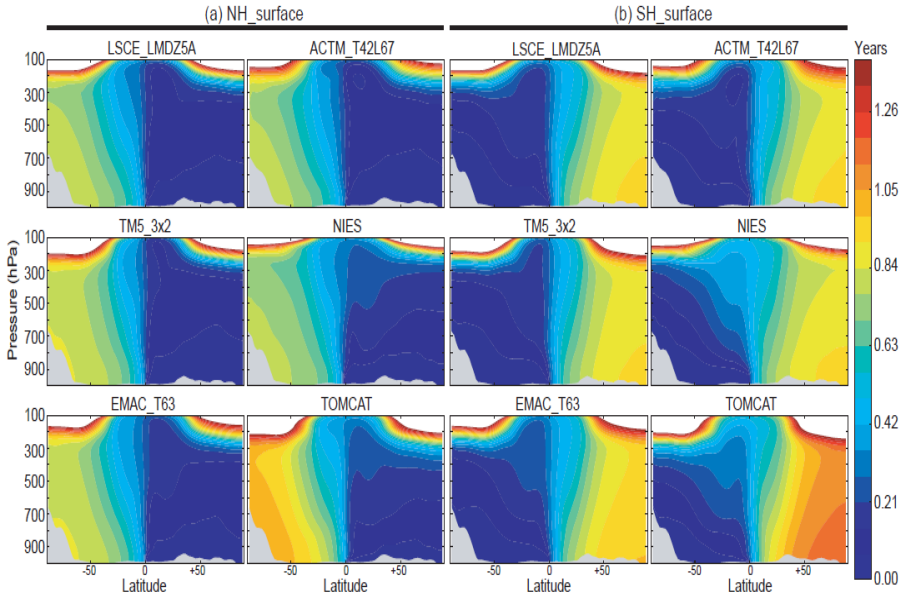

Figure 4.3. Zonal averages of **(a)** NH and **(b)** SH AoA tracers (years), averaged over 2000-2010 time period. White areas correspond to regions where air is older than 1.4 years. From Krol *et al.*, 2018 .

4.2.2 TOMCAT AoA results with ERA-Interim updrafts

The TOMCAT model results shown in Krol *et al.*, (2018) are based on the implementation of the Tiedtke default convection scheme (Tiedtke, 1989) which has been in the model since the work of Stockwell and Chipperfield, (1999). This configuration of the model shows persistent low and slow interhemispheric transport and slow transport to upper

troposphere levels compared to the majority of other models (**Section 4.2.1**). Thus, modelling the vertical transport of short-lived-substances from surface to these levels in this version of TOMCAT might underestimate their actual mixing ratio. In order to try to solve this issue, an updated version of the convection scheme has been developed and used in the simulations of this subsection: ERA-Interim convective mass fluxes. The use of this convection scheme in the TOMCAT model builds on previous work; an earlier version of this scheme has already been successfully used to determine the model performance in the context of cloud convection (Feng *et al.*, 2011). This updated convection scheme showed significant enhancement of vertical transport in the Tropics at about 100 hPa compared to the results obtained with the default Tiedtke scheme (Feng *et al.*, 2011). This is a significant level, where the ASM anticyclone is well developed and pollutants originated on the surface are therein confined (see **Section 2**, Brunamonti *et al.*, 2018). Nevertheless, the work presented in this chapter (with an improved version of the scheme) represents the first long-term (multiannual) simulations with the archived convection terms in TOMCAT and the first evaluation with similar global CTMs.

In order to show that the implementation of the ERA-Interim convective mass fluxes in TOMCAT improves transport to UTLS levels, plots of the AoA tracers based on the protocol in **Table 4.1** are shown.

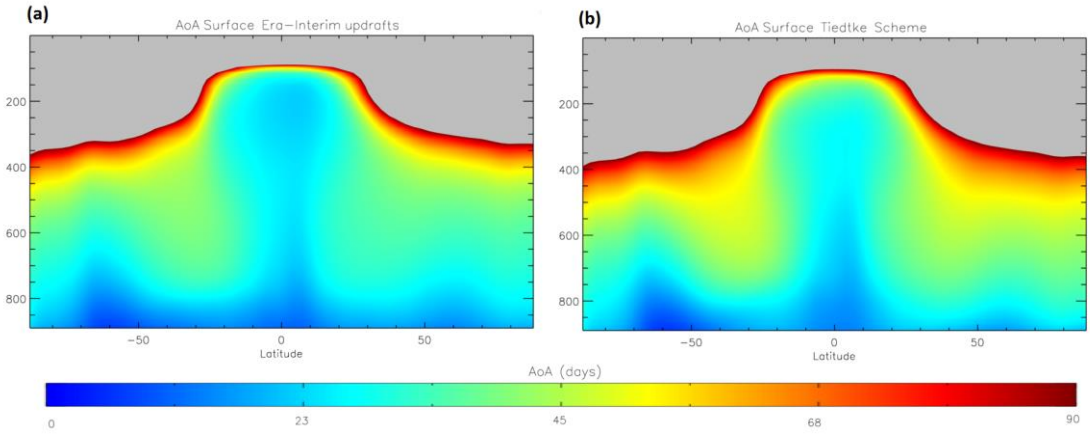

Figure 4.4. Latitude-vertical plots of TOMCAT zonal average AoA (days) from tracer emitted at surface, averaged over 2000-2010 time period. AoA is calculated from mixing ratio emitted according to the protocol specified in Table 4.1. Panel **(a)** shows results when ERA-Interim updrafts are used, while **(b)** refers to results with default Tiedtke scheme. Grey areas indicate AoA older than 100 days.

Figure 4.4. compares the results of the Surface tracer with the Tiedtke scheme (as in **Figure 4.2.**) and the ERA-Interim updraft scheme. The archived ERA-Interim fluxes cause a much stronger upward transport in the Tropics which produces much lower AoA values: for example 20 days at 200 hPa in the Tropics compared to around 40 with the default Tiedtke scheme. The pattern of the AoA tracer with the archived convection also gives a characteristic distribution of outflow in the UT, i.e. a larger region of young AoA than at mid-levels. With the new convection scheme there is also a general reduction in the AoA values in the mid-latitude mid troposphere.

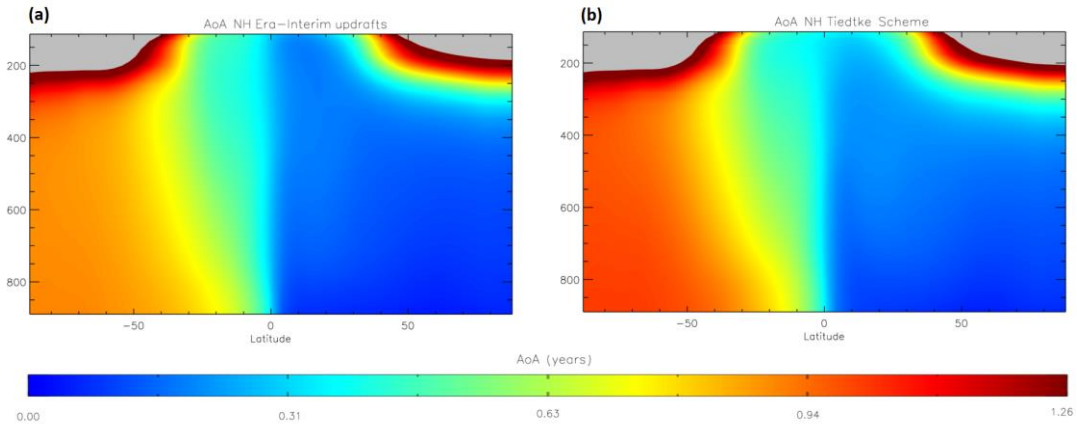

Figure 4.5. Latitude-vertical plots of zonal average AoA emitted at NH surface, averaged over 2000-2010 time period. AoA is calculated from mixing ratio emitted according to the protocol specified in Table 4.1. Panel **(a)** shows results when ERA-Interim updrafts are used, while **(b)** refers to results when defaults Tiedtke scheme is implemented. Grey areas indicate AoA older than 1.4 years.

Figures 4.5 and **4.6.** show the TOMCAT NH-emitted and SH-emitted tracers from the simulations with the two versions of the convection scheme. The results of the Tiedtke scheme are the same as those shown in **Figure 4.3.** For both tracers the new convection scheme decreases the AoA in the opposing hemisphere, though this is more noticeable at high latitudes for the NH tracer. The largest impact (decrease) on the AoA for the SH tracer is at northern mid-latitudes. The use of the new convection scheme reduces the difference between TOMCAT and the other models for these tracers (**Figure 4.3.**) but TOMCAT still shows some larger ages. For example, the AoA values for the SH tracer at northern high latitudes is still over a year with the archived scheme.

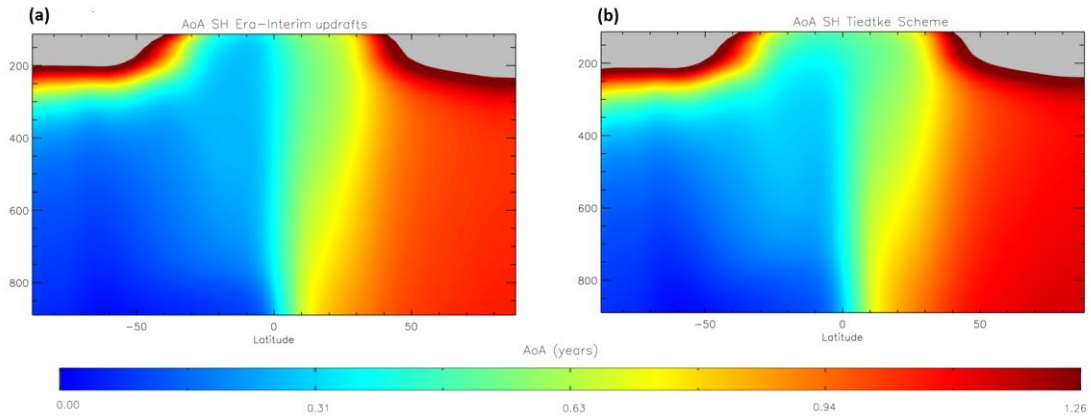

Figure 4.6. Latitude-vertical plots of zonal average AoA (years) diagnosed from tracer emitted at SH surface, averaged over 2000-2010 time period. AoA is calculated from specified mixing ratio according to the protocol specified in Table 4.1. Panel **(a)** shows results when ERA-Interim updrafts are used, while panel **(b)** shows results when default Tiedtke scheme is implemented. Grey areas indicate AoA older than 1.4 years.

Overall, the inclusion of the archived ERA-Interim convective fluxes has increased the rapid vertical motion in the TOMCAT model. This is to be expected as the Tiedtke scheme in the CTM aims to diagnose convection from large-scale analyses (temperature, moisture, horizontal winds) which have already been subject to convection (i.e. stabilized). It would be expected that these large-scale fields will not generate sufficient regions of small scale convective instability, though parameters in the Tiedtke scheme can be adjusted to negate this effect. The ERA-Interim archived convective mass fluxes are calculated at the full resolution of the reanalysis model (≈100 km) with meteorological fields at their full time resolution. Using the archived convection mass fluxes from the same assimilation system which produces the other model meteorology will also be more consistent. It should be noted that it is only the reanalyses products like ERA-Interim for which ECMWF provide accumulated convective mass fluxes as a diagnostic. Many past TOMCAT studies have used operational analyses for which the only option was to recalculate convection online (e.g. using the Tiedtke scheme).

4.2.3 Artificial tracer simulations in the ASM region

The Asian Summer Monsoon extends over an important region well known for the transport of climate-relevant gases from the troposphere to the stratosphere, as discussed

in **Chapter 2**. Recent work by several groups (Park *et al.*, 2007; Pan *et al.*, 2016; Ploeger *et al.*, 2017) have focused on quantifying processes which contribute to coupling in the upper troposphere-lower stratosphere (UTLS), including transport during the ASM period. Troposphere-to-stratosphere transport in this region has been the focus of a number of recent campaigns, including the EU "StratoClim campaign" in Greece 2016 and Nepal 2017 (see **Chapter 5**).

Anthropogenic compounds such as CO, Very Short-Lived Substances (VSLS), which destroy stratospheric ozone, and sulfur compounds, which maintain the stratospheric aerosol layer, are among the important species involved in large convective systems transport such as the ASM. An important question for halogenated VSLS is whether ASM-associated transport can take place on timescales which are short relative to their chemical lifetimes of days to months.

This subsection presents results from TOMCAT CTM simulations from 1989 through 2017 to investigate these issues using moderate-resolution simulations (2.8° × 2.8°, 60 levels from surface to 60 km). I created *ad hoc* artificial and idealized tracers to shed new light on the interannual variability of the transport via the ASM, considering three convective scenarios (Tiedtke default scheme, ERA-Interim archived mass fluxes and no convection, see **Chapter 3**). These simulations are based on the "simplified approach" described in **Section 3.4.1.** Computationally cheap simulations allow the model to run over multi-decadal time periods and therefore have been exploited here. This allows the global model to be used for a study on interannual variability which involves the transport via the ASM circulation. The tracers used in these simulations were chosen to span a range of relevant lifetimes and to have surface distributions which are uniform (easier to interpret) or representative of a pollution tracer. They are:

- **CO25**, **Carbon monoxide-like** tracer 25-day lifetime (e-folding time, see **Chapter 3**) realistic geographical emission distribution.
- **CO50**, **Carbon monoxide-like** tracer 50-day lifetime (e-folding time, see **Chapter 3**) realistic geographical emission distribution.
- **TR5**, 5-day lifetime (e-folding time, see **Chapter 3**), fixed 100 ppbv surface value within 32^{o}N-49^{o}N latitudinal band.
- **TR50,** 50-day lifetime (e-folding time, see **Chapter 3**), fixed 100 ppbv surface value within 32^{o}N-49^{o}N latitudinal band.

Maps of the surface mixing ratio tracers are summarized in **Figure 4.7.** The lifetimes of CO25 and CO50 were chosen according to the real CO lifetime which is between 1-2 months (Novelli *et al*., 1998; Petrenko *et al.*, 2013). TR5 and TR50 are initialized in the 32^{o}N-49^{o}N latitudinal band to represent highly polluted Chinese industrialized area and the chosen lifetime of the former reflects fast deep convective transport while the latter is related to slow ascent large scale structure (Chen *et al.*, 2012)

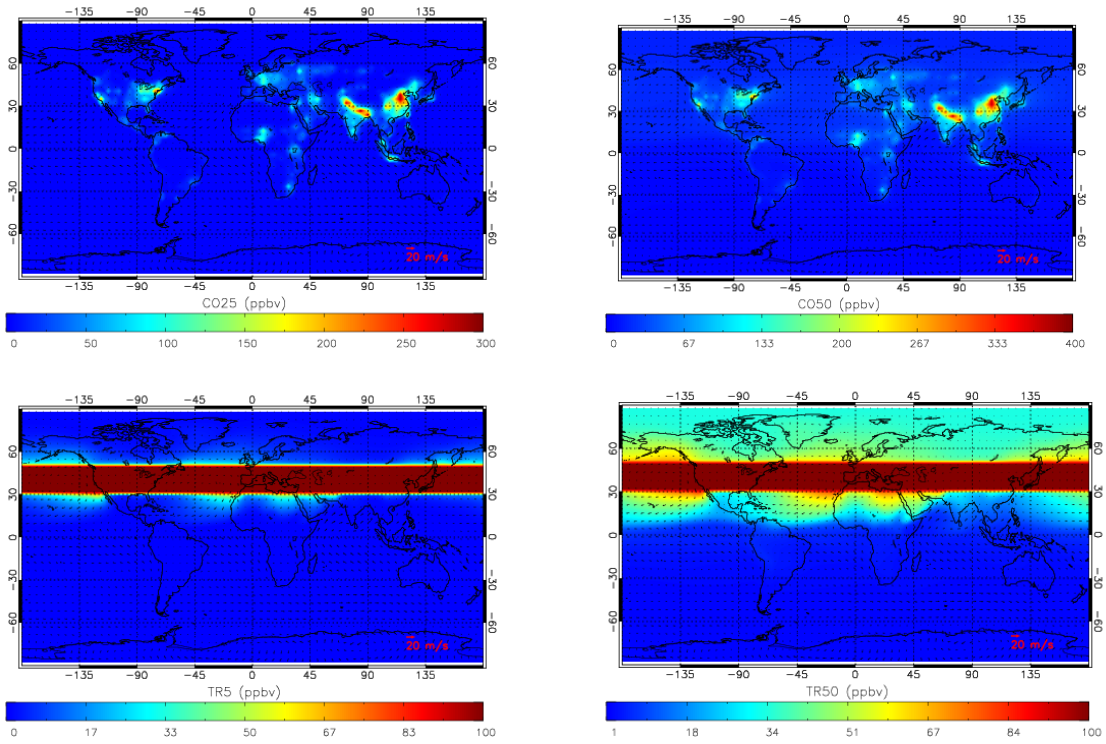

Figure 4.7. Surface 1989-2017 JJA average of tracers CO25 (top left) , CO50 (top right), TR5 (bottom left) and TR50 (bottom right).

Figures 4.8. shows the vertical profiles of model results of CO25 and CO50 from when the ERA-Interim archived mass fluxes (**a** and **c**), the Tiedtke scheme (**b** and **d**) and difference between the two schemes (**e** and **f**). The results are longitudinally averaged over the ASM area (0-140^{o}E). The plots show clear transport of both CO25 and CO50 in the vertical column which correspond to large emissions over India, around 25^{o}N (see **Figures 4.8. a**, **b**). As expected, CO50 is, in absolute terms, more abundant than CO25, due to its longer lifetime. However, both convection schemes agree on the shape and extent of the transport which fits with the location and height of the ASM anticyclone (Brunamonti *et al.*, 2018, Figure 6). The difference plots (**Figures 4.8.e** and **f**) show some

interesting features. **Figure 4.8.e** highlights that ERA-Interim archived convective updrafts provide stronger transport, than the Tiedtke scheme between 100-150 hPa at 25^{o}N, although some noisy patterns at lower altitudes are present. In contrast, CO50 (**Figure 4.8.f**) shows a clear net improvement when the default scheme is switched to the archived one, at the same height and latitude of CO25. However, a closer look shows that in relative terms the consequences on CO25 are greater than on CO50, especially at the upper limit of transport at around 100 hPa. The ameliorated performance of the ERA-Interim archived updrafts seem to have a greater effect on shorter lived substances than longer ones and that becomes more clear with interannual variability plots (**Figure 4.10.**, below). The vertical plots of TR5 and TR50 (**Figure 4.9.**) reflect the surface distribution. Due to its short lifetime, TR5 does not ascend to the same levels as CO25 and CO50. Only a small fraction (a few ppbv) of TR5 can reach pressure levels between 100-200 hPa. As its lifetime is comparable to the deep convective timescale (≈2 days, Chen *et al.*, 2012) the difference between the two convective schemes shows a noisy behaviour for TR5 with the Tiedtke scheme showing stronger transport to 200 hPa and above. TR50 (**Figure 4.9. c**, **d**, **f**) shows similar structure to TR5, although its greater lifetime makes this tracer able to reach UTLS levels around 25^{o}N, where tracers are confined within the ASM anticyclone (Brunamonti *et al.*, 2018). However, a positive net contribution from ERA-Interim archived mass fluxes is present at around 100 hPa, between 0-30^{o}N.

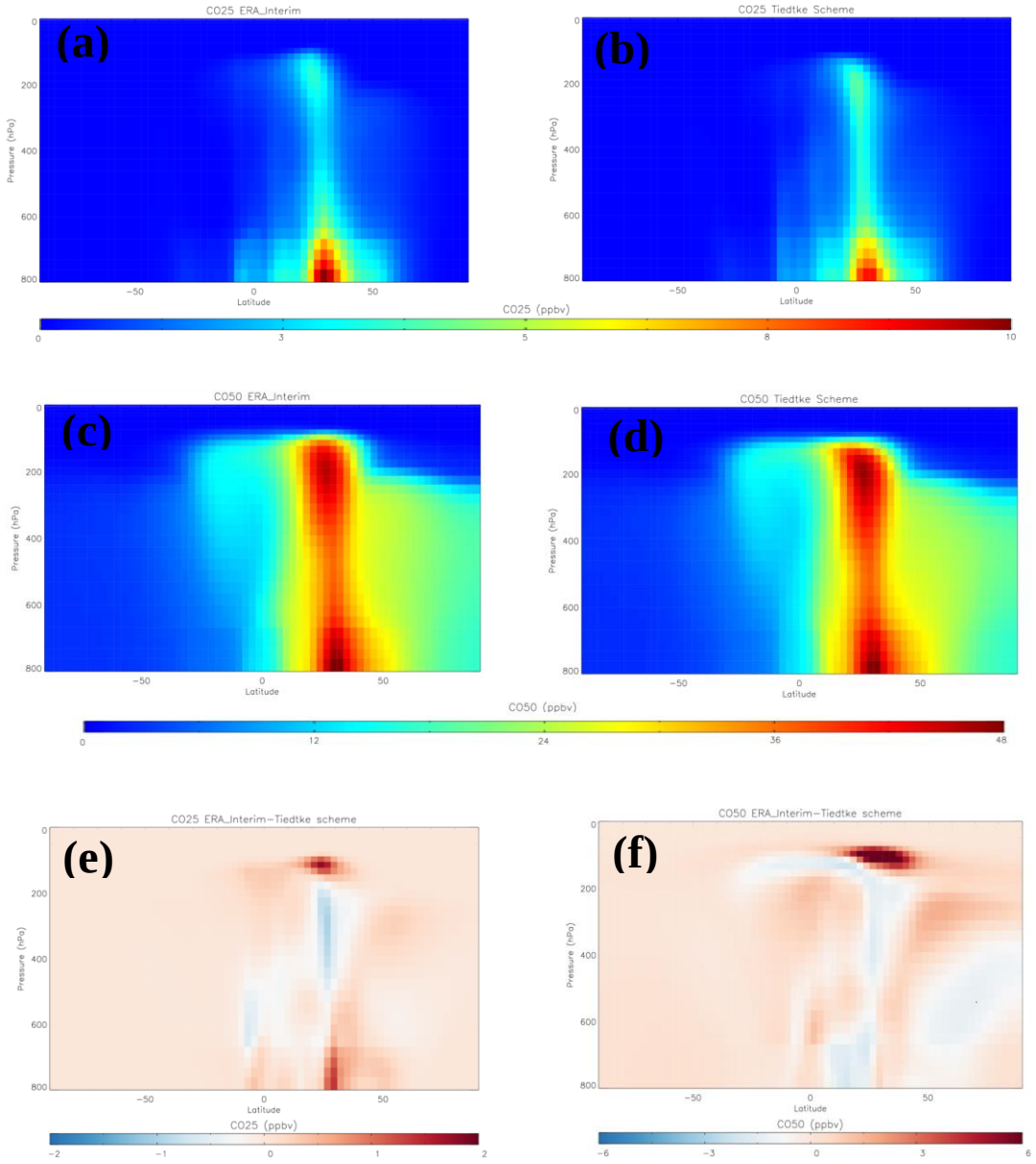

Figure 4.8. 1989-2017 JJA average over the ASM region (0-140ºE) of artificial and idealized tracers CO25 and CO50 with Tiedtke convection scheme (**a** and **c**) and ERA-Interim archived mass fluxes (**b** and **d**). Panels **(e)** and **(f)** show differences between the two convection schemes for CO25 and CO50, respectively.

The interannual variability of CO25, CO50, TR5 and TR50 from 1989-2017 (**Figure 4.10.a-d**) averaged in the ASM region (0-50ºN, 0-140ºE) at 100 hPa, when ERA-Interim archived mass fluxes, Tiedtke and no convection scheme are implemented is shown in **Figures 4.10.** The apparent discrepancy between the vertical plots of CO25 at 100 hPa (**Figures 4.9.c** and **d**) and the corresponding interannual variability plot (**Figure 4.10.c**),

which shows mixing ratio of just fractions of ppbvs, is explained by the fact that the latter is averaged over an area which comprises the horizontal extension of the ASM anticyclone (Popovic and Plumb, 2001; Vogel *et al.*, 2014) and the deep convective area in south east Asia which has been identified as a source region of species subsequently confined in the ASM anticyclone (Chen *et al.*, 2012) and therefore does not correspond with the area of high ASM anticyclone core occurrence (Ploeger *et al.*, 2015). Therefore, the averaging process over such an area produces lower mixing ratios than if included only the core of the ASM. The interannual variability of these tracers is essentially driven by the internal variability of the circulation in the ASM region. Although some connections between some large-scale phenomena like ENSO and structure, stability and evolution of the ASM anticyclone have been found (Yan *et al.*, 2018), complex interdependency between other factors such as volcanic eruptions, monsoon strength (Webster and Fasullo, 2003) and rainfall (Liu *et al.*, 2016) probably play a role. **Figure 4.10.** shows a rapid decline in JJA 1992, a year after the Pinatubo eruption (June1991) and interestingly is observed in all the convective scenarios (ERA-Interim archived updrafts, Tiedtke scheme and no convection). Its magnitude depends on the tracer, with longer-lived tracers showing nearly the same decay in all three scenarios (in absolute terms). The presence of an abrupt decrease even in idealized TR5 and TR50 tracers, suggest a dynamically-induced change by the eruption, rather than a purely chemically-induced one. The impact of such a large volcanic eruption on TR50 in case of "no_conv" might be due to the reduced lapse rate provoked by the aerosol loading generated by the eruption (Canty *et al.*, 2013), which in turn depressed the vertical lapse rate and then convection and vertical advection. It worth noting that a scenario with increased stratospheric aerosol loading is not only relevant to large volcanic eruptions, but also to Solar Radiation Management (SRM) techniques, in the context of geo-engineering strategies implementation as explained in **Chapter 6**. Furthermore, the effect of increased aerosol loading caused by the possible application of these strategies on the Asian Tropopause Aerosol Layer (ATAL, Vernier *et al.*, 2015) is as yet totally unexplored. The effect of large volcanic eruptions on the tracers we used in this study would likely be similar in case of injection of particles in the stratosphere (**Chapter 6**).

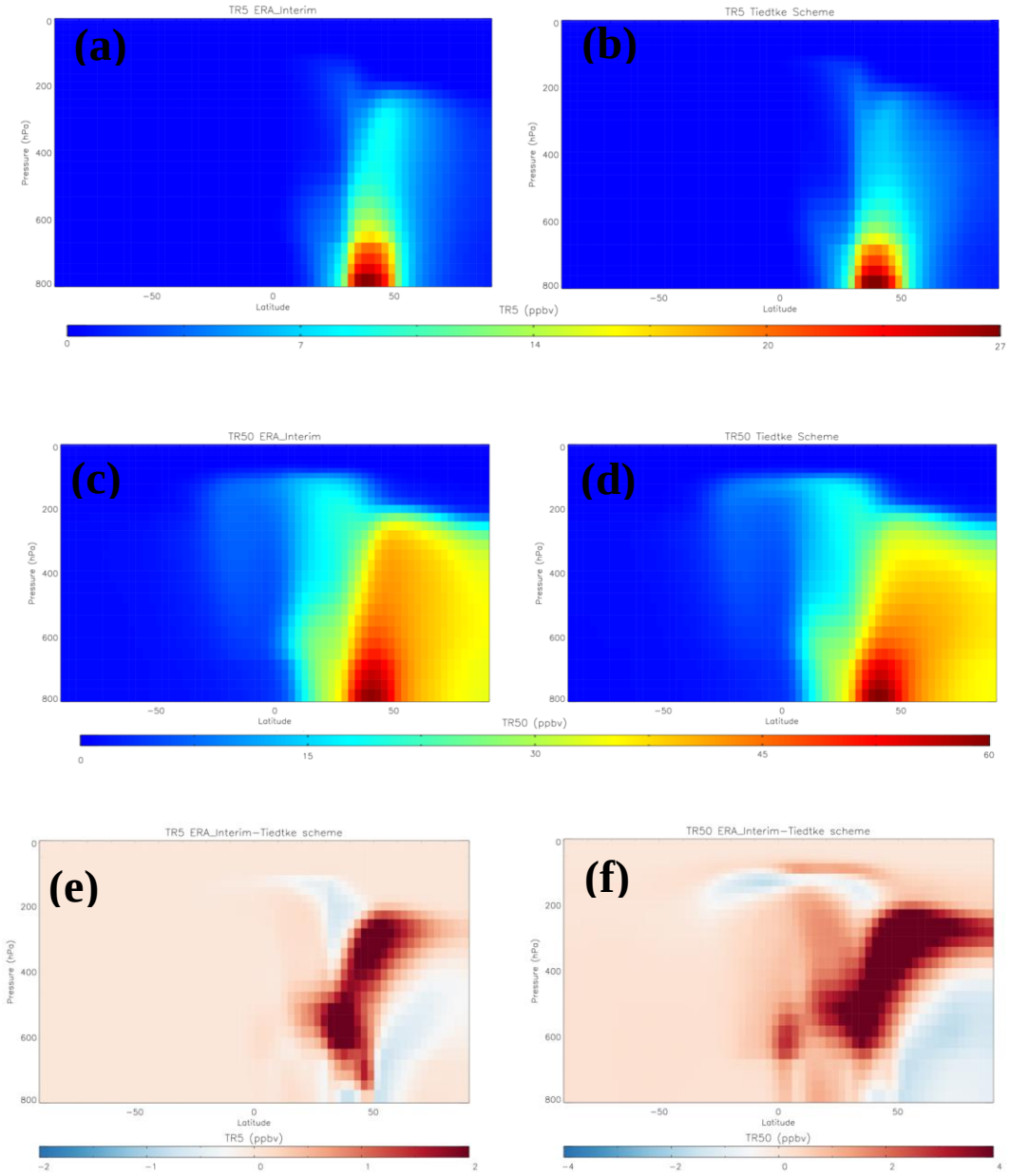

Figure 4.9. 1989-2017 JJA average over the ASM region (0-140^{o}E) of artificial tracers TR5 and TR50 with ERA-Interim archived mass fluxes (**a** and **c**) and Tiedtke convection scheme (**b** and **d**). Panels **(e)** and (f) show differences between the two convection schemes for tracers TR5 and TR50, respectively.

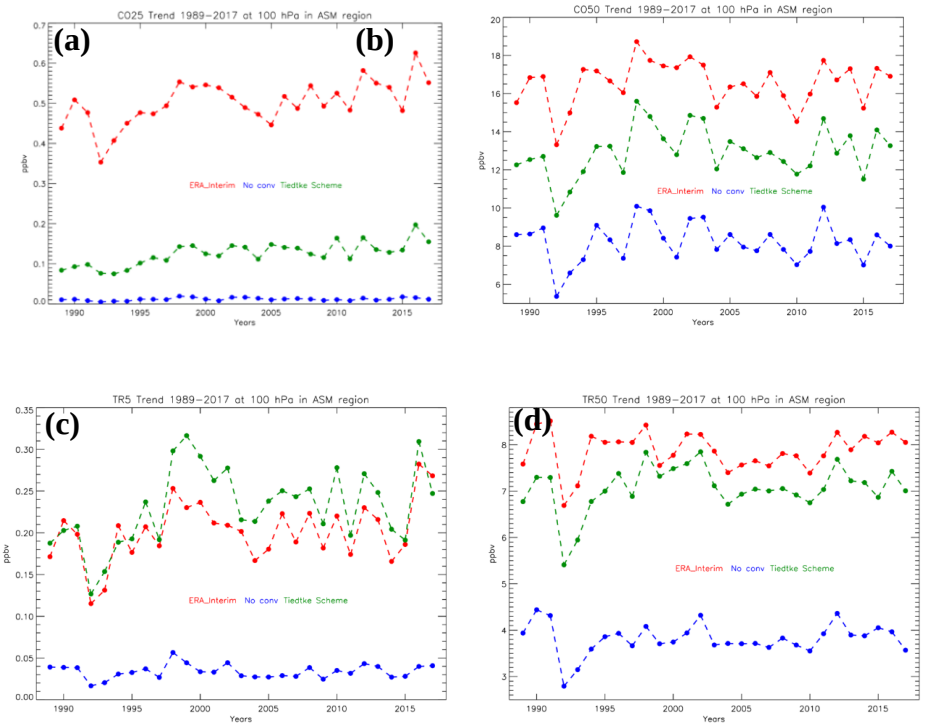

Figure 4.10. 1989-2017 JJA average over the ASM region (0-50^{o}N, 0-140^{o}E) of idealized tracers **(a)** CO25 and **(b)** CO50, and artificial tracers and **(c)** TR5 and **(d)** TR50 with Tiedtke convection scheme.

The tracers shown in this section are naturally subjected to variations in both local and global dynamical structures. The ASM itself is inextricably linked to ENSO, large volcanic eruptions, teleconnections and other aspects of the global climate (**Chapter 2**). One of the consequences of this interaction is obviously reflected in the ability of the ASM to vertically transport species from surface to upper atmospheric levels. To quantify the "strength" of the ASM, many indices have been created which describe different aspects of the ASM (e.g., circulation, convection, rainfall intensity) (Wang and Fan, 1999). The most commonly used indices are the Webster and Yang index (WYI) (Webster and Yang, 1992) and All Indian Summer Rainfall Index (AIRI) anomalies (Parthasarathy *et al.*, 1994) (**Figure 4.11**). The former is defined by the vertical shear of the zonal wind *U* between 850 hPa and 200 hPa to reflect the variability of the broad scale of the South East Asian Summer Monsoon averaged over 0°-20°N and from 40°E-110°E, during JJAS. The latter is a long rainfall dataset which cover the entire Indian nation and is available from 1871 till 2014, (available at https://www.tropmet.res.in/ visited on 20th of May 2020). To link the vertical transport and related confinement of the idealized tracers

used in this chapter to ASM anticyclonic levels (100 hPa at 0-50°N, 0-140°E) a slightly different version of the WYI has been used, according to the work of Wang and Fan, 1999 hereafter called WSI1. This adapted version differs from WYI in the averaging area (5°N-20°N, 40°E-80°E) (region **a** in **Figure 4.12**). This is motivated by the fact that such an index is well correlated with convective activity over India and the Bay of Bengal (region **b** in **Figure 4.12**) assessed using negative Outgoing Longwave Radiation (OLR) anomaly a typical proxy for convection as explained by Wang and Fan (1999).

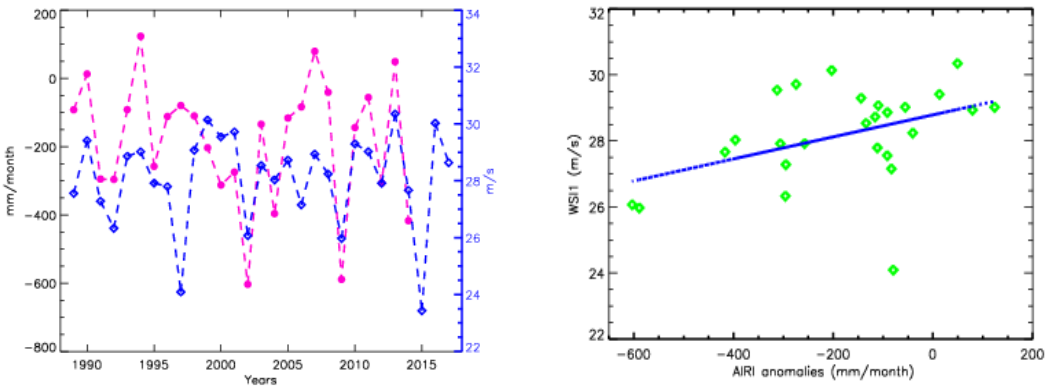

Figure 4.11. Interannual variability of WSI1 index (blue) and AIRI anomalies (pink), (left). The former is calculated for the 1989-2017 period while the latter refers to 1989-2014 (calculated wrt to the 1871-2014 average). Scatter plot (right) of WSI1 and AIRI anomalies for the 1989-2014 period with correlation coefficient equals to 0.43 and best fit line shown in blue.

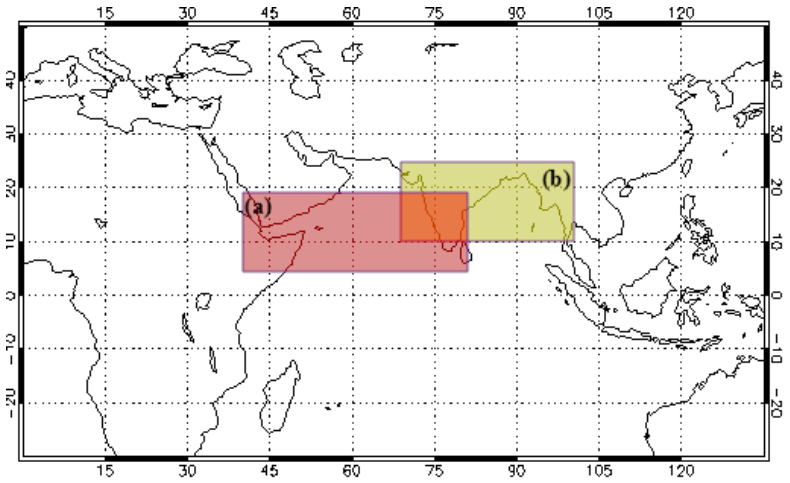

Figure 4.12. Averaging area of ASM index WSI1 (region a) and convective area over the Bay of Bengal (region b).

Correlation plots between the idealized/artificial tracers (CO25, CO50, TR5 and TR50) in the ASM anticyclone and indices WSI1 and AIRI are shown in **Figure 4.13** and summarized in **Table 4.3.**

	WSI1	**AIRI**
CO25 ERA-Interim	0.348	-0.098
Tiedtke scheme	0.219	-0.258
No convection	-0.044	-0.276
CO50 ERA-Interim	0.335	-0.043
Tiedtke scheme	0.311	-0.276
No convection	0.262	-0.223
TR5 ERA-Interim	0.401	0.177
Tiedtke scheme	0.460	-0.125
No convection	0.351	0.026
TR50 ERA-Interim	0.112	0.051
Tiedtke scheme	0.235	-0.110
No convection	0.008	-0.078

Table 4.3. Summary of correlation coefficients between idealized tracers at 100 hPa averaged in the ASM area and the indicesWSI1 and AIRI. For the latter, simulations have been limited to 2014, due to availability of the AIRI dataset.

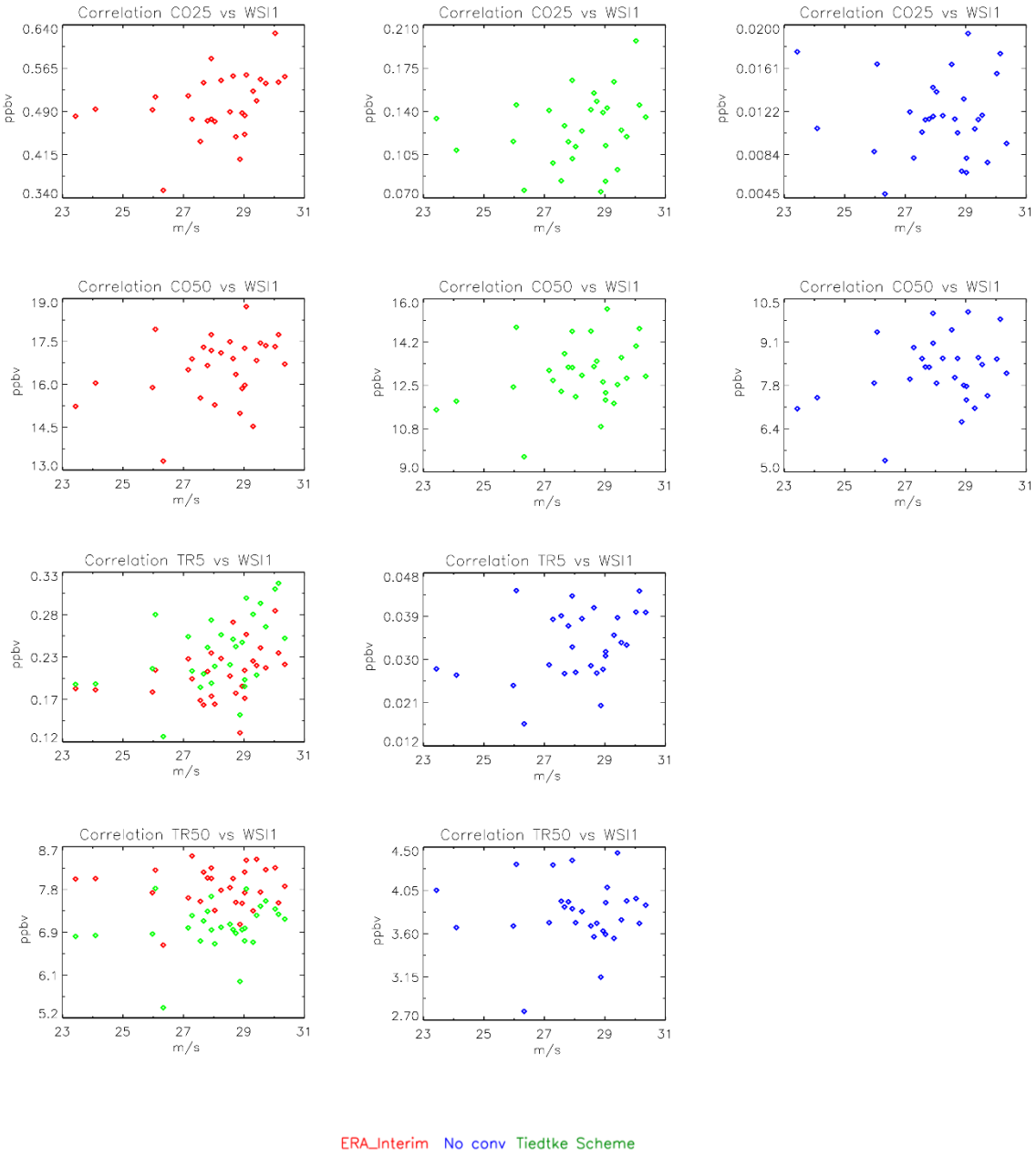

Figure 4.13. Correlation plots of tracers CO25, CO50, TR5 and TR50 (ppbv) versus ASM index WSI1 (m/s).

Table 4.3. shows that the correlation between the tracers and WSI1 is not more than 0.460. Moreover, it does not seem that the implementation of the ERA-Interim archived scheme is strongly linked with WSI1 and consequently with convective-induced vertical transport originating in India and BoB. Objections to this analysis could lie in the fact that the tracers have been averaged over JJA while the WSI1 and AIRI are averaged over JJAS. However, averaging over JJA is a common procedure in the relevant literature of the study of transport at anticyclonic level (Park *et al.*, 2008, 2013; Randel *et al.*, 2010).

In any case, calculation shows that averaging WSI1 and AIRI over JJA does not change the correlation coefficients significantly (not shown). Understandably, the "No convection" scenario shows chaotic or very small correlation with convection over India and BoB. We would expect better correlation between shorter lived tracers and WSI1 than longer lived ones, due to the convection time-scale (2-3 days, Chen *et al*., 2012) and it is actually the case for CO25 and TR5. The expected superiority of the ERA-Interim archived mass fluxes is not clear and the Tiedtke scheme produces high correlations for TR5 and TR50. These results suggest that the modelling of interannual variability of the confinement of tracers at ASM anticyclone levels (**Chapter 2**) is a combination of dynamical regimes which act on several time scales, including the internal variability of the ASM itself, convective source locations and convective parametrization included in the model. Also, the idealized and artificial tracers considered in these simulations are averaged on a fixed longitude-latitude regions, while the anticyclone and related confinement shows eddy shedding and bimodality, with a strong intraseasonal variability (Nützel *et al.*, 2016).

The AIRI 1989-2014 versus tracers (limited to 2014) connection is chaotic. Together with the limitations described above a further explanation could be that rainfalls are the result of a complex interaction between several aspects of the climate (e.g., land sea interaction, nucleation) and not simply on convection.

4.3 Summary

This chapter has described tracer experiments with the TOMCAT model aimed at testing a new version with improved treatment of convection and diagnosis of tracer transport in the ASM. The improved convection scheme applied archived ERA-Interim mass fluxes with careful averaging onto the lower resolution CTM grid in a mass-conserving approach. The new model was first tested against published results (Krol *et al.*, 2018) where the older version of TOMCAT had performed relatively poorly for convective transport. The updated model produced tracer results similar to other global CTMs that used archived convective mass fluxes.

The model was then applied to study multiannual variation of tracer transport related to the ASM over the period 1989-2017 using simplified, parameterised tracers with lifetimes ranging from 5 to 50 days. Using the archived ERA-Interim convective mass fluxes in

the model produced significantly faster vertical tracer transport in the tropical troposphere compared to the previous default Tiedtke scheme. The Tiedtke scheme is based on the CTM recalculating convection from the large-scale analyses while use of the archived convective fluxes (averaged onto the model grid from the higher resolution analyses) ensures that TOMCAT is including the full convection produced in the ECMWF assimilation model. This is therefore an important model improvement.

As expected, convection is an important component of the vertical transport in the analyzed 1989-2017 simulation although its impact is reduced the longer lived the tracer (i.e. smaller effect for 50-day lifetime tracer compared to 5-day lifetime) and in this case the large-scale slower ascent appears to dominate over convection. The impact of large volcanic eruptions (Pinatubo-like) greatly influences the extent of the vertical transport over the ASM region and analogies with the injection of stratospheric particle for SRM techniques have been suggested.

While the ERA-Interim archived mass fluxes show a better vertical transport ability when compared with an older version of the convection subroutine within the model (**Section 4.2.2**) and in a 1989-2017 simulation (**Section 4.2.3**), correlating this improved characteristics of the model with the strength of the ASM is not straightforward. A very commonly used index, namely WSI1, which is related to strong convective activity over the Bay of Bengal does not show a clear robust correlation with the ASM anticyclonic average of any tracer considered (CO25, CO50, TR5 and TR50) at 100 hPa. A possible explanation for this result might lie in the fact that a single index might not be accurate enough to describe a complex feature like the ASM (Wang and Fan, 1999) which suggests that comparison with a series of indices might be more appropriate. This kind of analysis would be a topic for future work.

5 Interpretation of UTLS Campaign Observations

5.1 Introduction

One of the foci of this thesis, as outlined in **Chapter 1**, is the evaluation of climate- and ozone-related species entering the stratosphere via the ASM. Although much progress has been made since the pivotal work of Dethof *et al.* in (1999), which firstly determined the role of the ASM in transporting water vapour in the stratosphere (Dethof *et al.*, 1999), a clear portrait of its mechanisms and impact is still missing. Thanks to the staging of the EU StratoClim campaign (**Chapter 2**), in-situ data of climate-relevant species within the ASM are starting to be analyzed (Brunamonti *et al.*, 2018, 2019). In this chapter the 'full chemistry' TOMCAT model is tested against temperature, water vapour and CO values from the StratoClim fight campaign (**Chapter 2**). While the StratoClim campaign was clearly focussed on understanding and quantifying the transport over the Indian Subcontinent (**Chapter 2**) many other well instrumented campaigns have probed the UTLS in recent years, providing a lot of complementary data. A notable example is NASA Airborne Tropical Tropopause Experiment (ATTREX) campaign (Werner *et al.*, 2017) which took place in Guam in 2013/2014. The ATTREX observational payload allowed a focus on the transport of bromine VSLSs, which typically a high ozone-depleting effect when they reach the stratosphere. Using the full chemistry troposphere-stratosphere version of TOMCAT, simulations were performed to quantify the concentration of these species in the UTLS above the East Pacific Ocean. The model results related to ATTREX have been included in a published peer-reviewed paper by Werner *et al.*, (2017).

Section 5.2 presents the performance of the TOMCAT/SLIMCAT model (**Chapter 3**), configured with the new archived convective mass fluxes (**Chapter 3**), when compared with the measurements of this campaign. Due to the ongoing debate on the source of the observed CO at UTLS levels in the ASMA (Pan *et al.*, 2016), in **Section 5.4** I assess whether targeted TOMCAT simulations are able to give a definitive answer on this issue,

highlighting the complexity of this topic and estimating the importance of the two main presumed contributors (Bay of Bengal, BOB and Tibetan Plateau, TP) to the observed UTLS CO values.

5.2 Temperature, water vapour and CO comparison

In order to compare the TOMCAT simulation results with corresponding observations of any chemical species, it is necessary that the model realistically represents water vapour mixing ratios and temperature fields. The water vapour values used for the comparison comes from the FLASH instrument on board the M55 Geophysica aircraft (**Chapter 2**, Sitnikov *et al.*, 2007) while the temperature values are taken directly from the aircraft flight data. CO measurements are taken using COLD (**Chapter 2**, Viciani *et al.*, 2018). **Table 5.1.** shows the flight dates, related availability and instruments used for water vapour, temperature and CO measurements (used in **Section 5.3**).

It is important to note that water vapour and temperature values in TOMCAT are not generated by the model itself but are instead specified from the forcing ECMWF ERA-Interim reanalyses, consistent with the convection scheme used in the simulations (**Chapter 3**). **Figures 5.1.** and **5.2.** show that the model water vapour and temperature values (sampled at aircraft location and time) are consistent with corresponding FLASH and aircraft measurements. However, a recent study (Brunamonti *et al.*, 2019) based on the analysis of balloon-borne measurements of UTLS water vapour over Nainital in 2016 and Dhulikel in 2017 (NT16 and DK17, **Chapter 2**) concluded that the ERA-Interim UTLS representation is very much too dry, with an average mixing ratio difference ranging from -38% (100-120 hPa) to 10% (40-60 hPa) when compared with balloon water vapour measurements. This difference is well above the systematic error which affects FLuorescent Airborne Stratospheric Hygrometer (FLASH) measurements (Sitnikov *et al.*, 2007).

	Water Vapour	CO	Temperature
1st Flight KAL 30.8.2016	×	✓	✓
2nd Flight KAL 01.09.2016	✓	×	✓
3rd Flight KAL 06.09.2016	×	×	✓
1st Flight KTM 27.7.2017	✓	✓	✓
2nd Flight KTM 29.7.2017	✓	✓	✓
3rd Flight KTM 31.7.2017	✓	✓	✓
4th Flight KTM 02.08.2017	✓	✓	✓
5th Flight KTM 04.08.2017	✓	✓	✓
6th Flight KTM 06.08.2017	✓	✓	✓
7th Flight KTM 08.08.2017	✓	✓	✓
8th Flight KTM 10.08.2017	✓	✓	✓

Table 5.1. Summary of the availability of water vapour, temperature and CO observations from the StratoClim flight campaign. Water vapour and CO values have been measured using FLASH and COLD, respectively (**Chapter 2**). Locations of the flights are represented in **Figure 2.13.** and **2.14.**

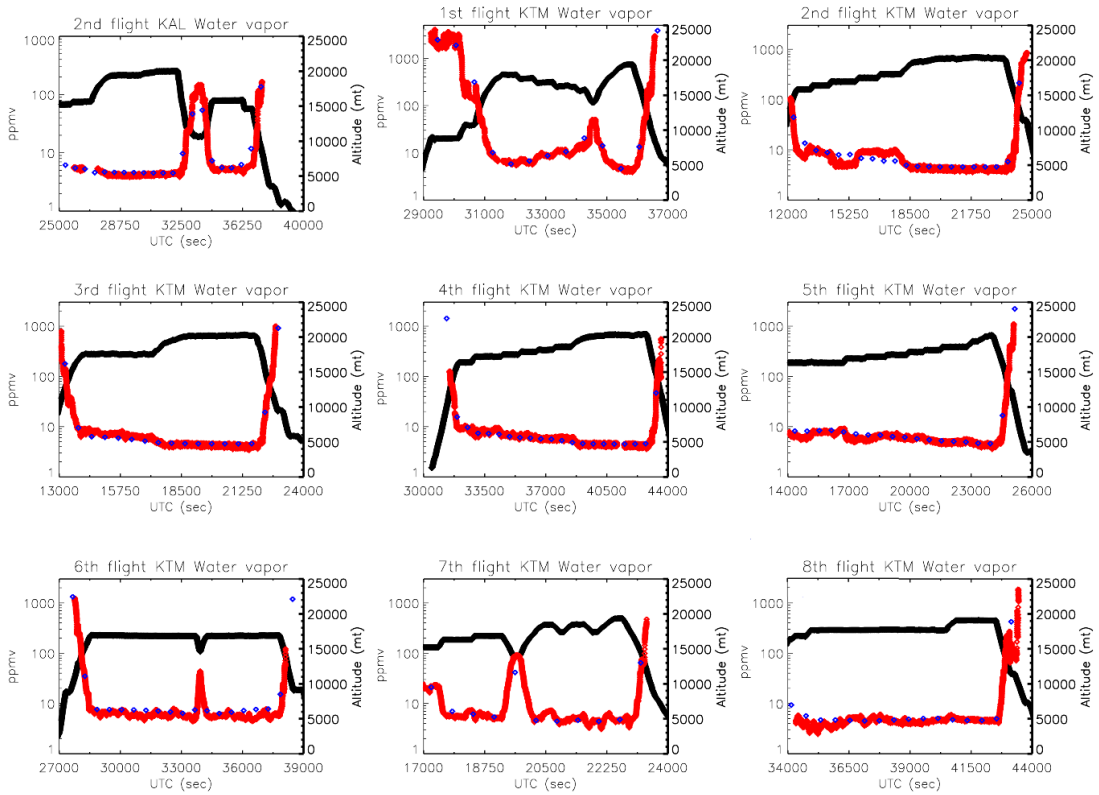

Figure 5.1. Plots of FLASH water vapour measurements (red dots) during the StratoClim campaigns. Results from TOMCAT model water vapour results (blue dots) and the aircraft altitude (black) are also shown. KAL refers to the flight during the campaign over Kalamata, Greece in 2016, while KTM refers to the campaign over Nepal in 2017.

In order to investigate further this problem, I quantified the discrepancy between the TOMCAT (ERA-Interim) water vapour and temperatures with corresponding data taken with FLASH and onboard instrumentation. This comparison aims to confirm or disprove the findings of Brunamonti *et al.*, (2019) which have important repercussions on the availability of the water vapour in the UTLS. To date this is the only published study on comparison of water vapour values from the StratoClim campaign with reanalysis data.

First, it is worth noting that this analysis has been limited to the Nepal (Katmandu) 2017 data, i.e. excluding similar data for the Kalamata (Greece) 2016 (although shown in **Figures 5.1** and **5.2**, flights tracks are in **Figures 2.13** and **2.14**). This is due to the fact that balloon data used in the study of Brunamonti *et al.*, (2019) were launched from Nainital (India) and Dhlikhel (Nepal).

The temperature model data, sampled every 600 seconds along the flight path, fit extremely well with the corresponding temperature data measured from M55 Geophysica. Calculations show that the average difference is about 1 K, with temperature range between 194-204 K in the UTLS. More interesting is the water vapour difference shown in **Table 5.2.** together with values from the balloon campaigns in NT and DK in 2016 and 2017, respectively, (Brunamonti *et al.,* 2017).

Pressure (hPa)	**ERA_Interim – Aircraft FLASH H_2O**	**ERA_Interim – Balloon H_2O (Brunamonti *et al.*, 2019)**
40-60	-1.31 ppmv (-31%) (18)	+0.46 ppmv (+10%)
60-80	-0.95 ppmv (-37%) (36)	-0.64 ppmv(-14%)
80-100	-2.48 ppmv(-40%) (18)	-1.68 ppmv (-30%)
100-120	-1.17 ppmv (-25%) (38)	-3.23 ppmv (-38%)

Table 5.2. Summary of water vapour comparison between averaged ERA-Interim database and FLASH measurements from all aircraft flights of the Nepal (KTM) campaign and the balloon campaigns binned into 4 altitude range. The latter data are taken from Brunamonti *et al.,* (2019). The values in brackets refer to the number of FLASH values over which the average has been carried out.

Likewise the temperature data, model water vapour has been sampled every 600 seconds. The results show a severe underestimation of the ERA-Interim water vapour in UTLS above the India and Nepal, probed by the aircraft, compared to FLASH values. Results show that the FLASH instrument identifies a pronounced drier the UTLS, although the percentage difference and the absolute value are different. For instance, a moister 40-60 hPa layer is not seen in the results shown here, while the LS (60-100 hPa) values are more in agreement. A temperature bias cannot be the explanation. However, the general

agreement between two independent instruments from the StratoClim campaign is a positive sign, although a further investigation is desirable. One of the aims of the StratoClim project is to have a clearer picture of the distribution of water vapour in the UTLS and consequently more realistic parametrizations of such species in CTM and CCMs (**Chapter 2**). Switching to different reanalyses, such as ERA5 (ECMWF, 2018) as suggested by Brunamonti *et al.*, (2019) might to help to pursue this aim, although positive bias (moister UTLS) is present, in favour of better vertical and horizontal resolution (137 levels, 0.5° × 0.5°).

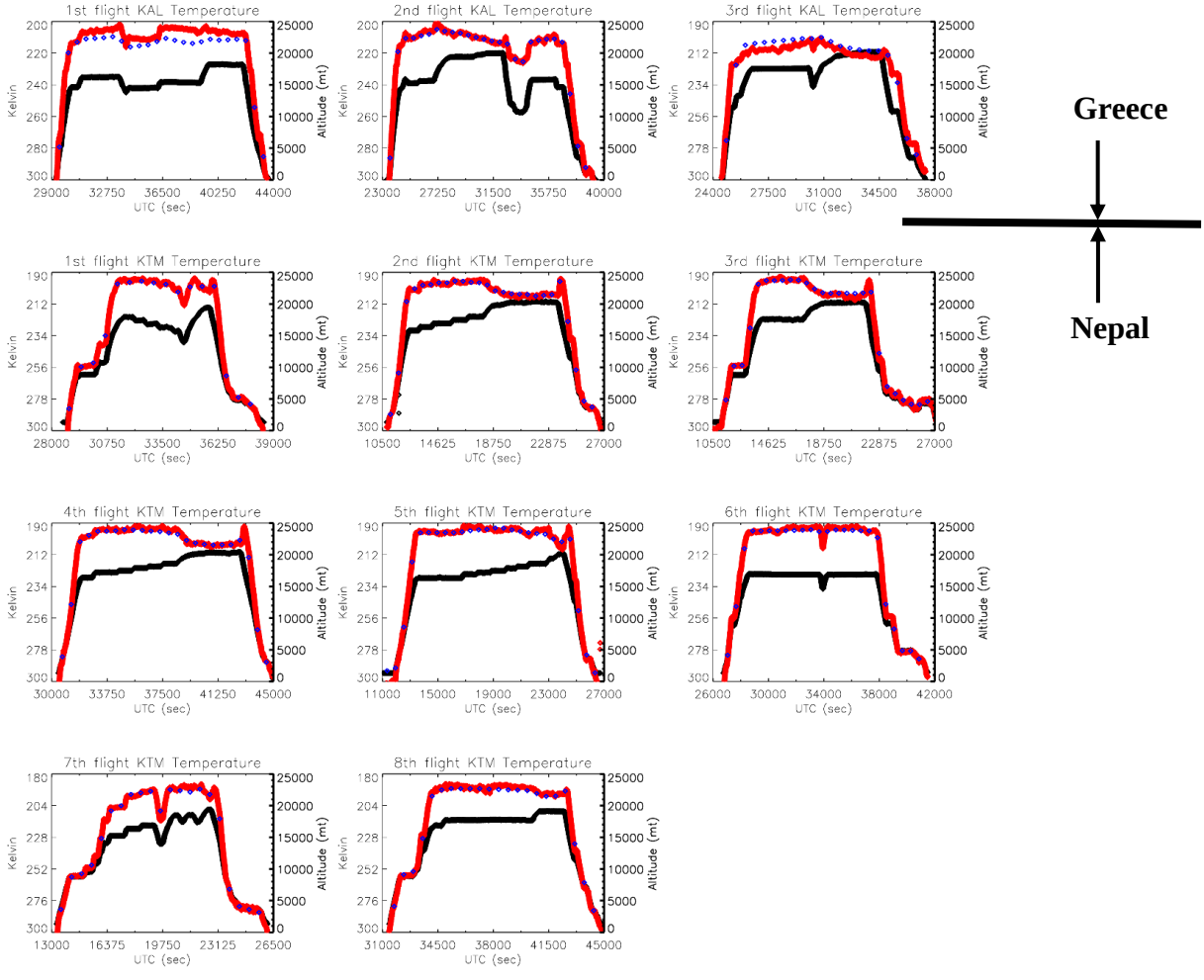

Figure 5.2. Plots of measured temperature values (K) during the StratoClim flights campaign (red dots). Samples of TOMCAT modelled temperature are shown in blue, while the aircraft altitude is shown in black. KAL refers to flights during the campaign over Kalamata, Greece in 2016, while KTM refers to the campaign over Nepal in 2017. Flights tracks are shown in **Figures 2.13.** and **2.14.**

While the water vapour and temperature comparisons test the accuracy of ECMWF reanalyses and the meteorological forcing, more information on the ability of the model to simulate the UTLS can be obtained by comparing chemically active tracers from the StratoClim campaign. For this three tropospheric full chemistry simulations (**Chapter 3**) were performed and the TOMCAT CO values are compared with COLD (Viciani *et al*., 2018) data from the flight campaign (**Figure 5.3.**). CO is a typical tropospheric chemical tracer and is not directly affected by the bias in water vapour in the UTLS as discussed before, although it is produced and destroyed in reactions involving OH, which has H_2O as its primary source. CO is also chosen because it was the tracer with the largest StratoClim observed dataset in the period following the campaign. The three model experiments different in their treatment of convection: archived convective mass fluxes, the Tiedtke scheme and no convection.

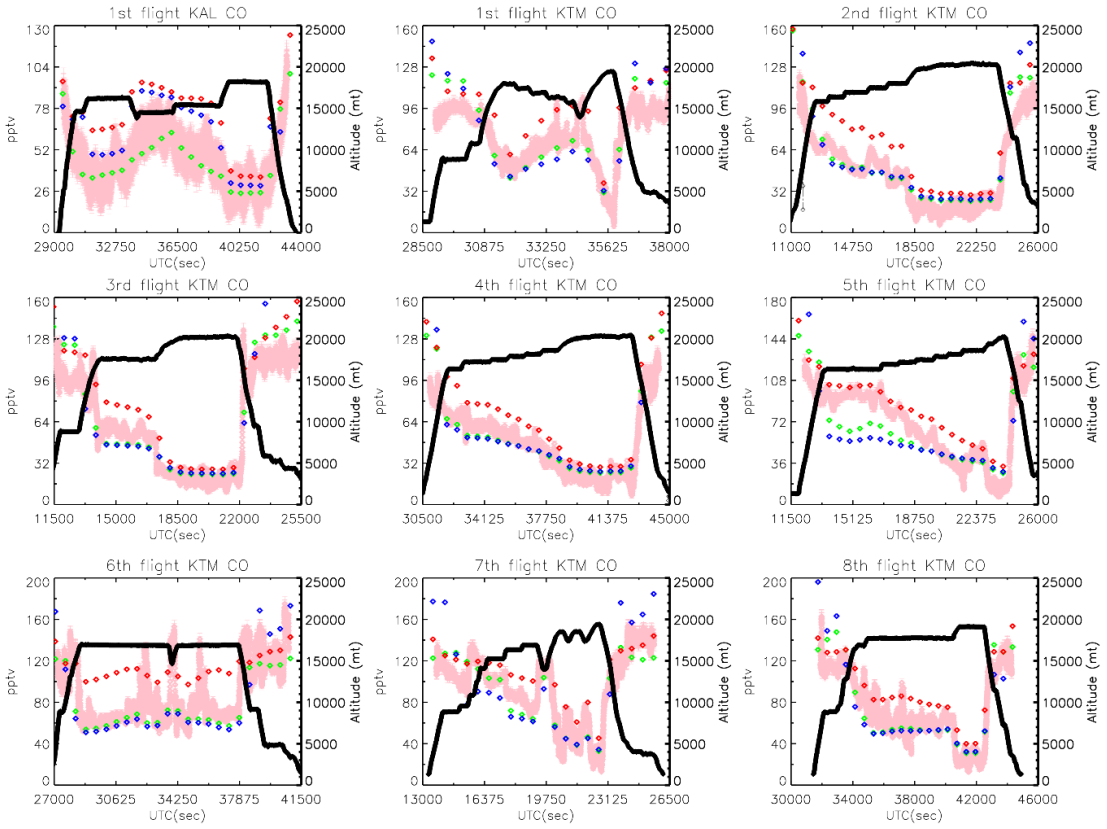

Figure 5.3. Time series of CO COLD mixing ratio along StratoClim flights (see **Table 5.1.**) are shown in pink. TOMCAT CO mixing ratio sampled at aircraft position, calculated with three different treatments of convection are shown. Red diamonds refer to run with archived mass fluxes, green diamonds describe run with the default convection

scheme (Tiedtke) while blue diamond refers to run with no convection scheme implemented. Black line refers to the aircraft altitude shown in meters on the right axys.

The results with the convective scenario (see also **Chapter 4**) do not give a definite answer on the "best" parametrization to use. Although the ERA-Interim convective mass fluxes (hereafter EICMF) sometimes overestimate the observed CO (see 1st KAL, 2nd KTM and 6th KTM flights) the simulation fits the observations better.

The correlation plots in **Figure 5.4.** show that simulation with EICMF generally overestimate the observed data, although it shows a less chaotic behaviour compared to other two schemes.

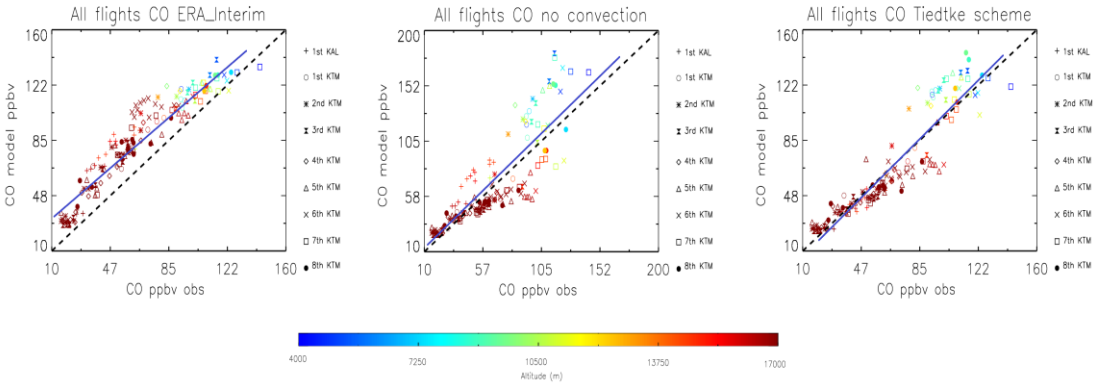

Figure 5.4. Correlation plots of observed (COLD data) and modelled (TOMCAT) CO for all available StratoClim flights. The data are shown for simulations with EICMF (**left**, correlation coefficient 0.95), no convection implemented (**centre**, correlation coefficient 0.86) and with default Tiedtke scheme (**right**, correlation coefficient 0.92). Best fit lines are plotted in blue. Mean absolute errors are 19.3 ppbv, 16.1 ppbv and 9.9 ppbv for EICMF, no convection and Tiedtke scheme respectively.

The Tiedtke scheme correlates well at higher altitude, but close to surface it tends to overestimate the observations. This suggests that the tracer stays at the surface rather than being vertically uplifted resulting in a non-realistic mixing ratio. The related (Pearson) correlation are as follows: **0.95 EICMF**, **0.86 no convection**, **0.92 Tiedtke scheme**. The ECMWF archived mass fluxes give the best agreement. Interestingly the correlation in the unrealistic run with no convection is still fairly high, suggesting that the improvement from the Tiedtke scheme to EICMF (0.92 to 0.95) is important. There results corroborate

the conclusions of the modelling study in **Chapter 4** and therefore this configuration of the model is the most appropriate to study the transport of species at stratospheric levels, over the tropical regions. This conclusion is in line of what found in a previous study focused on a similar topic with an early version of the EICMF scheme (Feng *et al.*, 2011).

5.3 NASA ATTREX campaign

The UTLS is the key region for species to be transported into the free stratosphere and therein impact ozone and other key components, particularly those which directly or indirectly affect its delicate radiative balance. Among these species the halogenated VSLSs, with lifetimes less than 6 months, generate concern due to their direct effect on stratospheric ozone and also due to the fact that they are not controlled in the Montreal Protocol (Montzka *et al.*, 2011; Hossaini *et al.*, 2016, WMO 2014). The Airborne Tropical Tropical Tropopause Experiment (ATTREX) was designed to measure a wide range of chemical tracers including various brominated species, such as CH_3Br, $CHBr_3$, CH_2Br_2 and Halon-1211 (H-1211) which have been identified as powerful ODSs (Seinfeld and Pandis, 2016). Measurements were taken via a large set of instrument aboard of the Global Hawk (GH) (Werner *et al.*, 2017). These data complement the more modest database of ASM observations from StratoClim and allow an investigation of the amount of brominated VSLS reaching the stratosphere in the East Pacific Ocean in early 2013 (**Figure 5.5.**, **left**). Satellite measurements (**Figure 5.5. right)** show that convection extended in the TTL (see **Figure 2.5.)** up to about 360 K is strong in the West Pacific above 10°N in Jan-Feb 2013, while deep convection reaching the TTL in the East-Central pacific is far less likely (occurrence frequency less than 1%, Jensen, *et al.*, 2017). Therefore, the data related to the ATTREX February 2013 flights represents a situation where convection doesn't seem to be the main driver of transport of species into the TTL. Comparison btw altitude and equivalent potential temperature (Bolton, 1980) (**Figures 5.7. a** and **j**), especially in the area III (Tropical TTL, see Werner *et al.*, 2017) confirm the relative vertical stability of this layer in agreement with the findings in **Figure 5.5.** right. As a matter of fact, EPT increases when the altitude does and the other way around and this reflects a condition vertically stable atmosphere (Holton, 2004).

Comparison of TOMCAT simulations with these data are a good test for the model table 4.2during the ASM (see **Section 2.3.**) the opposite (convection turned "ON") is a more realistic representation.

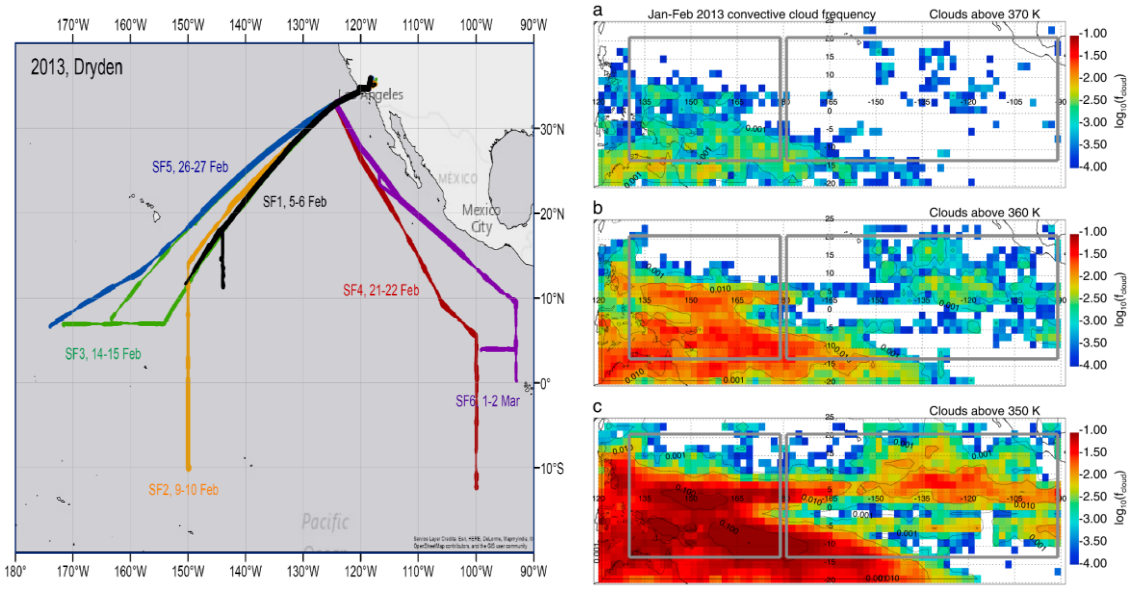

Figure 5.5. (**left**) Geographical location of NASA-ATTREX flights SF1-SF6, conducted from Dryden, California in 2013. The thickness of the line describes the flight altitude with thinnest line is for around 14 km and the thickest is for around 18 km. Figure taken from Werner et al., 2017. Further ATTREX flights took place from Guam in 2014. (**right**) Occurrence frequency of convection at levels above 370 K (**a**), 360 K (**b**) and 350 K (**c**), derived from satellite measurements, during January- February 2013. The grey boxes show the ATTREX campaign flights locations. Figure taken from Jensen *et al.*, 2017.

For these comparisons TOMCAT/SLIMCAT (**Chapter 3**) simulations with the stratospheric full chemistry scheme have been run with the ERA-Interim archived convective mass fluxes, due its better vertical transport performance, an important aspect in the Tropics where convection can be the dominant vertical transport regime **(Chapters 2** and **4**). First a low resolution simulation ($5.6^{o} \times 5.6^{o}$) was integrated from 1979 until 2013. The surface mixing ratio of long-lived source gases were specified from monthly global mean values based on observations. The long interation ensured that the model was fully spun-up, including the distribution of long-lived stratospheric tracers such as

CH_4, N_2O and CFCs. Brominated VSLS species were included with constant surface mixing ratios of: $CHBr_3$ = 1ppt, CH_2Br_2 = 1ppt and the sum of minor species a total of 1 ppt Br. Overall that added a further 6 ppt bromine to Br_y (WMO, 2014) Output from this run on January 1st 2013 was taken to initialise a higher resolution simulation ($1.2^o \times 1.2^o$) to cover the period of the 2013 ATTREX campaign. This run was sampled along the Global Hawk flightpaths to provide output for direct comparison with the aircraft data.

Example mixing ratio 'curtain plots' of selected TOMCAT species profiles along the flightrack of 14th February 2013 are shown in **Figure 5.6.** The Global Hawk flight track is shown in white. Methane shows high abundances in the troposphere which start to decay in the lower stratosphere, at the top of the plotted domain. The ozone distribution is anti-correlated with this and **Figure 5.6.** shows that the aircraft just probes the large stratospheric values around 30°N latitude. NO_2 and BrO are both short-lived radical species and need to be sampled at the correct local time for sensible model-data comparisons. **Figure 5.6.** shows the increasing abundance of these species in the overlying stratosphere. The lower panels of **Figure 5.6.** show the conversion of bromine from the organic source gas forms at lower altitudes (Br_y^{org}) to inorganic forms (Br_y^{inorg}) at higher altitudes.

Figure 5.7. compares the observed and modelled chemical tracers along the flight of 14th February 2013, including CH_4, O_3 and NO_2. Preliminary comparisons (not shown) revealed generally good, but not perfect, agreement between the modelled and observed CH_4 and O_3. These results pointed to a slight mismatch in the vertical profiles in the model. As the modelled and observed CH_4/O_3 ratios agreed very well (see Werner *et al*., 2017) ozone (with its stronger gradient) was used as a vertical coordinate to shift the model profiles. This correction was around 1 km or less. Consequently, in **Figure 5.7.** the model ozone field appears to agree perfectly. Given that, the model then does perform very well in the other comparisons, particularly for the longer lived CH_4. CH_4 measurement accuracy (~0.5%) and stability are calibrated by periodically replacing ambient air (4 min every 30 min) with NOAA-traceble gas standards, so the variations in CH_4 show real atmospheric variability (~ 0.2 ppbv, Werner *et al*., 2017)

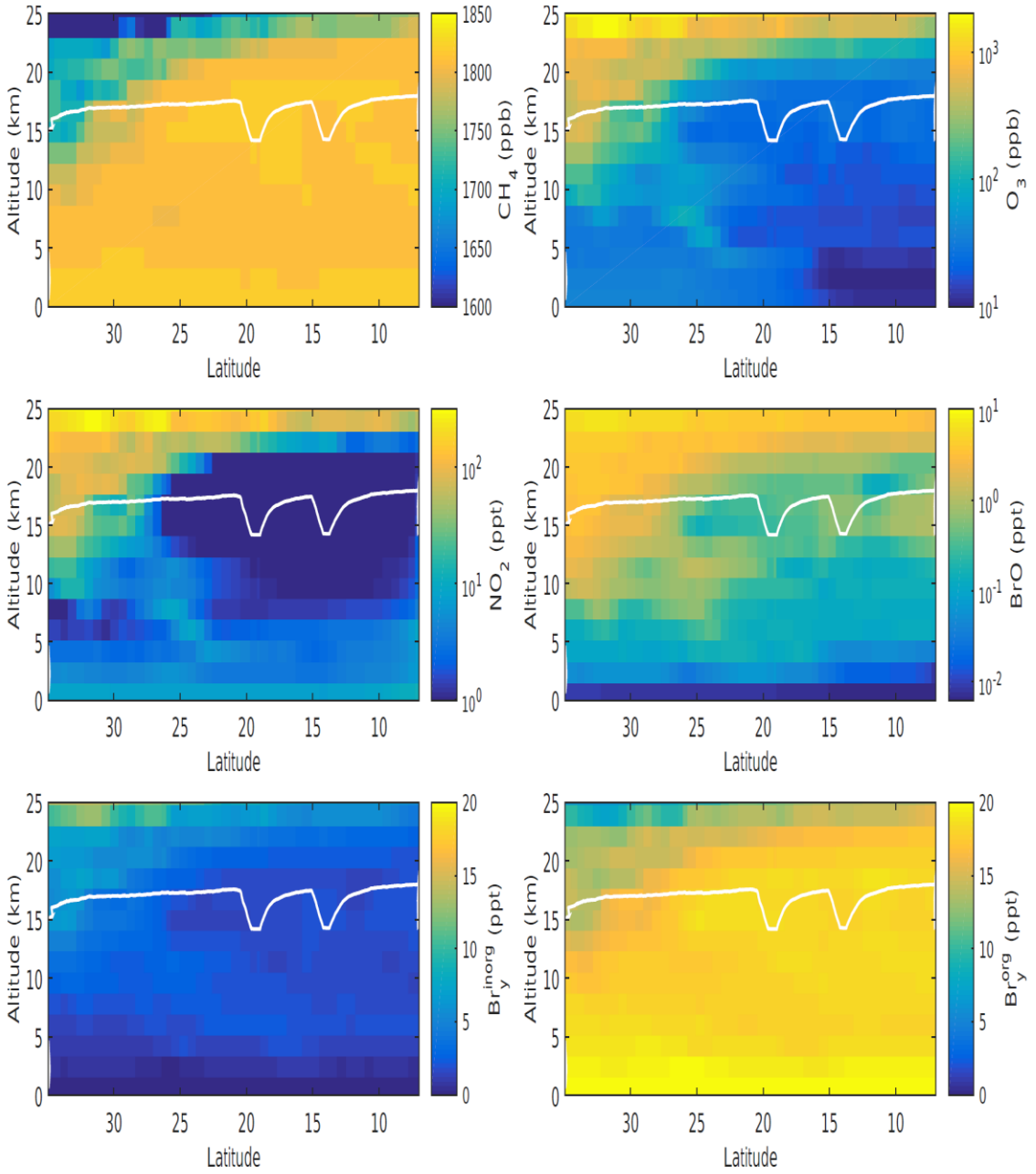

Figure 5.6. Latitude-height cross section of TOMCAT-simulated CH_4 (upper left), O_3 (upper right), NO_2 (middle left), BrO (middle right), Br_y^{inorg} (bottom left) and Br_y^{org} (bottom right) along the example ATTREX flightpath SF3-2013 (14 February 2013). The white line represents the Global Hawk trajectory. Figure taken from Werner *et al.*, 2017.

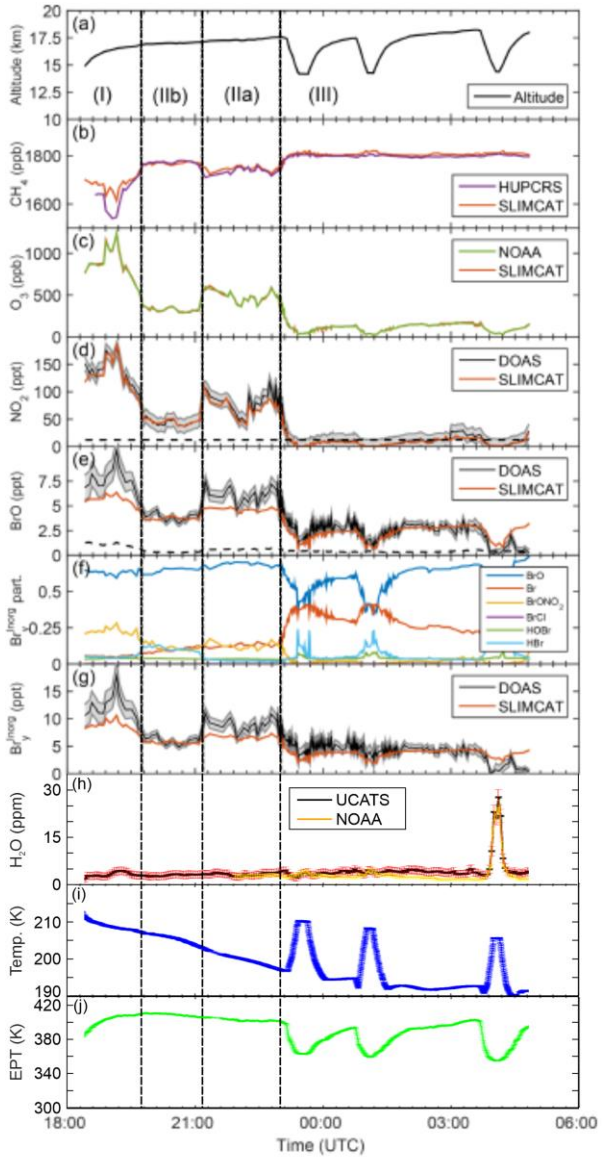

Figure 5.7. (a) Plot of time-altitude trajectory of the Global Hawk during ATTREX flight SF3-2013 (14-15 February 2013). Panels **(b)-(e)** show intercomparisons between the TOMCAT simulation and results of **(b)** CH_4 (HUPCRS), **(c)** O_3 (NOAA-2 polarized O_3 photometer), **(d)** NO_2 (mini DOAS) and **(e)** BrO (mini-DOAS). The grey shaded-error bars include all significant errors (see Figure 3 in Werner *et al.*, 2017 for details). Panel **(f)** shows the TOMCAT models partitioned Br_y for a control run. Panel **(g)** shows modelled and observed Br_y^{inorg}, with uncertainty grey band. **(h) H_2O** (UCTAS), and NOAA-2 polarized photometer measurements. Red and yellow bands represent significant errors for UCATS and NOAA-2 respectively. **(i)** temperature and **(j)** equivalent potential temperature (EPT) of the Global Hawk. Plots **(a)-(g)** are taken from Werner *et al.*, 2017 where more details can be found.

Figure 5.8. presents the correlation plots between modelled and measured CH_3Br(~62 days lifetime, Mellouki *et al*., 1992) , $CHBr_3$ (~26 days lifetime, WMO, 2014), CH_2Br_2 (~ 120 days lifetime, WMO, 2014) and Halon-1211 (H-1211, ~24 years lifetime, Volk, *et al*., 1997) from the Global hawk Whole Air Sampler (GWAS). The longer-lived species CH_3Br and Halon-1211 (specified at the surface from global mean observations) agree well between the model and observations. The VSLS $CHBr_3$, specified with a constant surface mixing ratio of 1 ppt also agrees well overall, but shows more scatter. This is likely due larger variability in it is source and distribution. In contrast, the agreement for the VSLS CH_2Br_2 is less good and varies from a model underestimate of ~0.1 ppt at high values (near the surface) to an overestimate at low values (higher altitude). There are likely various factors involved. The specified surface mixing ratio of CH_2Br_2 (1 ppt) is likely too low, together with a likely incorrect treatment of specified OH abundance which result in error in its lifetime and too little loss in the upper troposphere. The CH_3Br and $CHBr_3$ data scatter is reasonable but not very close, due instead to the variability of surface emission (Butler *et al*., 2010) encountered by the air masses sampled. As a matter of fact, emissions of natural brominated species, such as $CHBr_3$ and CH_2Br_2, are quite sparse and have a large spatial and temporal variability (Butler *et al.,* 2010).

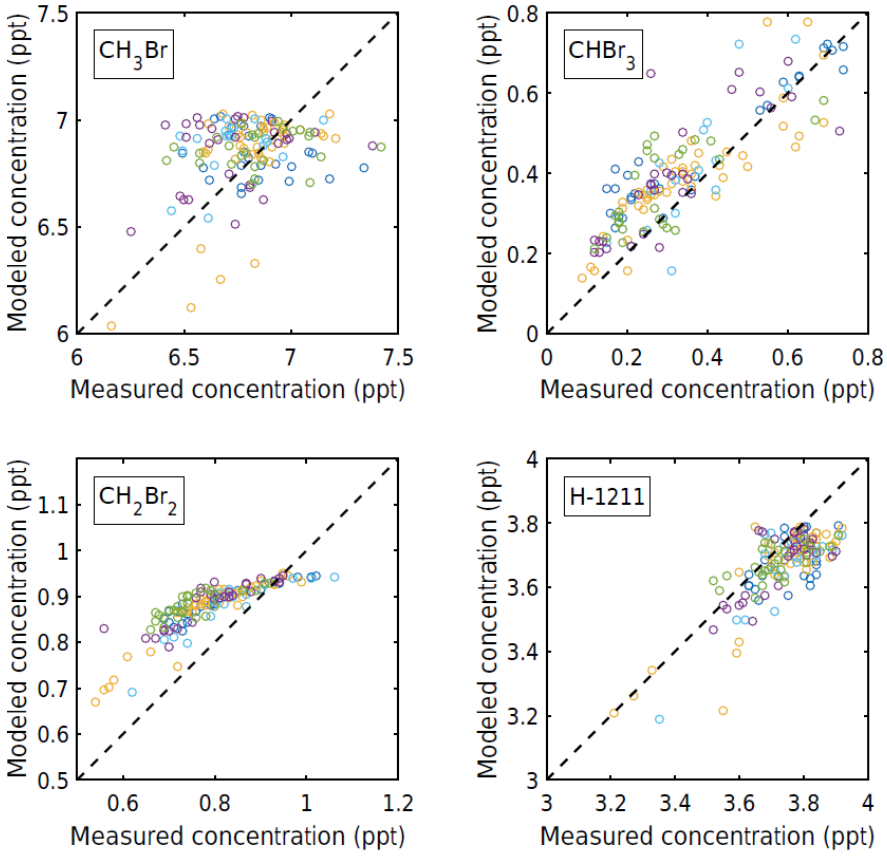

Figure 5.8. Correlation plots of measured tracers (ppt) from the ATTREX GWAS versus TOMCAT modelled CH_3Br (upper right), $CHBr_3$ (upper left), CH_2Br_2 (lower left) and Halon-1211 (H-1211) (bottom left). Flight SF1-2013 is indicated in blue, SF3-2013 in yellow, SF4-2013 in light blue, SF5-2013 in purple and SF6-2013 in green. Figure taken from Werner *et al.*, (2017).

Figure 5.7e compares the observed and modelled abundance of BrO. As an inorganic Br_y species, the abundance of BrO depends on the production from organic source gases. BrO is also the most widely observed Bry species and therefore the best species from which to infer the overall abundance of bromine. The figure shows generally good agreement between the model and observations, confirming the generally accurate abundance of the specified long-lived and short-lived bromine source gases. However, the model does underestimate the very largest BrO values near the start of the flight, which may point to direct injection of inorganic BrO into the stratosphere.

In summary, these TOMCAT/SLIMCAT simulations with the new convective scheme (**Chapter 4**) confirm the injection of around 6 ppt bromine derived from VSLS into the

stratosphere, but also show that this cannot account in all cases for the amount of inorganic bromine observed in the lower stratosphere. The validation of the model with the in-situ aircraft measurements is a further motivation to use the ERA-Interim archived mass fluxes to study the transport of VSLS originated at surface originated and then transported at stratospheric level. Further work should explore the variability of the surface sources rather than assume constant mixing ratios as done here.

5.4 Test of CO boundary layer sources

As shown in **Section 2.3.2**, the ASMA shows variability on several time scales. In **Chapter 4** the interannual variability of idealized CO25/CO50 and artificial TR5/TR50 tracers has been analysed and quantified. The subseasonal variability of the ASMA has been the object of a recent study (Pan *et al.*, 2016) which shows that CO at 100 hPa is characterized by two modes, namely the Tibetan Plateau (TP) and Iranian (IR) modes (**Figure 5.9**).

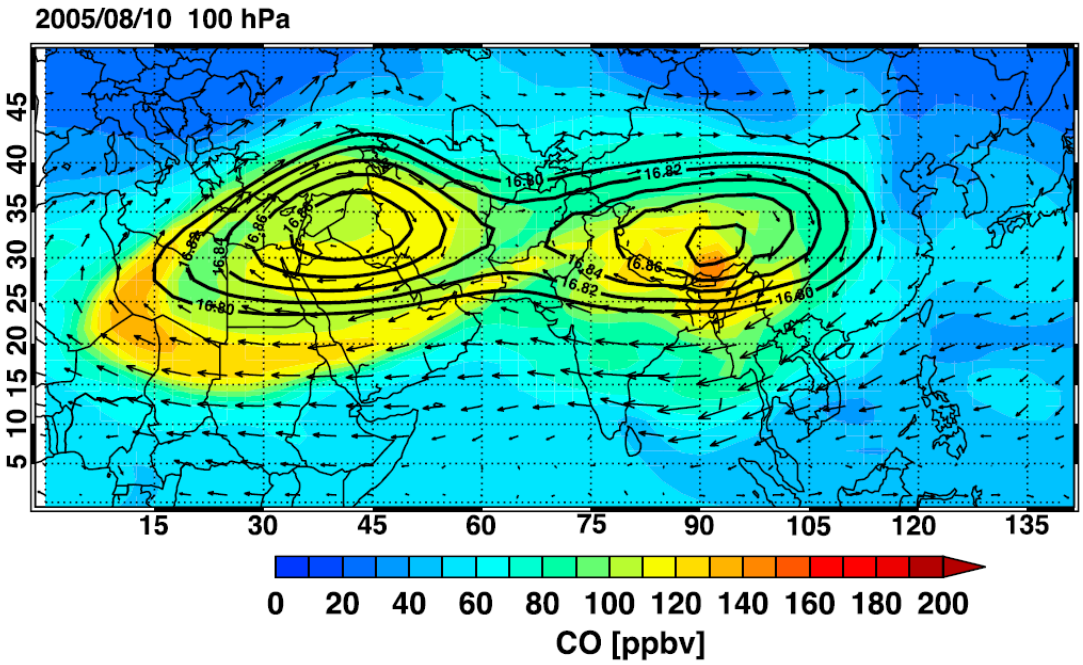

Figure 5.9. Simulated Whole Atmosphere Chemistry Climate Model (WACMM) CO field on August 10th 2005 at 100 hPa. Black contours show the geopotential height (km) and black arrows the horizontal winds at 100 hPa. Figure adapted from Pan *et al.*, (2016).

Pan and co-authors also identify the TP as the main contributor of CO at 100 hPa, which acts as chimney which feeds the Iranian mode (IR) via quasi-horizontal transport. Nevertheless, a previous study from Chen *et al.*, (2012) highlighted that together with the TP, the Bay of Bengal (BoB) and the Warm Pool (WP, East Pacific Ocean) contribute to the transport of air parcels from surface into the Asian Monsoon region. Among these, the TP contributes the least with only 12% while the BoB contributes the most with 21% of air parcels originating from the surface of these regions being transported to tropopause heights in the Asian Monsoon region.

In order to try and resolve this discussion with two conflicting hypotheses, I ran the TOMCAT model with the simplified chemistry scheme (**Chapter 3**) using the same CO50 used in **Chapter 4** but in four different convective scenarios. The first simulation is a control run, with EICMF. Three additional simulations were run with convection turned off over TP, BoB and TP+BoB, respectively. The model simulations covered the period of summer 2017. From the available output, August 9th 18 UTC to study an interesting three-mode configuration (IR+TP+WP) in tracer CO50 at 150 hPa, has been chosen. The main source regions are northern India and North East China (**Figure 5.10. left**).

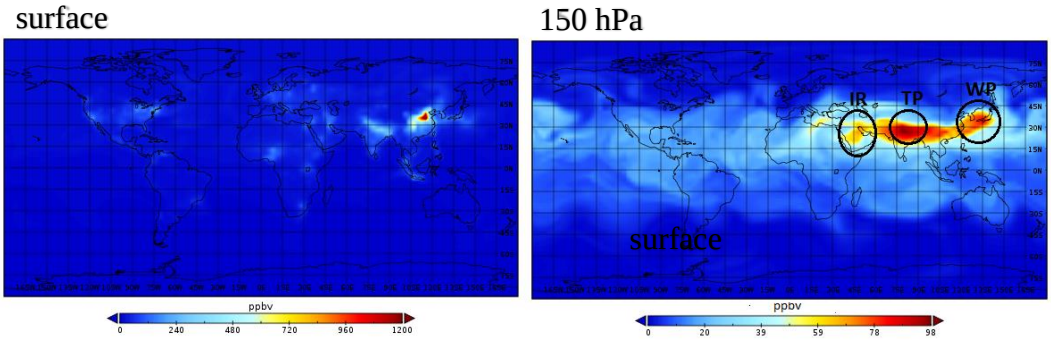

Figure 5.10. TOMCAT modelled tracer CO50 at 150 hPa on Aug 9th 2017 18 UTC at surface (**left**) and at 150hPa (**right**). The Tibetan Plateau (TP), Iranian (IR) and Western Pacific (WP) modes are indicated.

This structure is lost when time averaging longer than 6 hours is applied (**Figure 5.10. right**). Furthermore at 100 hPa this structure is less clear and the WP mode tends to disappear (not shown). Similar behaviour is found in case of CO25 (not shown). **Figure 5.11.** shows the difference between the control run and the respective area of "no

convection". A drastic reduction in the concentration of tracer CO50 over Northern India is evident when convection over TP is switched off (up to nearly 50%). The contribution of convection over BoB is minimal and the combination of TP+BoB is dominated by TP alone. Lack of convection on these two key areas, however, does not neutralize the three modes, suggesting that the modelled CO50 tracer distribution is the result of different transport regimes (e.g. large-scale ascent). This case study seems to negate the hypothesis that BoB is a main contributor of air in the ASMA region, although the level analysed here is lower (150 hPa rather than 100 hPa). Nevertheless, it unlikely that air coming from the BoB contributes only at 100 hPa thus skipping the 150 hPa level, implying a non-realistic air pathway to explain such a behaviour. Also, given the surface CO50 geographical distribution focused on northern India and North-East China, it is hard to speculate a vertical direct, fast deep transport from the BoB itself.brother More interestingly is the attempt to explain the disappearance of the WP mode at 100 hPa which leaves the open hypothesis of an autonomous boundary source which feeds exclusively the WP with peculiar time scales and characteristics. This analysis of this hypothesis is left for future works.

In terms of the model used here, it is worth noting that the analysis made here is somewhat complementary to the other two studies mentioned above. While Pan *et al.*, (2016) used WACCM, with the meteorology nudged to MERRA, Chen *et al.*, (2012) used FLEXPART a trajectory model whose winds come from ERA-Interim Reanalysis. The TOMCAT model, is an off-line model with detailed tropospheric and stratospheric chemistry schemes (**Chapter 5**) and so its findings come from a different standpoint which help to shed new light on the discussion developed here.

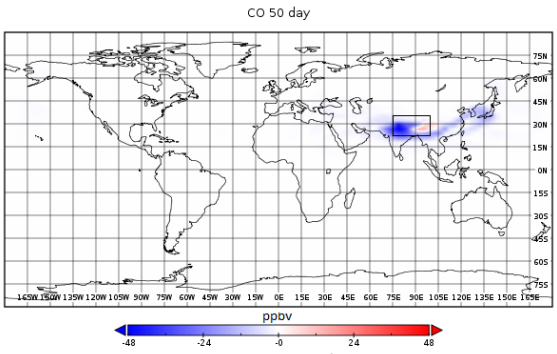

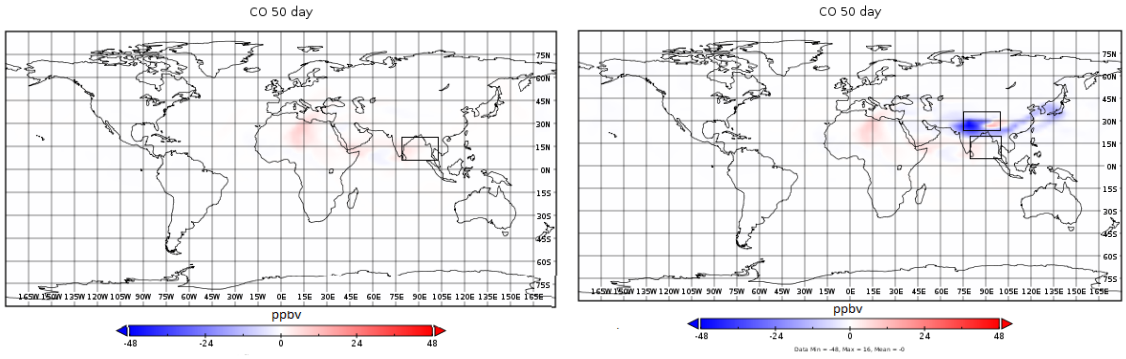

Figure 5.11. Plots of the difference (ppbv) between the CO50 control run and $CO50_{TP}$ (top), $CO50_{BoB}$ (bottom left) and $CO50_{TP+BoB}$ (bottom right) tracers at 150 hPa, on August 9th 2017, 18 UTC. Areas of "no convection" are shown by the black rectangle.

5.5 Summary

This chapter has been devoted to the analysis of temperature, water vapour and CO data from the StratoClim campaign and brominated species from the ATTREX project. Moreover, a TOMCAT modelling study designed to try to give new insight on the long-standing issue on the boundary sources of the ASMA has been conducted.

First, the model was compared with FLASH water vapour and aircraft temperature data taken during the StratoClim campaign of 2016 and 2017. This analysis aimed to compare results derived by the balloon measurements of the StratoClim campaign (now recently published), which shows that the UTLS over the Asian Monsoon in the ERA-Interim reanalyses is far too dry (up to -38% relative to balloon data, (Brunamonti *et al.*, 2019)). This ERA-Interim dataset is used in all TOMCAT simulations, as tropospheric water vapour is not calculated within the model. Therefore, it is important to understand whether or not a bias is present in the treatment of water vapour in the ERA-Interim in the UTLS. The dryness found in balloon measurements are generally confirmed by independent FLASH data. As FLASH is a highly precise fluorescent airborne stratosphere hygrometer, designed specifically for measurements in the UTLS (Sitnikov *et al.*, 2007) an issue with the ERA-Interim dataset might be present, following Brunamonti *et al.*, (2019). Switching to ERA5 water vapour database might be beneficial, although a positive bias (too moist UTLS) is present in this dataset.

The StratoClim COLD instrument gives a precious and unique portrait of CO in the UTLS

over the ASM. Following the rationale of **Chapter 4**, the model has been run using three different convection schemes (EICMF, Tiedtke scheme and no convection) to test which one fits the observations best. Both of the convective schemes give good correlation scores (above 0.92), but understandably the Tiedtke scheme overestimates the mixing ratio at surface and lacks the "strength" to transport CO upward. EICMF simulations have a correlation coefficient of about 0.95 when compared with COLD CO data, confirming the better ability of this scheme to reproduce the observations. This is further evidence of the successful comparison of the model in this configuration with in-situ measurements.

In the context of the 2013 ATTREX campaign in the Eastern Pacific, designed to probe the UTLS abundances of powerful halogen ODSs such as $CHBr_3$, CH_3Br, CH_2Br_2 and H-1211, the model agrees well with the observations. These studies are complementary to StratoClim and provide a much greater coverage of species. Simulations of TOMCAT/SLIMCAT with the new convective scheme based on archived mass fluxes confirm the injection of around 6 ppt bromine derived from VSLS into the stratosphere, but also show that this cannot account in all cases for the amount of inorganic bromine observed in the lower stratosphere. Direct injection of significant levels (few ppt) of inorganic bromine appear to occur, as further discussed in Werner *et al*., (2017).

The understanding of the vertical transport regimes, which uplift tracers from surface to UTLS is still a highly debated topic. CO is a tropospheric tracer originated at surface and eventually transport upward. It is typically used to try to discern the geographical areas which eventually supply it UTLS during the ASM. Recent evidence points out that the TP and BoB are the main important near-surface source regions, nevertheless they disagree on which is the dominant one. The model simulations, using computationally cheap idealized CO with 50-day lifetime, suggest that the BoB contributes little to the CO mixing ratio at 150 hPa, unlike the TP which shows a reduction up to 48 ppbv (corresponding to about 50%) when it is excluded from the convective sources. Analysis of daily summertime model fields shows also reveals a tri-modal CO structure at 150 hPa, which does not dissipate completely when the convection is turned off in both TP and BoB. This suggests that assuming TP and BoB as the sole main contributors may in itself be an oversimplification.

6 Impact of the injection of TiO_2 particles on Stratospheric Composition

6.1 Introduction

Concern about climate change has led to the proposals that humans could act to modify the Earth or its atmosphere to counteract these changes (Crutzen, 2006; Keith *et al.*, 2010). This topic is summarized by the term 'geoengineering'. Given the serious consequences of climate change, these ideas are being widely discussed and therefore need to be informed as accurately as possible. In addition to the significant technical and ethical issues of geoengineering, there are also questions related to atmospheric composition. In particular, could attempts to modify the Earth's climate have undesired consequences on other parts of the Earth system such as the ozone layer? This is where models of stratospheric chemistry, which have been thoroughly tested against atmospheric observations (e.g. see **Chapters 4** and **5**), play a critical role in assessing the possible negative consequences.

This chapter investigates the potential impact of titanium dioxide (TiO_2) particles on stratospheric composition. TiO_2 particles have been proposed as a means of geoengineering through solar radiation management because of their high reflectivity (Pope *et al.*, 2012). However, their injection into the lower stratosphere could cause impacts on chemistry through heterogeneous reactions, similar to those that occur on sulfate aerosols and on polar stratospheric clouds. Laboratory data for the rates of some possible heterogeneous reactions on TiO_2 are now becoming available and forms the basis for the model experiments discussed here. Some results from the modelling work in this chapter have been published in Moon *et al.*, (2018), which specifically looked at the role of HO_2 loss on TiO_2 particles.

The layout of this chapter is as follows: **Section 6.2** provides some background of the historical context of geoengineering. **Section 6.3** reviews recent literature and laboratory studies related to the use of TiO_2 particles in the atmosphere. **Sections 6.4** and **6.5**

describe results of TOMCAT simulations related to the impact of TiO_2 particles on stratospheric ozone. The key results of this chapter are summarized in **Section 6.6.**

6.2 Historical Context

Weather and climate modification is far from being a new concept in our modern times. Societies from many parts of the globe have always desired to control the weather, mostly through some kind of ritualistic "rainmaking" (National Science Foundation, 1966). In modern times many methods have been suggested to try to increase rainfall in certain areas. For instance, before the 20th century two U.S. Government patents on rainfall management were registered (National Research Council, 1966). However, the history of 'geoengineering', a term which will be defined below, had its turning point around the publication of an influential paper from Nobel Laureate Paul Crutzen (Crutzen, 2006). From 2006 a large number of scientists, politicians, and scholars of moral issues have become involved in the assessment of several aspect of geoengineering.

Shortly after WWII, few American scientists understood that since the human beings have an effect on local weather, e.g. emitting NOx and deforesting rural areas, similar procedures can be undertaken to modify the weather on purpose. From 1945 until well into the 1970s, both of the two superpowers invested large sums of government money to explore projects to harm each other's local weather, e.g. to ruin the Soviet harvest by creating a drought. These actions were part of a wider theory, so-called *climatological warfare* (Fleming, 2010), a term which alongside the race with Soviet Union to produce more lethal nuclear weapons, suggested a similar decisive competition to control the weather (Neumann, 1955). The idea of "cloud seeding" **(Figure 6.1.)** remained the main weather-modification project until the mid-1970s. In this process silver iodide particles cause cloud moisture to freeze and create ice crystals, changing the microphysics of clouds and allowing rain drops or snow to form.

Although concerns around the negative effects on rainfall were raised (Lambright and Changnon, 1989), research efforts and funding for cloud-seeding projects continued throughout the 1960s with questionable results (National Academy of Sciences, 1966). In the early 1970s the U.S. government invested more than $20 million dollars per year on cloud seeding projects, although in the late 1970s and 1980s funding and attention

suffered a steady substantial decline (Lambright and Changnon, 1989). After that, both the USA and Soviet Union abandoned these kinds of projects to pursue a different aim. Awareness of *global warming* effects started to grow and some scientists thought that human intervention to counteract it should not be considered as a taboo. Research then developed from manipulation of the conditions of the atmosphere on a local, temporally limited scale (weather) to a global, temporally long basis (climate).

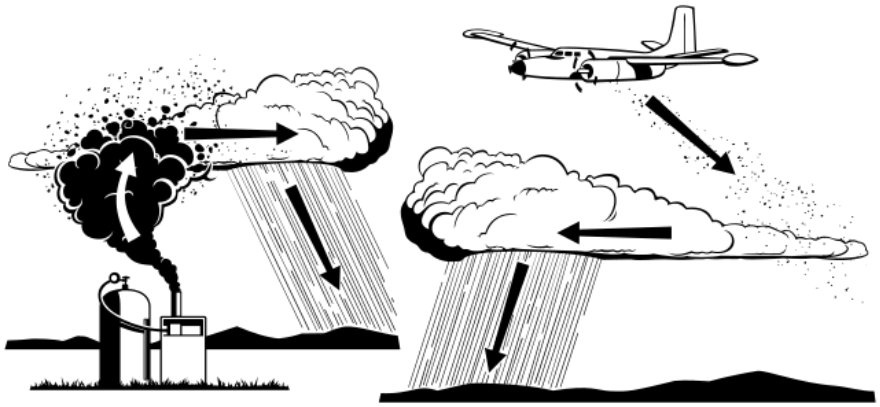

Figure 6.1. Illustration showing how cloud seeding works: targeted clouds are fed with silver iodide particles, via an aircraft or an in-situ generator, which aid in the formation of ice crystals, eventually becoming large enough to fall and create snow or rain. Figure from https://en.wikipedia.org/wiki/Cloud_seeding#

As mentioned above, research in this direction was stimulated in August 2006 when Paul Crutzen published an article (Crutzen, 2006) which reinvigorated the debate around "solutions" to escalating climate change. A clear definition of *geoengineering* as the "intentional manipulation of the environment to counteract the negative impacts of the global warming" finally took hold. Carbon dioxide removal (CDR) and solar radiation management (SRM) are currently the two main techniques proposed to try to mitigate the effect of climate change, the former based on the removal of CO_2 from the atmosphere, while the latter aims to enhance the back-scattering of the incoming radiation to reduce the consequential surface heating. These two methods can be applied through several techniques, some of which illustrated in **Figure 6.2.**

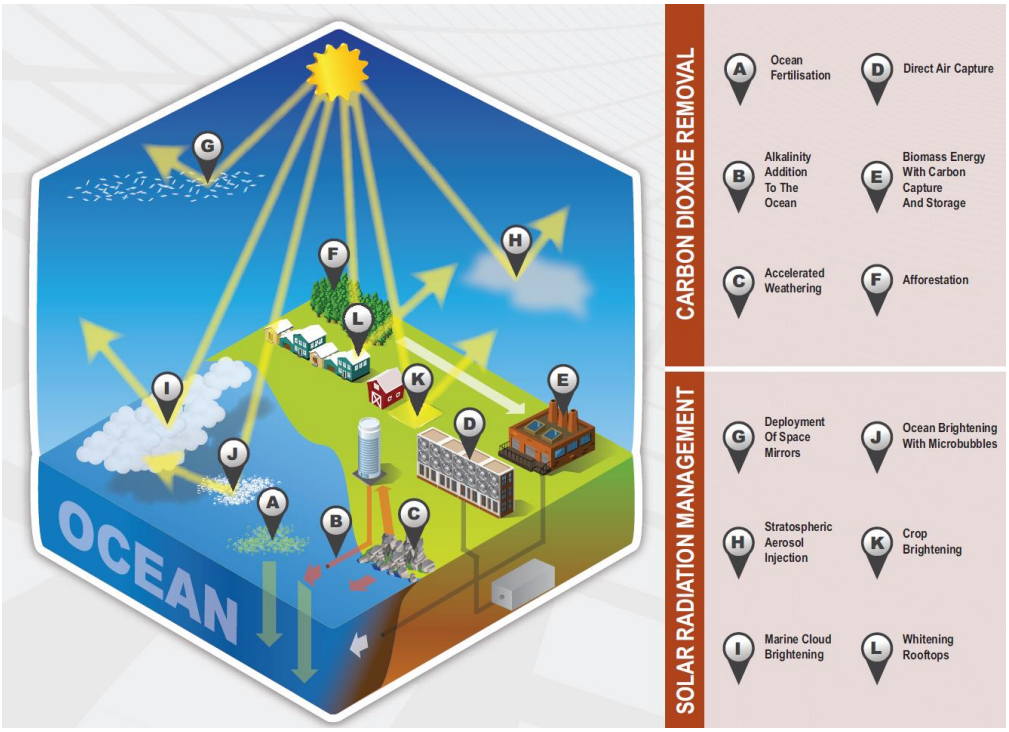

Figure 6.2. Overview of main geoengineering methods divided between CDR and SRM techniques. (A) Ocean Fertilization, based on the enhancement of CO_2 uptake due to the increment of nutrients; (B) Alkalinity Addition to the Ocean: solid minerals are injected in the ocean to enhance the dissolution of atmospheric CO_2; (C) Accelerated Weathering: dissolved silicate and carbonate mineral rocks applied in coastal environment are transported to the ocean to enhance ocean CO_2 uptake; (D) Direct Air Capture: underground or oceanic storage of chemically captured CO_2; (E) Biomass Energy With Carbon Capture and Storage: electric power production using biomass, CO_2 captured and stored either underground or in the ocean; (F) Afforestation: planting new trees enhance natural CO_2 storage in forest ecosystems; (G) Deployment of Space Mirrors: space reflectors at appropriate distance reflect solar radiation; (H) Stratospheric Aerosol Injection: highly reflective particles indirectly producing aerosols are injected at stratospheric levels; (I) Marine Cloud Brightening: marine stratocumulus clouds coverage can be artificially increased through appropriate cloud seeding; (J) Ocean Brightening with Microbubbles: increment of microbubbles in ship wakes resulting in a more reflective ocean surface; (K) Crop Brightening: more reflective crops can increase backscatter of solar radiation; (L) Whitening Rooftops: whitening roofs and other constructions increases the brightness of urban and rural environments. Figure taken from (IPCC, 2013).

6.3 Proposed Use of TiO_2 for Solar Radiation Management

Among the SRM techniques, injection of aerosols at stratospheric levels is currently one of the most widely studied. In particular, research on this topic accelerated in August 2006, when Nobel laureate Paul Crutzen published an editorial essay (Crutzen, 2006), which reviewed in detail the pros and cons of injecting sulfuric acid aerosols in the stratosphere to reduce the incoming shortwave radiation and thus cooling the surface. Those aerosols occur naturally in the stratosphere mostly due to the transport of volcanic emission of SO_2 and biogenic (oceanic) emissions of OCS (Seinfeld and Pandis, 2016). The stratospheric sulfur burden during a reduced volcanic activity is about 0.65±0.2 Tg (*SPARC,* 2006). In this context, the international modelling project GeoMIP (Geoengineering Model Intercomparison, (Robock, 2014)) attempted to assess the impact of sulfur geoengineering on temperature, precipitation and radiative balance, through a comprehensive chemistry–climate modelling research effort. However, a unique occasion to study the impact of the injection of large quantities of aerosols in the stratosphere was provided by the Pinatubo eruption in 1991, when it has been estimated that about 30 Tg of H_2SO_4 accumulated in the stratosphere (McCormick and Veiga, 1992) causing global-average surface cooling of about 0.5 K (Dutton and Christy, 1992) although a recent work has reduced this value to about 0.14 K (Canty *et al.*, 2013) (see **Figure 6.3.**).

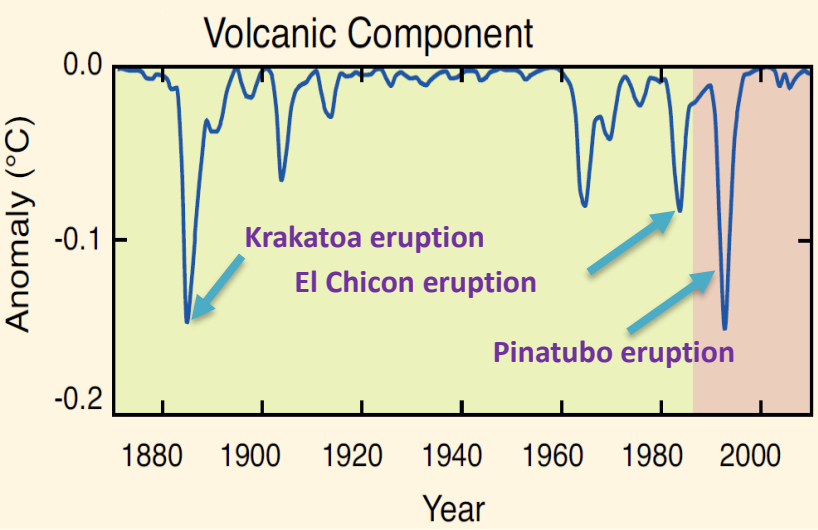

Figure 6.3. Estimated model global mean surface temperature response (°C) to large volcanic eruptions (IPCC, 2013).

Following this idea, the artificial recreation of large volcanic eruptions has been suggested as a way to 'engineer' the climate. However, together with the desired temperature mitigation, other undesired aspects are associated with large volcanic eruptions, which should be avoided in case of the implementation of any geoengineering strategy. For instance, observations evidenced a minimum in stratospheric ozone values after the eruption (McCormick *et al.*, 1995), and particularly up to 30% in the tropical stratosphere (**Figure 6.4.**). The reason for this is the involvement of changes in the dynamics, photolysis rates and heterogeneous chemistry induced by the volcanic event (Grant, *et al.*, 1994).

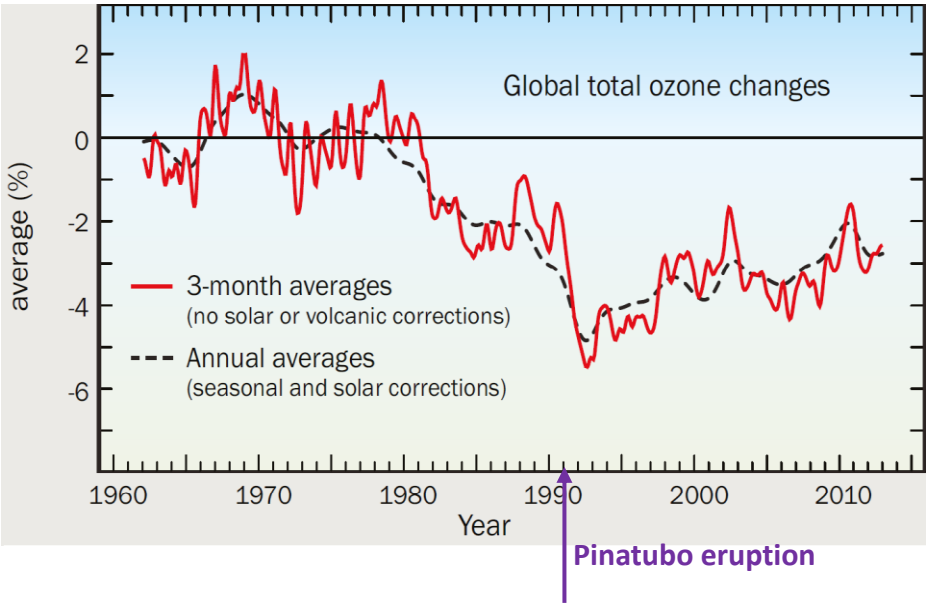

Figure 6.4. Change in global average total column ozone (%) relative to 1964-1980 average. Figure taken from (World Meteorological Organization (WMO), 2014).

As the mechanisms of the impact of sulfate aerosols on stratospheric ozone are well understood, and given the consequential (negative) effects which followed the Pinatubo eruptions, alternatives to sulfate have been sought and found in mineral dusts particles (Pope *et al.*, 2012). A comprehensive review of sulfate particles for geo-engineering strategies can be found in (Visioni, *et al.*, 2017). Nevertheless, suitable alternatives to sulfur particles for stratospheric injection must have comparable scattering efficiencies and avoid the abovementioned undesirable effects on ozone. Likewise, aerosols in the stratosphere affect the temperature field through the absorption-emission of long wave radiation and then eventually changing the circulation there. In turn, that could alter the

ozone distribution and also, they are constantly subject to removal processes. Ideally, a candidate for SRM techniques should have low impact on the longwave radiation balance and long residence time, to avoid negative influence on the dynamics and constant re-introduction of particles from the surface. Recent laboratory and modelling studies have determined that TiO_2 particles show slower sedimentation time and less heating effect than sulfur particles (Ferraro *et al.*, 2011 ; Benduhn and Lawrence, 2013) as shown in **Figure 6.5.**

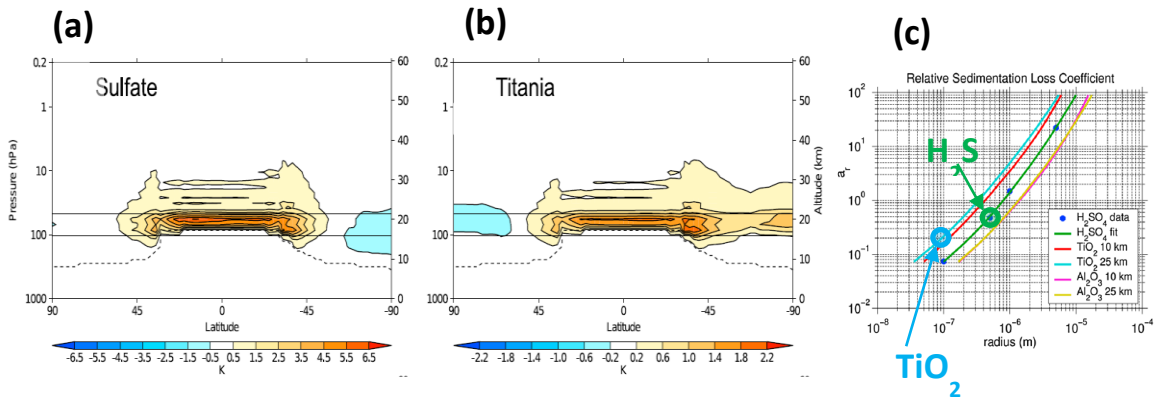

Figure 6.5. Modelled DJF zonal mean temperature change (K) due to the stratospheric injection of aerosols composed of **(a)** sulfuric acid (sulfate) and **(b)** titanium dioxide (titania), from Ferraro, Highwood and Charlton-Perez, 2011. **(c)** Relative sedimentation loss coefficient for sulfate aerosols (H_2SO_4) and TiO_2 particles for sizes typical of geoengineering studies, Figures taken from Benduhn and Lawrence, 2013.

In their influential paper (Pope *et al.*, 2012) first reviewed the chemical characteristics of mineral dust particles with potential for SRM use and, among these, SiO_2 and TiO_2 particles have been the object of subsequent work focused on assessing the impact on HO_2, nitrogen species and chlorine radical activation (Tang *et al.*, 2014; Tang *et al.*, 2016; Moon *et al.*, 2018). Mineral dust particles are widely spread in the troposphere and account the largest fraction of the tropospheric aerosol burden (Textor *et al.*, 2006; Huneeus *et al.*, 2011) with TiO_2 accounting for up to 10% of the all mineral dust loading (Usher, *et al.*, 2003). In particular, TiO_2 particles, have been suggested as convenient for SRM schemes due to their large refractive indices (Pope *et al.*, 2012). It has been estimated that the use of TiO_2 particles requires a factor of 3 less in mass (and a factor of 7 less in volume) of sulfuric acid particles in order to achieve the same cooling effect due to the Pinatubo eruption, as the refractive index of TiO_2 at 550 nm is 2.5 compared to a

value of 1.5 for naturally occurring sulfate aerosols (Pope *et al.,* 2012). However, the injection of particles in the atmosphere, provides surfaces for heterogeneous reactions to occur and this is especially important at stratospheric levels, where the ozone concentration is maximum.

In order to understand the impact of TiO_2 particle injection on climate-relevant species, e.g. ozone, recent laboratory experiments studies (Tang *et al.,* 2014; Tang *et al.,* 2016) have focused on the investigation of the efficiency of those particles to hydrolyse N_2O_5 and $ClONO_2$ via the following reactions:

$$N_2O_5 + H_2O + surface \rightarrow 2HNO_3 \quad \text{(R1)}$$

$$ClONO_2 + H_2O + surface \rightarrow HNO_3 + HOCl \quad \text{(R2)}$$

The dissolution of N_2O_5 and $ClONO_2$ has been widely observed after the Mt Pinatubo eruption together with the activation of chlorine radicals formed by the photolysis of Cl_2 derived from reaction of $ClONO_2$ with HCl (Fahey, *et al.,* 1993).

$$ClONO_2 + HCl + surface \rightarrow HNO_3 + Cl_2 \quad \text{(R3)}$$

A further study (Moon *et al.*, 2018) tested the uptake of HO_2 on TiO_2 particles, a radical responsible for up to 40% of ozone depletion in the lower stratosphere via the catalytic cycle

$$\begin{cases} OH + O_3 \rightarrow HO_2 + O_2 \\ HO_2 + O_3 \rightarrow OH + 2O_2 \\ Net: \ 2O_3 \rightarrow 3O_2 \end{cases}$$

The source of HOx (OH + HO_2) in the stratosphere is water vapour. HOx is short-lived and there is a strong cycling in/out of the H_2O reservoir. Source of stratospheric water

vapour is transport from the troposphere (through the temperature minimum at the tropopause) and oxidation of CH_4 (Seinfeld and Pandis, 2016).

6.4 TOMCAT Model Experiments

The TOMCAT off-line three-dimensional (3-D) (Chipperfield, 1999, 2006) has been used to assess the impact of the heterogeneous reactions on TiO_2 particles on stratospheric composition. As described in **Chapter 3**, the model has been widely used in previous studies of stratospheric chemistry and performs well in reproducing stratospheric ozone and the trace species which control its distribution (Chipperfield *et al.*, 2015). The model includes a detailed treatment of stratospheric chemistry of O_x, HO_x, NO_y, Cl_y and Br_y species along with the main source gases. The model has a comprehensive gas-phase chemistry scheme and includes a number of heterogeneous reactions on stratospheric sulfate aerosols and polar stratospheric clouds (Chipperfield, 1999).

The loss rate of a gas-phase chemical species (HO_2, N_2O_5, $ClONO_2$) due to heterogeneous reaction with TiO_2 was included in the model as:

$$k = 0.25\, S_a\, w\, \gamma \qquad \text{(Eqn. 1)}$$

where S_a is the surface area density of TiO_2, w is the mean velocity of the reacting molecules (ms^{-1}) and γ is the uptake coefficient which is based on laboratory data as described above. Two sets of TOMCAT experiments, one for 2008 and the other one for time period 2000-2049 were performed (see **Table 6.1.**).

The first set included four TOMCAT simulations, performed at a horizontal resolution of $5.6^o \times 5.6^o$ and 32 levels from the surface to ~60 km. The aim of these shorter experiments was to assess the impact of TiO_2 particles under present-day conditions. The model was forced with wind and temperature fields from the European Centre for Medium-Range Weather Forecasts (ECMWF) ERA-Interim reanalyses and integrated for 2 years from January 2007 until December 2008, initialised with the output from a standard TOMCAT run which had spun-up from 1977. The first simulation (CNTL_2008), similar to that presented in Chipperfield *et al.*, (2015), did not include TiO_2 particles. A specified latitude-height distribution of TiO_2 particles was then included

in two simulations with an effective aerosol surface area density equal to that of sulfate aerosols in 1992 following the eruption of Mt Pinatubo. This is an assumption which allows for the fact that less TiO_2 mass is needed in order to produce the same radiative impact as sulfate aerosol from Mt Pinatubo, but the TiO_2 particle size is smaller. Hence these effects largely cancel (Tang *et al.* (2014)).

Experiment Label	Time Period	γ(R1)	γ(R2)	γ(R3)	$\gamma_{HO2} = 1$
CNTL_2008	2007-2008	0	0	0	0
R1_2008	2007-2008	0.005	0	0	0
R2_2008	2007-2008	0.005	0	0	1
R3_2008	2007-2008	0.005	0.0015	0	0
R4_2008	2007-2008	0.005	0.0015	0.02	0
CNTL_2049	2000-2049	0	0	0	0
R4_2049	2000-2049	0.005	0.0015	0.02	0

Table 6.1. Summary of the TOMCAT 3-D CTM simulations performed to assess the impact of TiO_2 particles on relevant stratospheric species, with the assigned coefficient uptakes (γ).

Simulation CNTL_2008 is a control simulation using 2008 meteorology and chemical conditions without the inclusion of TiO_2 particles. The first of the sensitivity simulations (R1_2008) included only the loss of N_2O_5 on TiO_2 particles with γ(R1) = 0.005, the upper limit used in the modelling of Tang *et al.* (2014), which allows comparison with their study. Simulation R2_2008 also included the loss of HO_2 on TiO_2 particles with a γ_{HO2} = 1, as discussed above. Simulation R3_2008 was the same as R1_2008 but also included

the hydrolysis of $ClONO_2$ was included (γ(R2)=0.0015, according to lab results of Tang *et al.,* 2016). Finally, a run with γ(R1)s=0.005, γ(R2)=0.0015 and γ(R3)=0.02 (Molina *et al.,* 1997) was performed (R4_2008). These last two runs did not include loss of HO_2 because of the negligible impact of the titanium dioxide particles on this species, as shown below for R2_2008.

The second set of TOMCAT simulations were performed to assess how the impact of TiO_2 particles may change as the composition of the stratosphere changes, notably as the halogen loading declines in response to the effects of the Montreal Protocol. As this is the timescale on which geoengineering may take place, it is important to see the time dependence of any effects on ozone. Therefore, two additional simulations (with and without TiO_2) were performed to investigate the combined impact of reactions (R1), (R2) and (R3) for time period from 2000-2049, particularly in terms of chlorine activation which is a key step in stratospheric ozone depletion. For the future model years, the meteorology was fixed to 2012 values from 2018 onwards. In order to investigate the interaction of geoengineering and large volcanic eruptions, which of course may still occur, these future runs include the eruption of a Pinatubo-like volcano every 10 years (in 2021, 2031, 2041, etc.). The varying effect of the interaction of aerosols and TiO_2 particles can also be studied. Uptake coefficients used for these simulations have been object of studies led by M. Tang (Tang *et al.*, 2016) and M.J. Molina (Molina *et al.,* 1997), respectively. Limitations in the former study meant that laboratory experiments were only conducted at room temperature (296±2 K), while in the latter study conditions were typical of the mid-latitude lower stratosphere but α-alumina (Al_2O_3) particles were used. The simulation, R4_2049 was conducted with γ(R1)=0.005 (same as the simulations for 2008 conditions), γ(R2)=0.0015 (Tang *et al.,* 2016) and γ(R3)=0.02 (Molina *et al.,* 1997). The control simulation CNTL_2049 assumed no particle injection, therefore $\gamma(R1) = \gamma(R2) = \gamma(R3) = 0$.

6.5 Results

This section describes and discuss the simulation results obtained according to the methodology described in the previous section. The findings relate to the third set of research questions that guided this study as explained in **Section 1.1**.

6.5.1 Reaction of N_2O_5

The impact of N_2O_5 loss on TiO_2 particles has been assessed by (Tang *et al.*, 2014) using a nudged chemistry-climate model (CCM). Therefore, results from TOMCAT simulation R1_2008 can be used to compare with that study as a test of the model setup.

Figure 6.6.b shows the impact of including heterogeneous loss of N_2O_5 on TiO_2 particles in the model, with γ(R1)=0.005 (R1_2008 simulation). N_2O_5 is decreased by up to 0.5% in the region of TiO_2 particles, which is assumed to follow the distribution of sulfate particles after the Mt Pinatubo eruption. The zonal means at 20 km, for January-December 2008 (**Figures 6.7a,b**) shows some latitudinal discrepancies which follow, at least for N_2O_5, the seasonal minimum temperature conditions. Nevertheless, the effect on N_2O_5 is is only a minor effect and considerably smaller than the impact of around -20% modelled by (Tang *et al.*, 2014, **Figure 6.8.**) for the same assumed γ(R1)=0.005. The reasons for this are not clear, although it is noted that the effect modelled in the off-line chemical transport model used here, with specified meteorology, is clearly confined to regions of high aerosol loading. The impacts modelled in the nudged CCM study of Tang *et al.*, 2014 are not confined to the region of high aerosol and even extend to the upper stratosphere. Large N_2O_5 increases (>10%) in the Tropics between 30-40 km at the North Pole between 40-50 km, raise some doubts due to the separation from the main TiO_2 particle distribution (**Figure 6.9.**). It is possible that their simulations, although nudged, also include some feedback due to dynamical variability, which enhances an otherwise small signal, or that there was model variability between the different sensitivity simulations (i.e. the nudging was not a strong constraint). **Figure 6.6a** shows that the resulting impact on O_3 in TOMCAT simulation R1_2008 is small with changes less than 0.02%. The model produces a region of slight decrease in the very low stratosphere, with a region of slight increase above.

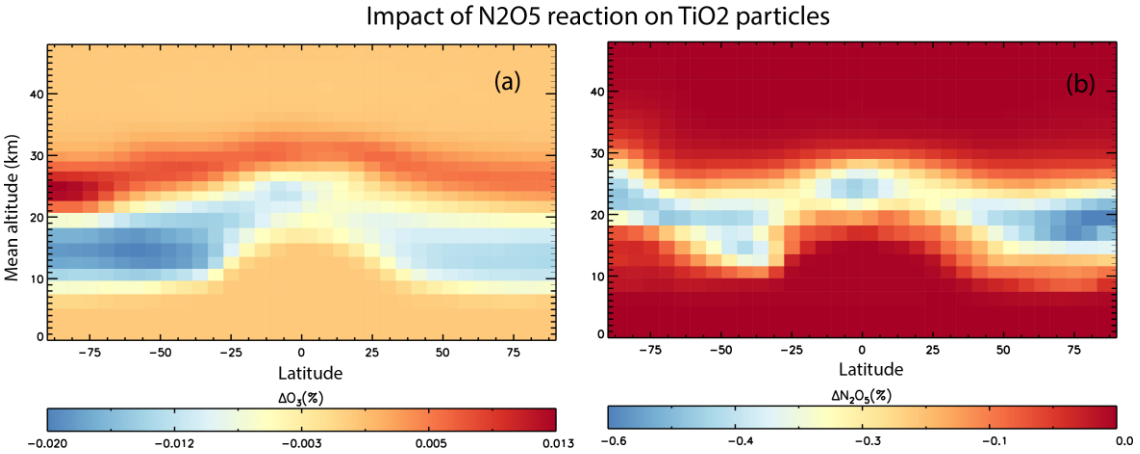

Figure 6.6. Annual mean zonal mean difference (%) in atmospheric **(a)** O_3 and **(b)** N_2O_5 for 2008 derived from TOMCAT simulation R1_2008 compared to simulation CNTL_2008 Figure also shown in Moon *et al.*, 2018.

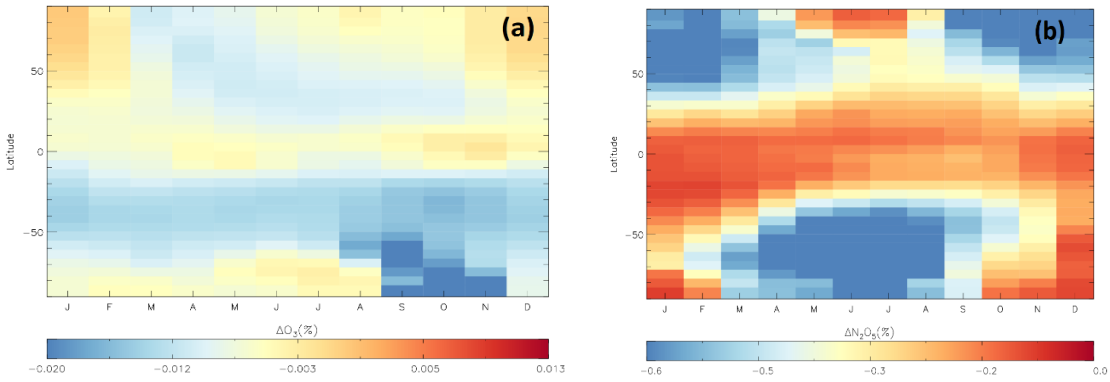

Figure 6.7. 2008 January-December monthly zonal mean difference mean at 20 km (%) vs latitude in atmospheric **(a)** O_3 and **(b)** N_2O_5 for derived from TOMCAT simulation R1_2008 compared to simulation CNTL_2008.

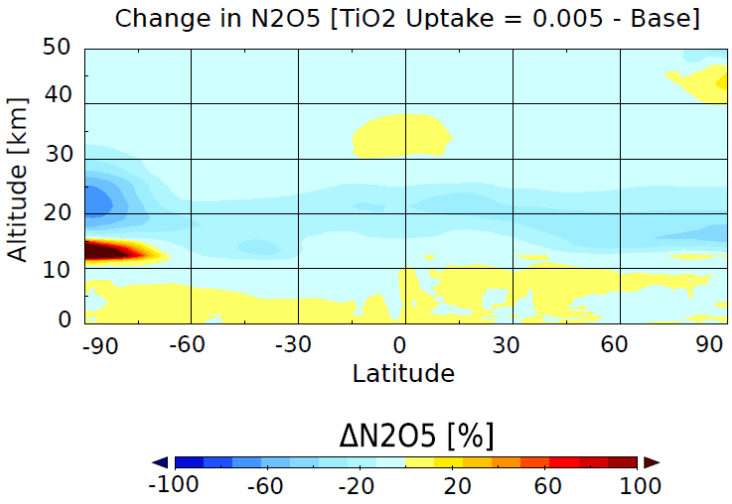

Figure 6.8. Simulated changes in N_2O_5 concentrations (%) caused by TiO_2 injection (see **Figure 6.9.**) with γ(R1)=0.005 using the UKCA nudged chemistry-climate model. Figure taken from Tang *et al.*, (2014).

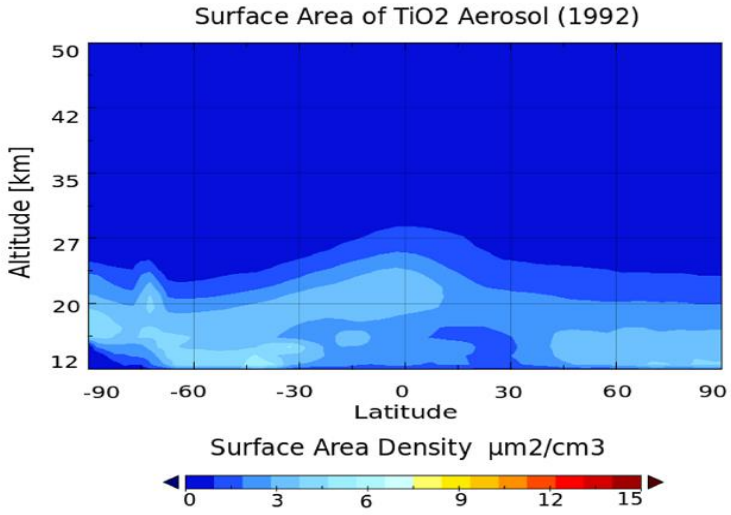

Figure 6.9. Surface area density (μm^2 cm^{-3}) of TiO_2 particles which is estimated to generate the same radiative effect as the sulfate particles derived from the Pinatubo eruption. Figure taken from Tang et al., 2014.

6.5.2 Reaction of HO_2

The effect of HO_2 uptake onto TiO_2 particles for stratospheric concentrations of HO_2 and O_3 was assessed using the TOMCAT model. At relative humidities (RH) relevant to the lower stratosphere (<40%) (Moon *et al.*, 2018) showed that $\gamma(HO_2)$ is in the range 0.020-

0.028 at 295 K. At stratospherically relevant temperatures (T = 200 - 220 K), $\gamma(HO_2)$ is likely to be considerably larger (Thornton *et al.*, 2008), due to a negative temperature dependence (Moon *et al.*, 2018) suggesting that considerably larger $\gamma(HO_2)$ values are realistic (Gershenzon *et al.*, 1995). Given this uncertainty, and to assess the extreme case, $\gamma(HO_2)$ = 1 was used in the model simulation R2_2008 to represent an upper limit (see **Table 6.1**).

It is evident that HO_2 loss due to heterogeneous reaction between HO_2 and TiO_2 particles in 2008 is <1% and is confined to the lower stratosphere where the assumed TiO_2 particles are located. **Figure 6.10a** shows that the subsequent effect of the TiO_2 particles on the O_3 concentrations through the effects of this reaction is also small (<0.1%), with a small decrease in the tropical upper troposphere/lower stratosphere and a small increase at all latitudes in the lower stratosphere. This small effect of TiO_2 particles on stratospheric HO_2 and O_3 concentrations is due to the reactive nature and short lifetime of HO_2 (order of seconds). The species readily reacts with other gas phase species (e.g. O_3) and so loss on TiO_2 surfaces does not compete significantly. The analysis of plots in **Figure 6.11** agrees with this interpretation. Therefore, loss of HO_2 was not considered in the further TOMCAT simulations.

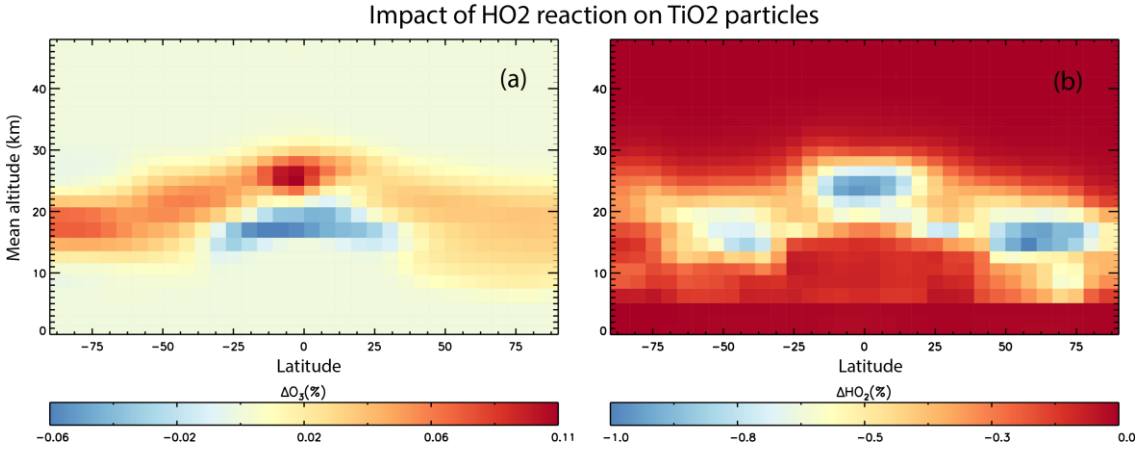

Figure 6.10. Annual mean zonal mean difference (%) in **(a)** O_3 and **(b)** HO_2 for 2008 from TOMCAT simulation R2_2008 compared to CNTL_2008. Figure also shown in (Moon et al., 2018).

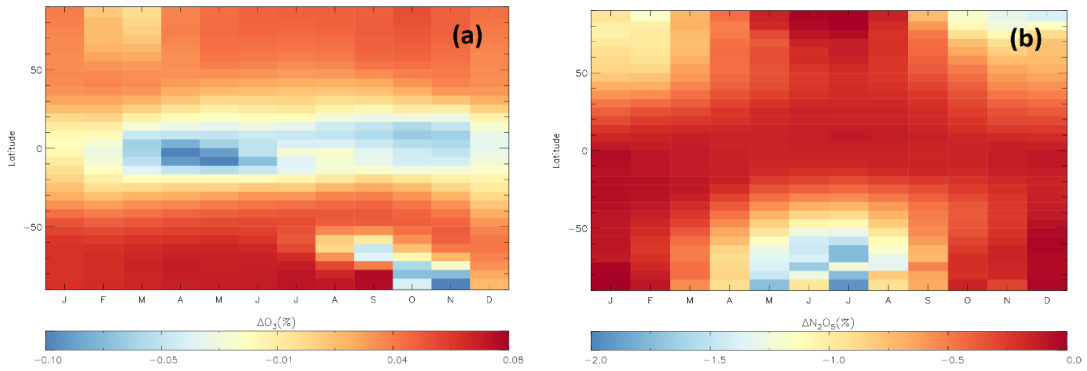

Figure 6.11. 2008 January-December monthly zonal mean difference mean at 20 km (%) vs latitude in atmospheric **(a)** O_3 and **(b)** N_2O_5 for derived from TOMCAT simulation R2_2008 compared to simulation CNTL_2008.

6.5.3 Chlorine activation reactions

A particularly important impact of the injection of TiO_2 particles may be due to their potential role in the activation of chlorine radicals which are very well known to cause depletion of stratospheric ozone, most notably in the Antarctic ozone hole (Seinfeld and Pandis, 2016; Farman, *et al.*, 1985). For this reason, simulations R3_2008 and R4_2008 (see **Table 6.1)** were performed with the treatment of heterogeneous processing of HCl and $ClONO_2$. The simulation results of R4_2008 are shown in **Figure 6.12.** and **Figure 6.13.**

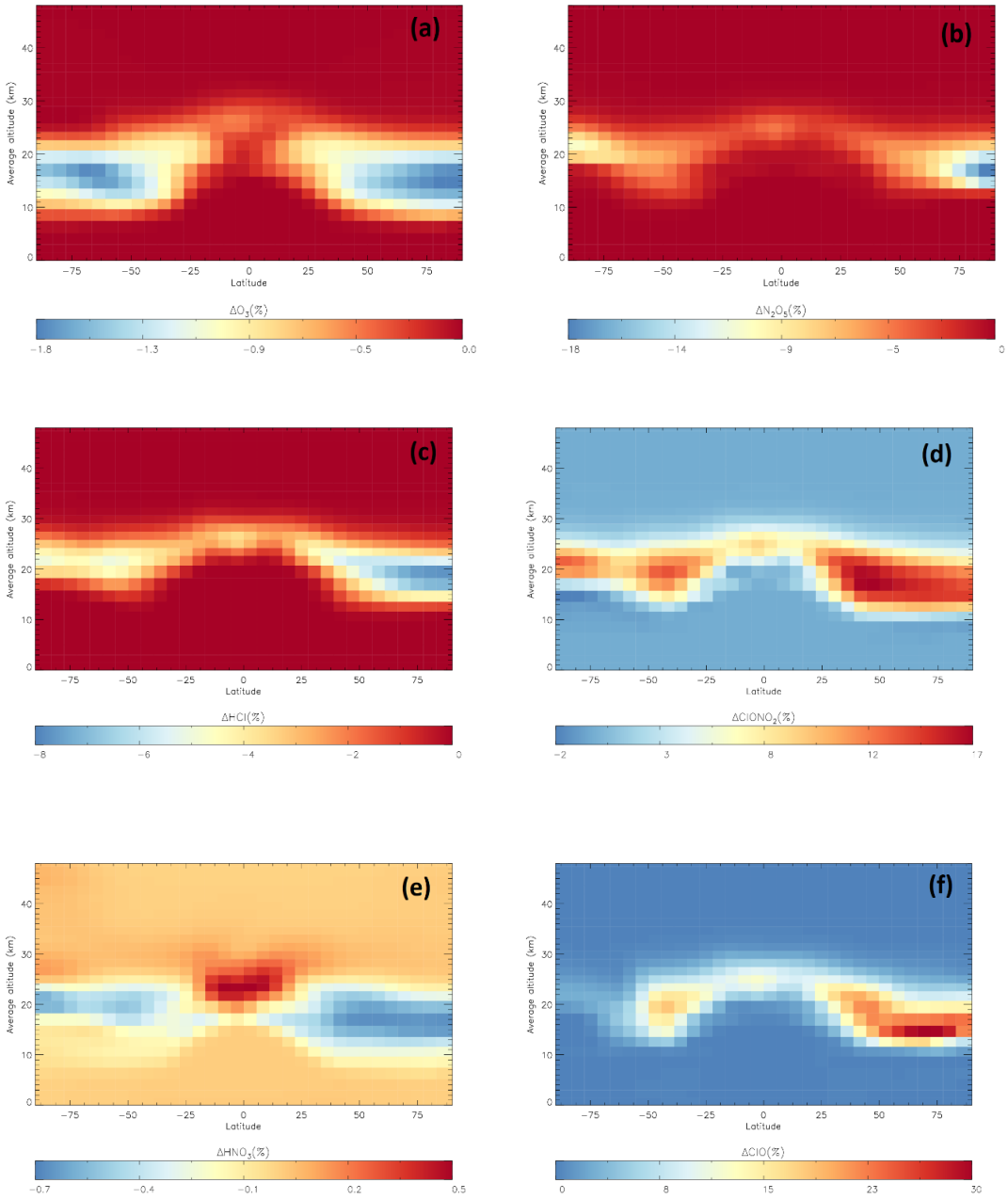

Figure 6.12. Annual mean zonal mean difference (%) in **(a)** O_3, **(b)** N_2O_5, **(c)** HCl, **(d)** $ClONO_2$, **(e)** HNO_3 and **(f)** ClO for 2008 from simulation R4_2008 compared to CNTL_2008.

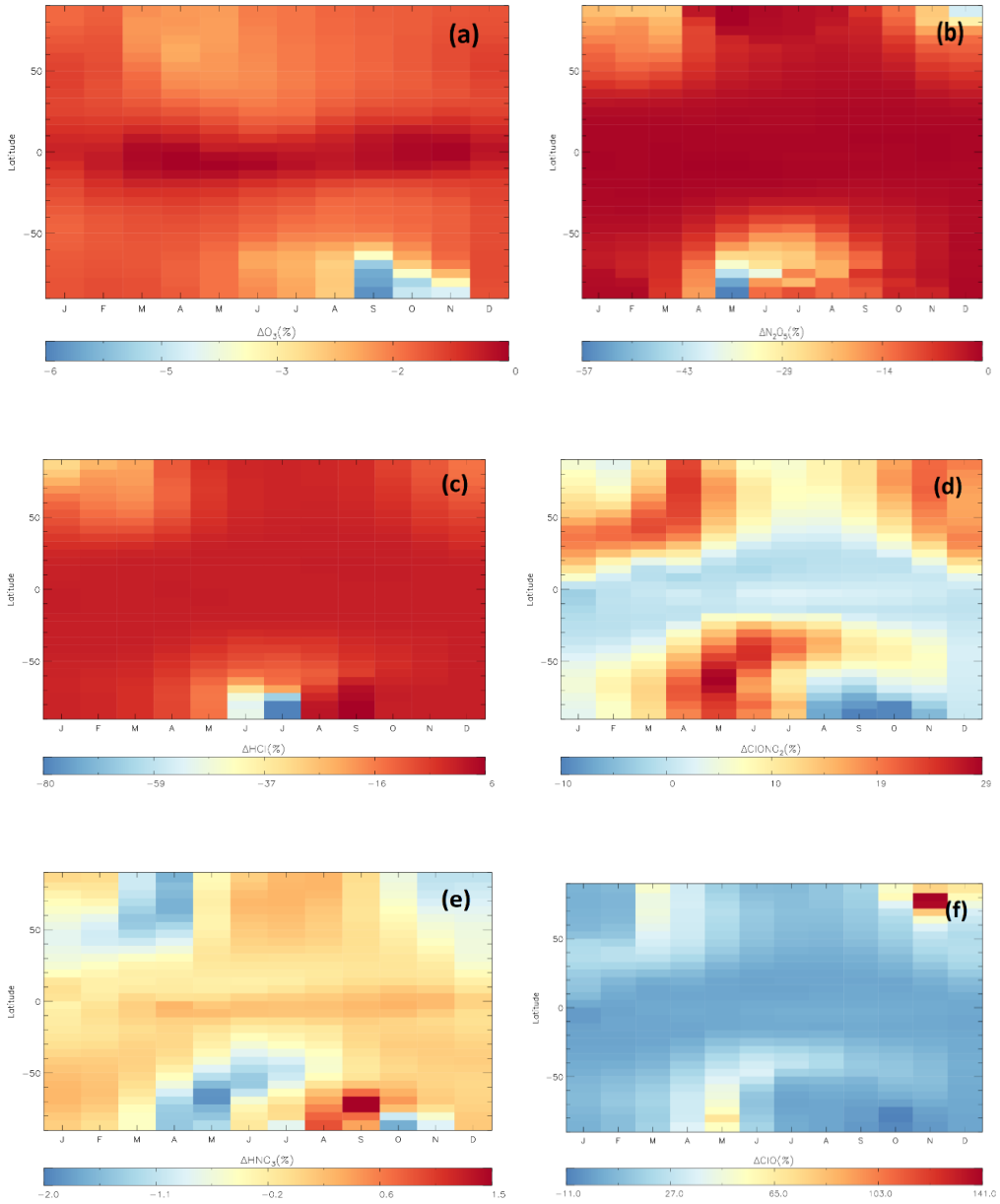

Figure 6.13. 2008 January-December monthly zonal mean difference mean at 20 km (%) versus latitude in atmospheric **(a)** O_3 and **(b)** N_2O_5 for derived from simulation R4_2008 compared to simulation CNTL_2008.

The 2008 O_3 annual change (**Figure 6.12a**) shows similar depletion patterns to the R1_2008 simulation although the inclusion of reaction R3 and R2 enhances the depletion up to -1.8%, between 10 and 20 km. The hydrolysis of $ClONO_2$ (R2) produces HNO_3 and reduce NO_x ($NO+NO_2$) which in turn depletes ozone, as the hydrolysis of N_2O_5 does (R1). Moreover, at extreme low temperatures (below 200 K) hydrolysis of $ClONO_2$ (R2) equals the contribution of R1 to deplete ozone (Fahey *et al.*, 1993). In our case, the ozone

reduction is, in absolute terms, more than double the reduction due to the sole R1 (-0.020%), suggesting that the additional effect is due to R3 via the reaction between reservoir $ClONO_2$ and HCl (Fahey, *et al.*, 1993). Furthermore, it is not surprising that the greatest ozone reduction is detected at the poles where temperatures below 200 K are normal during winter periods. More interestingly, the N_2O_5 concentration is strongly influenced by R2 and R3 as a comparison between **Figures 6.6b** and **6.12b** show. Although the N_2O_5 (**Figure 6.12b**) distribution follows the same as for R1_2008 (**Figure 6.6b**), the negative contribution is about an order of magnitude stronger up to -18% at the North Pole. To disentangle the role of R3 in this strong depletion, plots of O_3 and N_2O_5 from R3_2008 (**Table 6.1.**) are presented in **Figures 6.14.** and **6.15.**

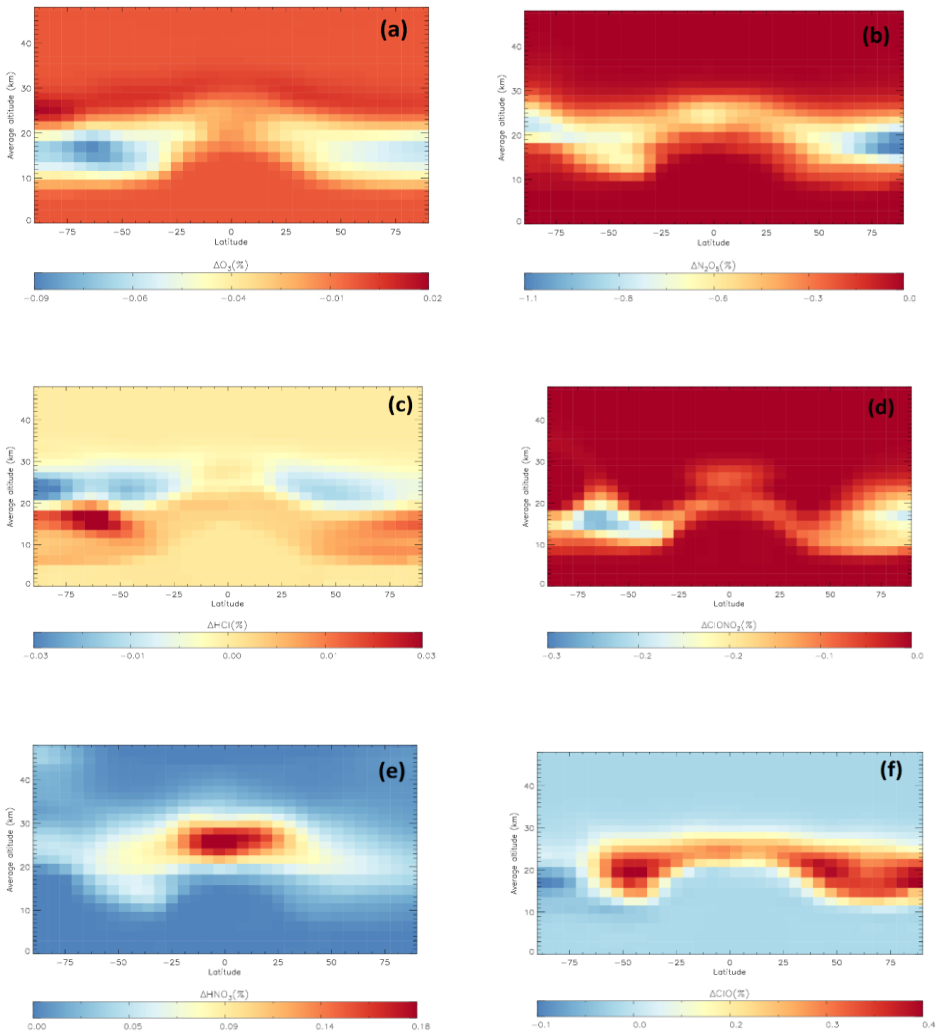

Figure 6.14. 2008 zonal mean difference (%) in **(a)** O_3, **(b)** N_2O_5, **(c)** HCl, **(d)** $ClONO_2$, **(e)** HNO_3 and **(f)** ClO from simulation R3_2008 compared to CNTL_2008.

.

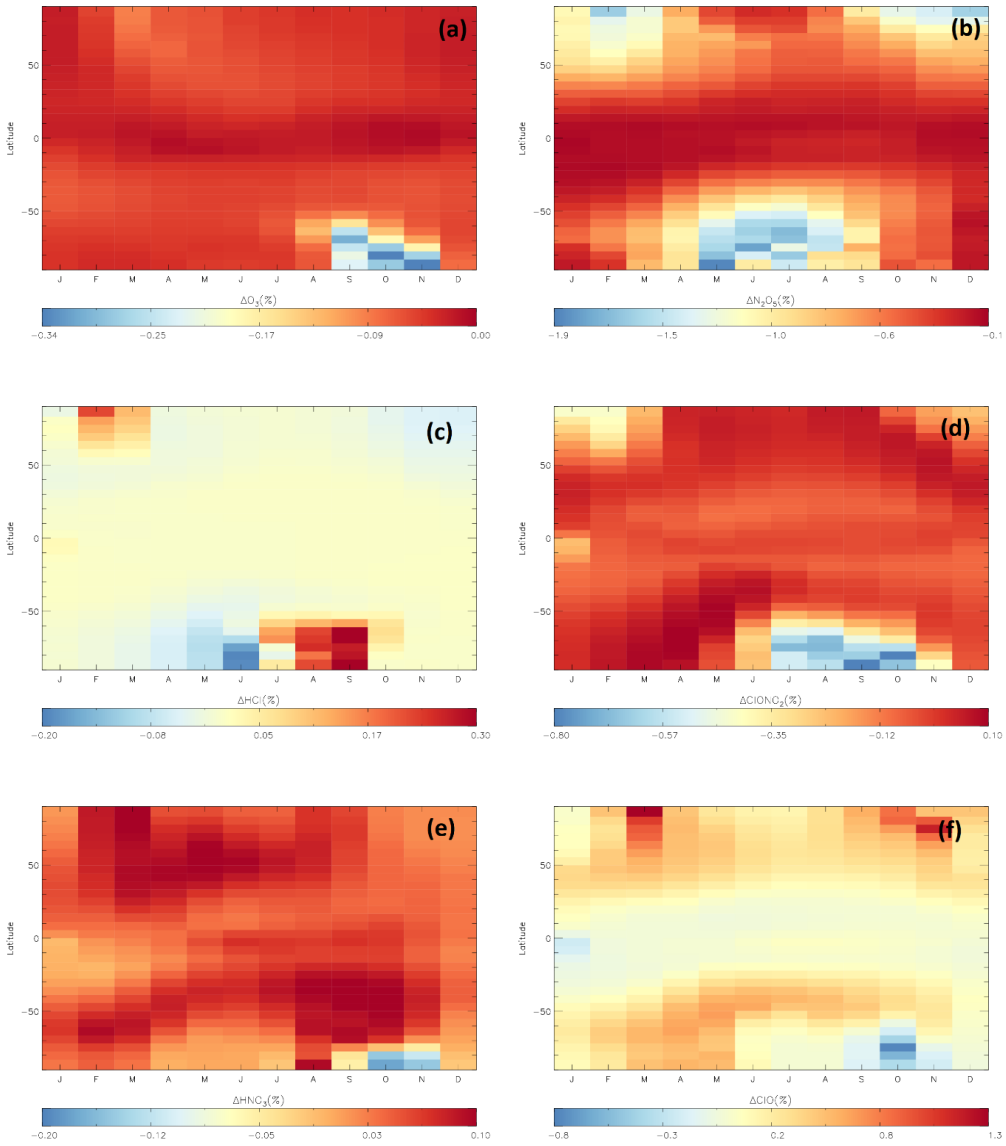

Figure 6.15. 2008 January-December monthly zonal mean difference mean at 20 km (%) versus latitude for atmospheric **(a)** O_3 and **(b)** N_2O_5 for derived from simulation R3_2008 compared to simulation CNTL_2008.

The minimum ozone value (**Figure 6.14a**) stays between the corresponding value for R1_2008 (-0.020%) and R4_2008 (-1.8%), although this value does not double the R1_2008 one, as previously explained. The difference should be due to the effect of inclusion of R3. While this is of minor importance for ozone, the jump from up -1.1%,

R3_2008 (**Figure 6.14b**), to up to -18% (**Figure 6.12b**) due to R4_2008 suggests the strong influence of the sole radical chlorine activation on the N_2O_5 balance. The reason behind that could be the effect of perturbation on the NO_x balance, a primary source of N_2O_5, due to the production of Cl_2 and ClO. (Fahey *et al.*, 1993).

6.5.4 Impact of TiO_2 Particles in a Future Atmosphere

As the effect of chlorine activation produced by the injection of TiO_2 particles, particularly via R3, is so relevant for ozone, TOMCAT simulations from 2000 until 2049 have been run including a TiO_2 particles field designed to "mimic" the same cooling effect recorded a year after Pinatubo eruption. The evaluation was focused on on O_3, N_2O_5, HCl and $ClONO_2$ (see reaction (R1), (R2) and (R3)). The negligible uptake of HO_2 on TiO_2 particles was not included in these simulations (see **Section 6.5.2**). In the lower stratosphere about 90% is contained (Seinfeld and Pandis, 2016) and consequently we focused our attention in 20 km level which is comprised in this layer. Moreover, the simulations involving the chlorine activation (R3_2008 and R4_2008) show that this level is affected by the ozone depletion the most, although up to a few percent (**Figures 6.12a** and **6.14a**).

To better understand the effect the injection of the TiO_2 particles on the chemistry of the ozone-relevant species $ClONO_2$, HCl, O_3 and N_2O_5 interannual variability of the mixing ratio plots are shown in **Figure 6.15.** for the Tropics ($-20^oN <$ latitude $< 20^oN$) and Antarctic regions (latitude $< -65^oN$). **Figure 6.15a** shows that the inclusion of reaction (R2) and (R3) causes a net increase in $ClONO_2$ especially in Antarctica. $ClONO_2$ is produced by re-combination of NO_2 and ClO (Fahey *et al.*, 1993). However, it is clear analysing **Figure 6.12b** and **Figure 6.16d** that N_2O_5 is negatively affected by TiO_2 particles injection. N_2O_5 forms through combination between NO_2 and NO_3, the latter produced in the reaction of NO_2 and ozone. Consequently, the sole effect of R2 on $ClONO_2$ should be a net reduction. The reason behind a net increase should be sought in the effect of R3 because it is worth noting that $ClONO_2$ is not touched (**Figure 6.16a**) by the nearly total depletion of N_2O_5 the year after every Pinatubo-like eruption (2012, 2022, 2032, ..., see also **Figure 6.16.**). Nevertheless, **Figure 6.15.** shows that, as expected, the absolute concentration of $ClONO_2$ is

reducing over time. The global decline of the stratospheric chlorine burden is also evident in the HCl mixing ratio (**Figure 6.16b**).

Figures 6.18. show the (%) interannual variability of $ClONO_2$, HCl, N_2O_5 and O_3 from 2000 until 2049 for Antarctic, Tropics (-20°N < latitude < 20°N) and Arctic (latitude > 65°N). The first thing to note is that, aside from $ClONO_2$, where the particles injection increase produces a net increment as shown above, all the other species show negative percent difference (%), meaning that the TiO_2 particles cause a net depletion, due to the adsorption of those species on the surface provided by them. The Arctic seems to be the most sensitive region. Moreover, the effect of TiO_2 uptake decreases with time, according to a scenario where atmospheric chlorine burden is reducing and thus removing the possibility of reactions (R2) and (R3) to occur. While O_3 and N_2O_5 decreases linearly with time toward 0%, HCl seems to converge asymptotically to about -7%, as it is possible to infer from **Figure 6.13c**. Comparing **Figure 6.6b** with **6.18d** draws the conclusion that including reactions (R2) and (R3) causes a general reduction of more than an order of magnitude of N_2O_5 in the Arctic, compared to the effect of the hydrolysis alone. Ozone does not seem to be particularly affected by the activation on chlorine radicals. Although the maximum depletion increases from -0.06% (**Figure 6.12a**) to -2.4% (**Figure. 6.18c**), it cannot be considered as a large effect. In addition, from **Figure 6.17d** is clear that TiO_2 particle injection is responsible for maximum 9% depletion of N_2O_5, while during large volcanic eruptions the value goes up to about 70 pptv (**Figure 6.16d**, Antarctic_control simulation), which leads to speculation that the uplift of sulfur particles has much more impact on N_2O_5, compared to TiO_2 particles. It is worth noting that the Tropics are left nearly intact from the injection of particles either sulfuric or mineral.

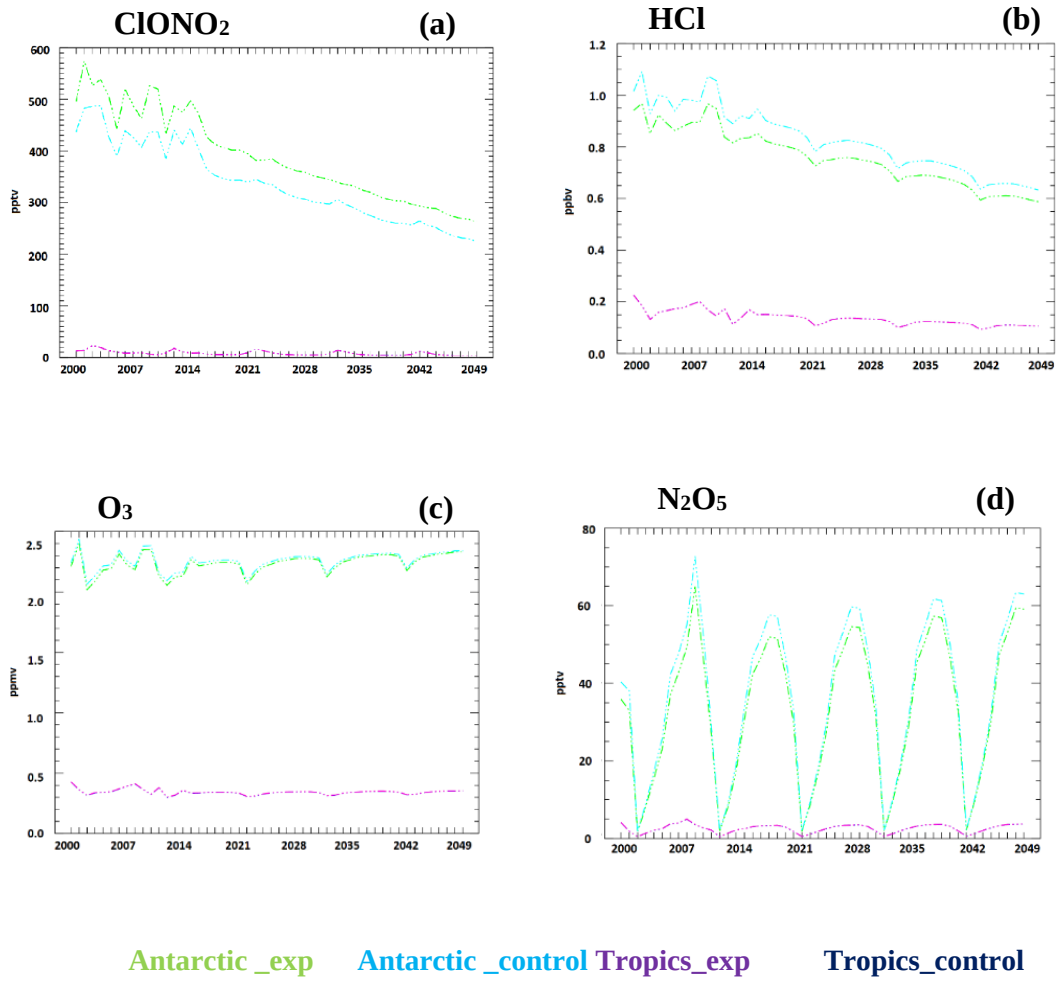

Figure 6.16.: Modelled annual mixing ratio (%) from 2000 to 2049 in **(a)** $ClONO_2$, **(b)** HCl, **(c)** O_3 and **(d)** N_2O_5 at 20 km.v**Antarctic_exp**, shows the model results including reaction (R1), (R2) and (R3), limited to Antarctica. **Tropics_exp,** same as **Antarctic_exp** but for the tropical region. Control runs in Antarctica and Tropics are indicated as **Antarctic_control** and **Tropics_control,** respectively.

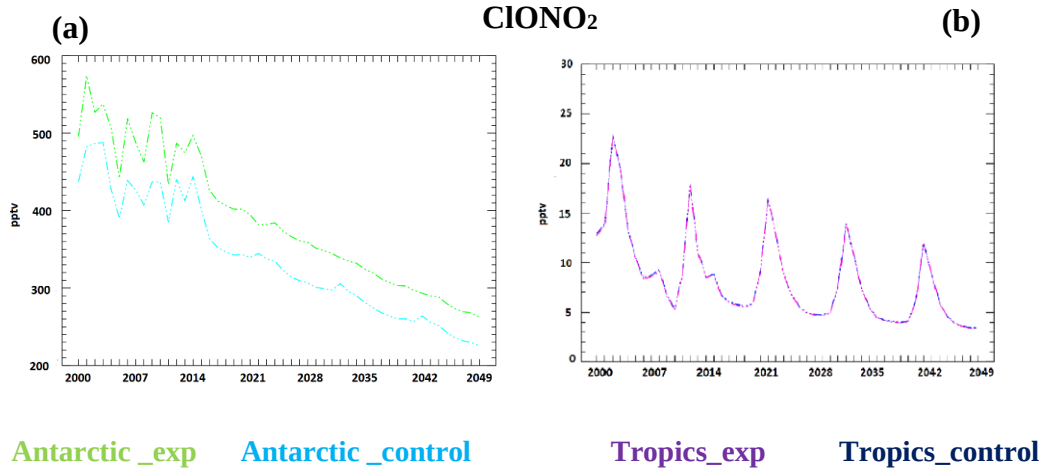

Figure 6.17. Enlargement of **Figure 6.16.a** for **(a)** Antarctica and **(b)** Tropics**.**

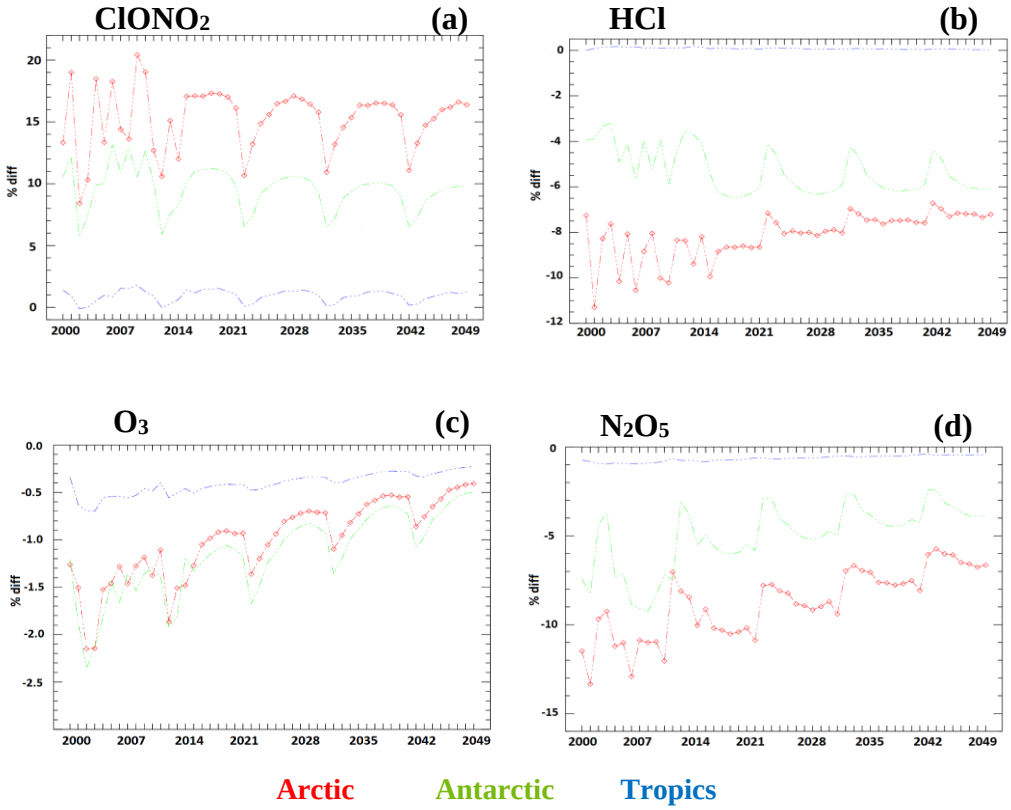

Figure 6.18. Annual mean zonal mean percent difference (%) between TOMCAT model experiment R3_2049 and control run CNTL_2049 from 2000 to 2049 at 20 km altitude for **(a)** $ClONO_2$, **(b)** HCl, **(c)** O_3 **(c)** and **(d)** N_2O_5. The experiment R4_2049 includes reactions (R1), (R2) and (R3) with coefficient uptakes described in the text (**Table 6.1**).

6.6 Summary

This chapter presented the results of the TOMCAT CTM simulations to evaluate the impact of the injection of TiO_2 particles on stratospheric chemistry, and in particular ozone. The first part of this study, whose results are presented in (Moon *et al.*, 2018), show the small effect of the uptake of both N_2O_5 and HO_2 (part of the ozone-destroying HO_x family) on the abovementioned particles, injected in a manner to "mimic" the same radiative effect as the 1991 Pinatubo eruptions. Although these results diverge from those shown in a recent previous study (Tang *et al.*, 2014), I am confident that the use of an off-line model avoids unrealistic feedback effects typical of CCM simulations. I find that the TOMCAT modelled stratospheric depletion is minimal (up to -0.06%).

The second part of this chapter has been devoted to the investigation of the long term effects (2000-2049) of the adsorption of stratospheric relevant chlorine species, namely $ClONO_2$ and HCl, on titanium dioxide particles. I found that a scenario where the emissions of chlorine are reducing and large volcanic eruptions occur every 10 years are appropriate for the scope. The overall modelling results suggest that related impact on the stratospheric ozone concentration is small. Latitudinal dependence is present but the impact is no larger than -2.5%. The concentration of $ClONO_2$ and HCl follows a steady decline, although $ClONO_2$ seems to be indirectly produced by the presence of the newly injected particles. In contrast, N_2O_5 shows remarkable opposite effect although a closer look show that sulfur injection caused by large volcanic eruptions play a much greater role.

The results shown in this chapter are limited by the paucity of recent laboratory coefficient uptakes, particularly for the reaction HCl + $ClONO_2$ (R3). However, the overall conclusion is that the chemical impact on the ozone layer of using TiO_2 particles for geoengineering is likely modest and will decrease with time as the chlorine loading decays. However, changes in stratospheric heating associated with the presence of the TiO_2 particles, which are not considered here, could affect the distribution of ozone through dynamical changes.

A possible microphysical interactions btw volcanic aerosol and TiO_2 particles cannot be *a priori* excluded. The eventuality of insoluble mineral dust particles, such as TiO_2 , to

be become cloud condensation nuclei when in contact with (convective) clouds and sulfates has been investigated (Yin *et al.,* 2002). This unexplored subject, in the context of SRM techniques, appears to be important especially in the event of large volcanic eruptions, where the plumes can reach the UTLS and where TiO_2 are located. Moreover, this kind of microphysical interactions are likely to occur in the Tropics especially in regions where the deep convection is more likely to happen, to say, the Indian Subcontinent, East Asia and the West Pacific (**Chapters 2** and **5**).

7 Conclusions

The final chapter of this thesis summarises the main results obtained during my PhD project and presented in **Chapters 4**, **5** and **6**. These results in turn address the research questions given in **Section 1.1**. This summary is provided in **Section 7.1**. Suggestions for follow-on studies and extensions of this work are provided in **Section 7.2**.

7.1 Summary

The TOMCAT 3-D CTM has been used throughout this work to evaluate the role of the vertical transport associated with the Asian summer monsoon (ASM), to transport species from surface to the UTLS. In conjunction with this, a study of the impact of TiO_2, a substance able to efficiently reflect solar radiation, on stratospheric ozone and chlorine has conducted.

In order to quantify the vertical transport of species due to the action of the ASM, a comprehensive diagnosis of the convection performance of the TOMCAT model was necessary. Motivated by a previous study which showed the relatively poor performance of the default Tiedtke convection scheme, this was replaced with a scheme based on ERA-Interim archived convective mass fluxes, in which the convection is calculated by the ECMWF model. Intercomparison with similar state-of-the-art chemical transport models, show that this “new” convective scheme largely improves both vertical and interhemispheric transport (**Section 4.2.1**). The analysis of a 1989-2017 simulation, designed using idealized tracers of 5, 25 and 50-day lifetimes, presents some interesting

aspects. The mixing ratio at 100 hPa, averaged over the ASM region is dominated by convective activity, but its effect is evident only for the shorter lived tracers (5- and 25-day lifetimes). This does not come as a surprise, because the convection timescale is on the order of days. Large volcanic eruptions, like Mt Pinatubo in 1991 have an apparent impact over the extent of the vertical transport (**Section 4.2.2**). While the test of the ERA-Interim archived mass fluxes, using age-of-air and other specific artificial tracers, gives clear evidence of the amelioration of the model, this is not the case when the same method is applied to a complex system like ASM. The correlation plots between the lifetime tracers (CO25, CO50, TR5 and TR50) and a widely used called WSI1, which is related to the convective activity over the Bay of Bengal (BoB), does not lead to clear conclusions.

In order to test the accuracy of the simulated distribution of chemical species in the UTLS the model needs to be validated by observations. In **Chapter 5**, comparison between water vapour, CO and temperature data from the StratoClim campaign have been performed (**Section 5.2**). The temperature measured by the M55 Geophysica, during the StratoClim campaign fits extremely well with the model temperature data, which are directly specified by the ECMWF ERA-Interim reanalyses. Unfortunately, these data when compared with in-situ FLASH water vapour data do not match very well, highlighting a negative bias (drier UTLS, in the Asian Monsoon region), confirming recently published results using balloon data. CO aircraft data have been tested against three convective scenarios (ERA-Interim convective mass fluxes (EICMF), Tiedtke scheme and no convection) to have a further evidence of performance of the new scheme developed here. The correlation between modelled and observed CO in this case is high and equal to 0.95.

CO is often used to identify the area which contributes most to transport to the upper troposphere. Two convective sources are usually identified as the main ones: the Tibetan Plateau (TP) and the BoB. Nevertheless, it is has not been established in the literature which one dominates. A three-step simulation for summer 2017 has been run, turning off the convection at each step either over TP, BoB or both. According to the results discussed here, the TP is the main contributor and its exclusion causes a reduction of about 50% of CO, compared to a normal scenario where convection occurs.

Section 5.3 presents some results of the 2013 ATTREX campaign, where measurements

of relevant halogenated species have been taken in the Eastern Pacific. The ATTREX campaign was designed to probe the UTLS abundances of a wide range of trace gases in a much more comprehensive way than StratoClim. Therefore, this dataset provided the best opportunity to investigate brominated VSLS over the timescale of this thesis. Simulations of TOMCAT/SLIMCAT with the new convective scheme based on archived mass fluxes agree well with UTLS observations of $CHBr_3$, CH_3Br, CH_2Br_2 and H-1211, the model agrees well with the observations. This confirms the injection of around 6 ppt bromine derived from VSLS into the stratosphere, but also shows that this cannot account in all cases for the amount of inorganic bromine observed in the lower stratosphere. Direct injection of significant levels (few ppt) of inorganic bromine appear to occur, as further discussed in Werner *et al*., (2017).

Concerns over climate change, has led many scientists and engineers to explore feasible options to try to limit its effects. Among them, the injection of highly reflective TiO_2 particles in the stratosphere has gained the attention of the researchers. In **Sections 6.5.1** and **6.5.2**, full-chemistry simulations have been run to see the effect of the surface provided by TiO_2 to initiate heterogeneous reactions which impact the overall stratospheric chemistry, in particular ozone. The TiO_2 burden was designed to reproduce the same cooling caused by the large Mt Pinatubo eruption in 1991. The simulations show that TiO_2 has a negligible impact on ozone (-0.06%) and on N_2O_5 and HO_2 which once transformed in NO_2 and OH can deplete ozone, even when the hydrolysis of $ClONO_2$ and the reaction $ClONO_2 + HCl + surface \rightarrow HNO_3 + Cl_2$ is included in the simulations. **Section 6.5.4** contains the results of a 2000-2049 simulation, conceived to see the effect of a permanent TiO_2 injection on the chlorine species in the stratosphere, which in turn can easily and rapidly destroy ozone. Large volcanic eruptions were assumed to occur every 10 years and the chlorine stratospheric loading steadily declines in accord with the Montreal Protocol. Modelled HCl follows this decline, while $ClONO_2$ slightly increases. Remarkably, N_2O_5 also increases, but maybe the net effect of TiO_2 is masked by the presence of sulfur generated by the large volcanic eruptions. It is worth emphasising that for they key reaction HCl + $ClONO_2$ (R3) in **Section 6.3,** accurate estimation of the coefficient are currently missing.

7.2 Future work

This study has helped to answer the questions posed in **Section 1.1**. Nevertheless, it has also given new insights on how to extend the research shown in this thesis. The new convective scheme improved the TOMCAT model in its ability to describe the transport in the UTLS. Linking the variability of species in the UTLS to the strength of the ASM requires an appropriate set of diverse indices describing, for example, dynamics, convection and rainfall. Future work in this regard could go in the simulation of improved idealized tropospheric tracers such as CO and HCN designed with realistic surface emissions. Such tracers are computationally cheap and can be run for long time periods, to study the interannual variability of the transport. Comparison with available satellite data (MLS, MIPAS) will help to validate the model.

Once the results from the StratoClim campaign are finalised, released and evaluated, they will drive modelling efforts toward detailed and targeted simulations aimed to describe the underlying mechanisms behind the ASM transport at UTLS levels and above. So far, the balloon water vapour data together with the analysis of FLASH data suggest to explore the potential of the ECMWF ERA5 dataset, not only in terms of water vapour. Its high horizontal (0.5° × 0.5°) and vertical resolutions (137 levels from surface to 1Pa, 80 km) will allow the models to study processes in the UTLS and above with improved accuracy.

The focus of the StratoClim campaign on the ASM region has prompted interest within the community. In particular, NASA and NSF in the USA are planning a similar campaign in summer 2020. The Asian Summer Monsoon Chemical and Climate Project (ACCLIP, PIs Laura Pan and Paul Newman, www2.acom.ucar.edu/acclip) will be based in Japan from July 15th to August 31st and use the NSF/NCAR GV and NASA WB-57 aircraft. These heavily instrumented aircraft will make extensive chemistry and aerosol measurements in an around the ASM. The campaign's primary goal is to 'investigate the impacts of Asian gas and aerosol emissions on global chemistry and climate via the linkage of ASM convection and associated large-scale dynamics' which will clearly extend on the basis provided by StratoClim.

Geoengineering techniques are being explored worldwide, also prompted by the current sensitivity of public opinion on the issues related to climate change. The simulations

performed for this study provide a positive feedback on the eventual use of TiO_2 for solar radiation management. However, laboratory evaluation of coefficient uptakes, particularly for chlorine-activating reactions are still missing. A growing number of modelling studies might encourage related laboratory studies which in turn would have the positive effect of improving the reliability of the simulations which test geo-engineering techniques. The implementation of any of these methods requires extra-care which is maybe unique in climate and atmospheric studies, due to the enormous implications that these have on the life of a huge number of individuals. For this reason an interplay between modelling and laboratory communities is crucial to pursue the ambitious aims which are inherent in geo-engineering itself.

8 References

Ammann, M., Cox, R. A., Crowley, J. N., Jenkin, M. E., Mellouki, A., Rossi, M. J., Troe, J., and Wallington, T. J. (2013) 'Evaluated kinetic and photochemical data for atmospheric chemistry: Volume VI - Heterogeneous reactions with liquid substrates', *Atmospheric Chemistry and Physics*, **13**(16), pp. 8045–8228. doi: 10.5194/acp-13-8045-2013.

Baldwin, M. P., Gray, L. J., Dunkerton, T. J., Hamilton, K., Haynes, P. H., Holton, J. R., Alexander, M. J., Hirota, I., Horinouchi, T., Jones, D. B. A., Marquardt, C., Sato, K., and Takahashi, M. (2001) 'The Quasi Biennal Oscillation', *Reviews of Geophysics*, **39**(2), pp. 179–229. doi :10.1029/1999RG000073

Belikov, D. A., Maksyutov, S., Krol, M., Fraser, A., Rigby, M., Bian, H., Agusti-Panareda, A., Bergmann, D., Bousquet, P, Cameron-Smith, P., Chipperfield, M. P., Fortems-Cheiney, A., Gloor, E., Haynes, K., Hess, P., Houweling, S., Kawa, S. R., Law, R. M., Loh, Z., Meng, L., Palmer, P. I., Patra, P. K., Prinn, R. G., Saito, R., and Wilson, C. (2013) 'Off-line algorithm for calculation of vertical tracer transport in the troposphere due to deep convection', *Atmospheric Chemistry and Physics*, **13,** pp. 1093–1114. doi: 10.5194/acp-13-1093-2013.

Benduhn, F,. and Lawrence, M. G. (2013) 'An investigation of the role of sedimentation for stratospheric solar radiation management', *Journal of Geophysical Research Atmospheres*, **118**(14), pp. 7905–7921. doi: 10.1002/jgrd.50622.

Bergman, J. W., Jensen, E. J., Pfister, L., and Yang, Q. (2012) 'Seasonal differences of vertical-transport efficiency in the tropical tropopause layer: On the interplay between tropical deep convection, large-scale vertical ascent, and horizontal circulations', *Journal of Geophysical Research Atmospheres*, **117**(5), pp. 1–20. doi: 10.1029/2011JD016992.

Bollasina, M. A., Ming, Y., and Ramaswamy, V. (2011) 'Anthropogenic Aerosols and the Weakening of the South Asian Summer Monsoon', *Science*, **334**(6055), pp. 502–505. doi: 10.1126/science.1204994.

Bolton, D., (1980) 'The Computation of Equivalent Temperature', *Monthly Weather Review,* **108**, pp. 1046-1053.

Bourassa, A. E., Robock, A., Randel, W. J., Deshler, T., Rieger, L. A., Lloyd, N. D., Llewellyn, E. J., and Degenstein, D. A. (2013) 'Response to Comments on "Large Volcanic Aerosol Load in the Stratosphere Linked to Asian Monsoon Transport', *Science*, **339**(6120), pp. 647–647. doi: 10.1126/science.1227961.

Brewer, A. W. (1949) 'Evidence for a world circulation provided by the measurements of helium and water vapour distribution in the stratosphere', *Quarterly Journal of the Royal Meteorological Sociery*, **75**, pp. 351–363.

Brunamonti, S., Jorge, T., Oelsner, P., Hanumanthu, S., Singh, B. S., Kumar, K. R., Sonbawne, S., Meier, S., Singh, D., Wienhold, F. G., Luo, B. P., Boettcher, M., Poltera, Y., Jauhiainen, H., Kayastha, R., Karmacharya, J., Dirksen, R., Naja, M., Rex, M., Fadnavis, S., and Peter, T., (2018) 'Balloon-borne measurements of temperature, water vapor, ozone and aerosol backscatter at the southern slopes of the Himalayas during StratoClim 2016-2017', **18**, pp. 15937–15957. doi: 10.5194/acp-2018-222.

Brunamonti, S., Füzér, L., Jorge, T., Poltera, Y., Oelsner, P., Meier, S., Dirksen, R., and Naja, M. (2019) 'Water Vapor in the Asian Summer Monsoon Anticyclone : Comparison of Balloon-Borne Measurements and ECMWF Data', *Journal of Geophysical Research Atmospheres*, **124**, pp. 7053–7068. doi: 10.1029/2018JD030000.

Burkholder, J., Sander, S. P., Abbatt, J., Barker, J. R., Huie, R. E., Kolb, C. E, and Wine, P. H. (2015) 'Chemical Kinetics and Photochemical Data for Use in Atmospheric Studies–Evaluation Number 18', *Nasa panel for data evaluation technical report*, **17**(10), pp. 1135–1151. doi: 10.1002/kin.550171010.

Burroughs, W. J. (1999) *The Climate Revealed*. Cambridge, UK: Cambridge University Press.

Butchart, N. (2014) 'The Brewer-Dobson circulation', *Review of Geophysics*, **52**, pp. 157–184. doi: 10.1002/2013RG000448.

Butler, J. H., Bell, T. G., Hall, B. D., Quack, B., Carpenter, L. J., and Williams, J. (2010) 'Technical Note: Ensuring consistent, global measurements of very short-lived halocarbon gases in the ocean and atmosphere', *Atmospheric Chemistry and Physics*, **10**(2), pp. 327–330. doi: 10.5194/acp-10-327-2010.

Canty, T., Mascioli, N. R., Smarte, M. D., and Salawitch, R. J. (2013) 'An empirical model of global climate – Part 1: A critical evaluation of volcanic cooling', *Atmospheric Chemistry and Physics*, **13**(8), pp. 3997–4031. doi: 10.5194/acp-13-3997-2013.

Carver, G. D., Brown, P. D., and Wild, O. (1997) 'The ASAD atmospheric chemistry integration package and chemical reaction database', *Computer Physics Communications*, **105**, pp. 197–215. doi: 10.1016/S0010-4655(97)00056-8.

Charney, J. G., and Drazin, P. G. (1961) 'Propagation of planetary-scale disturbances from the lower into the upper atmosphere', *Journal of Geophysical Research*, **66**(1), pp. 83–109. doi: 10.1029/JZ066i001p00083.

Chen, B., Xu, X. D., Yang, S., and Zhao, T. L. (2012) 'Climatological perspectives of air transport from atmospheric boundary layer to tropopause layer over Asian monsoon regions during boreal summer inferred from Lagrangian approach', *Atmospheric Chemistry and Physics*, **12**(13), pp. 5827–5839. doi: 10.5194/acp-12-5827-2012.

Chipperfield, M. P., Cariolle, D., and Simon, P. (1993) 'A Three-Dimensional Modeling Study of Trace Species in the Arctic Lower Stratosphere During Winter 1989-1990', *Journal of Geophysical Research*, **98**(92), pp. 7199–7218. doi: 10.1029/92JD02977

Chipperfield, M. P. (1999) 'Multiannual simulations with a three-dimensional chemical transport model', *Journal of Geophysical Research Atmospheres*, **104**(D1), pp. 1781–1805. doi: 10.1029/98JD02597.

Chipperfield, M. P., (2006a) 'The TOMCAT/SLIMCAT Off-Line 3D CTM User's Manual'. Available at: http://homepages.see.leeds.ac.uk/~lecmc/papers/uniman0.8.pdf.

Chipperfield, M. P. (2006b) 'New version of the TOMCAT/SLIMCAT off-line chemical transport model: Intercomparison of stratospheric tracer experiments', *Quarterly Journal*

of the Royal Meteorological Society, **132**(617), pp. 1179–1203. doi: 10.1256/qj.05.51.

Chipperfield, M. P., Dhomse, S., Feng, W., McKenzie, R. L., Velders, G. J. M., and Pyle, J. A. (2015) 'Quantifying the ozone and ultraviolet benefits already achieved by the Montreal Protocol', *Nature Communications*. Nature Publishing Group, **6**(May), pp. 1–8. doi: 10.1038/ncomms8233.

Chipperfield, M. P., Bekki, S., Dhomse, S., Harris, N. R. P., Hassler, B., Hossaini, R., Steinbrecht, W., Thiéblemont, R., and Weber, M. (2017) 'Detecting recovery of the stratospheric ozone layer', *Nature*, **549**(7671), pp. 211–218. doi: 10.1038/nature23681.

Connor, F. M. O., Johnson, C. E., Morgenstern, O., Abraham, N. L., Braesicke, P., Dalvi, M., and Folberth, G. A. (2014) 'Evaluation of the new UKCA climate-composition model – Part 2 : The Troposphere', *Geoscientific Model Development*, **7**, pp. 41–91. doi: 10.5194/gmd-7-41-2014.

Crutzen, P. J. (2006) 'Albedo enhancement by stratospheric sulfur injections: A contribution to resolve a policy dilemma?', *Climatic Change*, **77**(3–4), pp. 211–219. doi: 10.1007/s10584-006-9101-y.

De Bort, L. T. (1902) 'Variations de la temperature de l'air libre dans la zone comprise entre 8 km et 13 km d'altitude', *Comptes rendus de l'Académie des Sciences de Paris*, **134**, pp. 978–989.

Dee, D. P., Uppala, S. M., Simmons, A. J., Berrisford, P., Poli, P., Kobayashi, S., Undrae, U., Balmaseda, M. A., Balsoamo, G., Bauer, P., Bechtold P., Beljaars, A. C. M., van de Berg, L., Bidlot, J., Bormann, N., Delsol, C., Dragani, R., Fuentes, M., Geera, A. J., Haimberger, L., Healy, S. B., Hersbach, H., Holm, E. V., Isaksen, L., Kallberg, P., Kohler, M., Matricardi, M., McNally, A. P., Monge-Sanz , B. M., Morcrette, J.-J., Park, B.-K., Peubey, C., de Rosnay, P., Tavolato, C., Thepaut, J.-N., and Vitart, F. (2011) 'The ERA-Interim reanalysis : configuration and performance of the data assimilation system', *Quarterly Journal of the Royal Meteorological Society*, **137**, pp. 553–597. doi: 10.1002/qj.828.

Dethof, A., O'Neill, A., Slingo, J. M., and Smit, H. G. J. (1999) 'A mechanism for moistening the lower stratosphere involving the Asian summer monsoon', *Quarterly Journal of the Royal Meteorological Society*, **125**(556), pp. 1079–1106. doi: 10.1002/qj.1999.49712555602.

Devasthale, A., and Fueglistaler, S. (2010) 'A climatological perspective of deep convection penetrating the TTL during the Indian summer monsoon from the AVHRR and MODIS instruments', *Atmospheric Chemistry and Physics*, **10**(10), pp. 4573–4582. doi: 10.5194/acp-10-4573-2010.

Dobson, G. M. B. (1956) 'Origin and distribution of the polyatomic molecules in the atmosphere', *Proceedings of the Royal Society A: Mathematical, Physical and Engineering Sciences*, **236**, pp. 187–193.

Dutton, E. G., and Christy, J. R. (1992) 'Solar radiative forcing at selected locations and evidence for global lower tropospheric cooling following the eruptions of El Chichón and Pinatubo', *Geophysical Research Letters*, **19**(23), pp. 2313–2316. doi: 10.1029/92GL02495.

ECMWF (2018) *What are the differences changes from ERA-Interim to ERA5?* Available : https://confluence.ecmwf.int//pages/viewpage.action?%0ApageId=74764925 (accessed 20 November 2019).

Eliasen, E. B., Machenhauer, B., and Rasmussen, E. (1970) 'On a numerical method for integration of the hydrodymical equations with a spectral representation of the horizontal fields. Rep. No. 2', Copenaghen, Denmark: Institut for Teoretisk Meteorologi, Kobenhavns Universitet.

Eyring, V., Shepherd, T., and Waugh, D. (2010) *SPARC, 2010: SPARC CCMVal Report N°5 Chemistry-Climate Validation.* Available at: www.sparc-climate.org/publications/sparc-reports/ (accessed 20 Novembe 2019).

Fahey, D. W., Kawa, S. R., Woodbridge, E. L., Tin, P., Wilson, J. C., Jonsson, H. H., Dye, J. E., Baumgardner, D., Borrmann, S., Toohey, D. W., Avallone, L. M., Proffitt, M.

H., Margitan, J., Loewenstein, M., Podolske, J. R., Salawitch, R. J., Wofsy, S. C., Ko, M. K. W., Anderson, D. E., Schoeber, M. R., and Chan, K. R. (1993) 'In situ measurements constraining the role of sulphate aerosols in mid-latitude ozone depletion', *Letters to Nature*, **363**, pp. 509–514.

Farman, J. C., Gardiner, B. G., and Shanklin, J. D. (1985) 'Large losses of total ozone in Antarctica reveal seasonal ClO_x/NO_x interaction', *Nature*, **315**(6016), pp. 207–210. doi: 10.1038/315207a0.

Feng, W., Chipperfield, M. P., Dhomse, S., Monge-Sanz, B. M., Yang, X., Zhang, K., and Ramonet, M. (2011) 'Evaluation of cloud convection and tracer transport in a three-dimensional chemical transport model', *Atmospheric Chemistry and Physics*, **11**(12), pp. 5783–5803. doi: 10.5194/acp-11-5783-2011.

Ferraro, A. J., Highwood, E. J., and Charlton-Perez, A. J. (2011) 'Stratospheric heating by potential geoengineering aerosols', *Geophysical Research Letters*, **38**(24), pp. 1–6. doi: 10.1029/2011GL049761.

Fischer, H., Birk, M., Blom, C., Carli, B., Carlotti, M., Clarmann, T., Von Delbouille, L., Dudhia, A., and Ehhalt, D. (2008) 'MIPAS : an instrument for atmospheric and climate research', *Atmospheric Chemistry and Physics*, **18**, pp. 15937–15957.

Fleming, J. R. (2010) *Fixing the sky: the checkered history of weather and climate control*. New York, USA: Columbia University Press.

Forster, P. M. D. F., and Shine, K. P. (1999) 'Stratospheric water vapour changes as a possible contributor to observed stratospheric cooling', *Geophysical Research Letters*, **26**(21), pp. 3309–3312. doi: 10.1029/1999GL010487.

Forster, P. M. D. F., and Shine, K. P. (2002) 'Assessing the climate impact of trends in stratospheric water vapor', *Geophysical Research Letters*, **29**(6), pp. 10-1-10–4. doi: 10.1029/2001GL013909.

Fromm, M., Nedoluha, G., and Charvat, Z. (2013) 'Comments on "Large Volcanic Aerosol Load in the Stratosphere Linked to Asian Monsoon Transport"', *Science*,

339(6120), pp. 647–647. doi: 10.1126/science.1227961.

Fu, R., Hu, Y., Wright, J. S., Jiang, J. H., Dickinson, R. E., Chen, M., Filipiak, M., Read, W. G., Waters, J. W., and Wu, D. L. (2006) 'Short circuit of water vapor and polluted air to the global stratosphere by convective transport over the Tibetan Plateau', *Proceedings of the National Academy of Sciences*, **103**(15), pp. 5664–5669. doi: 10.1073/pnas.0601584103.

Fueglistaler, S., Dessler, A. E., Dunkerton, T. J., Folkins, I., Fu, Q., and Ote, P. W. (2009) 'Tropical tropopause layer', *Review of Geophysics*, **47**(RG1004), doi(2008), p. 101029/. doi: 10.1029/2008RG000267.1.INTRODUCTION.

Garfinkel, C. I., and Hartmann, D. L. (2010) 'Influence of the quasi-biennial oscillation on the North Pacific and El Niño teleconnections', *Journal of Geophysical Research Atmospheres*, **115**(June), pp. 1–12. doi: 10.1029/2010JD014181.

Garny, H., and Randel, W. J. (2013) 'Dynamic variability of the Asian monsoon anticyclone observed in potential vorticity and correlations with tracer distributions', *Journal of Geophysical Research Atmospheres*, **118**(24), pp. 13421–13433. doi: 10.1002/2013JD020908.

Garrat, J., (1994) *The Atmospheric Boundary Layer*. Cambridge, UK: Cambridge University Press.

Gershenzon, Y. M., Grigorieva, V. M., Ivanov, A. V., and Remorov, R. G. (1995) 'O3 and OH sensitivity to heterogeneous sinks of HO_x and CH_3O_2 on aerosol particles', *Faraday Discussions*, **100**, p. 83-100. doi: 10.1039/fD9950000083

Gettelman, A., Kinnison, D. E., Dunkerton, T. J., and Brasseur, G. P. (2004) 'Impact of monsoon circulations on the upper troposphere and lower stratosphere', *Journal of Geophysical Research D: Atmospheres*, **109**(22), pp. 1–14. doi: 10.1029/2004JD004878.

Gettelman, A., Hegglin, M. I., Son, S. ‐ W., Kim, J., M. Fujiwara, M., Birner, T., Kremser, S., Rex, M., Añel, J. A., Akiyoshi, H., Austin, J., Bekki, S., Braesike, P., Brühl,

C., Butchart, N., Chipperfield, M., Dameris, M.,Dhomse, S., Garny, H., Hardiman, S. C., Jöckel, P., Kinnison, D. E., Lamarque, J. F., Mancini, E., Marchand, M., Michou, M., Morgenstern, O., Pawson, S., Pitari, G., Plummer, D., Pyle, J. A., Rozanov, E., Scinocca, J., Shepherd, T. G., Shibata, K., Smale, D., Teyssèdre, H., and Tian, W. (2010) 'Multimodel assessment of the upper troposphere and lower stratosphere: Tropics and global trends', *Journal of Geophysical Research*, **115**, p. D00M08. doi: 10.1029/2009JD013638.

Gettelman, A., Pan, L. L., Randel, W. J., Hoor, P., Birner, T., and Hegglin, M. I. (2011) 'the Extratropical Upper Troposphere and Lower Stratosphere', *Reviews of Geophysics*, **49**(3), pp. 1–31. doi: 10.1029/2011RG000355.1.INTRODUCTION.

Grant, W. B., Browel, E. V., Fishman, J., Brackett, V. G., Veiga, R. E., Neganga, D., Minga, A., Cros, B., Butler, C. F., Fenn, M. A., Craig, L. S., and Larry, S. L. (1994) 'Aerosol-associated changes in tropical stratospheric ozone following the eruption of Mount Pinatubo', *Journal of Geophysical Research*, **99**(D4), pp. 8197–8211. doi: 10.1029/93JD03314.

Hall, T. M., and Plumb, R. A. (1994) 'Age as a diagnostic of startospheric transport', *Journal of Geophysical Research*, **99**(D1), pp. 1059–1070. doi :10.1029/93JD03192

Heath, N. K. and Fuelberg, H. E. (2014) 'Using a WRF simulation to examine regions where convection impacts the Asian summer monsoon anticyclone', *Atmospheric Chemistry and Physics*, **14**(4), pp. 2055–2070. doi: 10.5194/acp-14-2055-2014.

Held, I. M. (1982) 'On the Height of the Tropopause and the Static Stability of the Troposphere', *Journal of the Atmospheric Sciences*, **39**, pp. 412–417. doi: 10.1175/1520-0469(1982)039<0412:OTHOTT>2.0.CO;2.

Highwood, E. J., and Hoskins B. J. (1998) 'The tropical tropopause', *Quarterly Journal of the Royal Meteorological Society*, **124**, pp. 1579-1604. doi: 10.1002/qj.49712454911

Holton, J. R., Haynes, P. H., McIntyre, M. E., Douglass, A. R., Rood, R. B., and Pfister, L. (1995) 'Stratosphere-troposphere exchange', *Reviews of Geophysics*, **33**(4), pp. 403–

439. doi: 10.1029/95RG02097.

Holton, J. R., (2004) '*An Introduction to Dynamic Meteorology*', 3rd edition. Amsterdam: Amsterdam: Elsevier Academic Press.

Holtslag, A. A. M., and Boville, B. A. (1993) 'Local versus nonlocal boundary-layer diffusion in a global climate model', *Journal of Climate*, **6**, pp. 1825–1842. doi: 10.1175/1520-0442(1993)006<1825:LVNBLD>2.0.CO;2.

Holzer, M., and Hall, T. M. (2000) 'Transit-Time and Tracer-Age Distributions in Geophysical Flows', *Journal of the Atmospheric Sciences*, **57**(21), pp. 3539–3558. doi: 10.1175/1520-0469(2000)057<3539:TTATAD>2.0.CO;2.

Holzer, M., and Waugh, D. W. (2015) 'Interhemispheric transit time distributions and path-dependent lifetimes constrained by measurements of SF_6 , CFCs , and CFC replacements', *Geophysical Research Letters*, **42**, pp. 4581–4589. doi: doi: 10.1002/2015GL064172.

Homan, C. D., Volk, C. M., Kuhn, A. C., Werner, A., Baehr, J., Viciani, S., Ulanovski, A., and Ravegnani, F. (2010) 'Tracer measurements in the tropical tropopause layer during the AMMA/SCOUT-O3 aircraft campaign', *Atmospheric Chemistry and Physics*, **10**, pp. 3615–3627.

Höpfner, M., Volkamer, R., Grabowski, U., Grutter, M., Orphal, J., Stiller, G., Von Clarmann, T., and Wetzel, G. (2016) 'First detection of ammonia (NH_3) in the Asian summer monsoon upper troposphere', *Atmospheric Chemistry and Physics*, **16**(22), pp. 14357–14369. doi: 10.5194/acp-16-14357-2016.

Hossaini, R., Chipperfield, M. P., Monge-Sanz, B. M., Richards, N. A. D., Atlas, E., and Blake, D. R. (2010) 'Bromoform and dibromomethane in the tropics: a 3-D model study of chemistry and transport', *Atmospheric Chemistry and Physics Discussions*, **10**(4), pp. 719–735. doi: 10.5194/acpd-9-16811-2009.

Hossaini, R., Chipperfield, M. P., Feng, W., Breider, T. J., Atlas, E., Montzka, S. A., Miller, B. R., Moore, F., and Elkins, J. (2012) 'The contribution of natural and

anthropogenic very short-lived species to stratospheric bromine', *Atmospheric Chemistry and Physics*, **12**(1), pp. 371–380. doi: 10.5194/acp-12-371-2012.

Hossaini, R., Patra, P. K., Leeson, A. A., Krysztofiak, G., Abraham, N. L., Andrews, S. J., Archibald, A. T., Aschmann, J., Atlas, E. L., Belikov, D. A., Bönisch, H., Carpenter, L. J., Dhomse, S., Dorf, M., Engel, A., Feng, W., Fuhlbrügge, S., Griffiths, P. T., Harris, N. R. P., Hommel, R., Keber, T., Krüger, K., Lennartz, S. T., Maksyutov, S., Mantle, H., Mills, G. P., Mille, B., Montzka, S. A., Moore, F., Navarro, M. A., Oram, D. E., Pfeilsticker, K., Pyle, J. A., Quack, B., Robinson, A. D., Saikawa, E., Saiz-Lopez, A., Sala, S., Sinnhuber, B.-M., Taguchi, S., Tegtmeier, S., Lidster, R. T., Wilson, C., and Ziska, F. (2016) 'A multi-model intercomparison of halogenated very short-lived substances (TransCom-VSLS): Linking oceanic emissions and tropospheric transport for a reconciled estimate of the stratospheric source gas injection of bromine', *Atmospheric Chemistry and Physics*, **16**(14), pp. 9163–9187. doi: 10.5194/acp-16-9163-2016.

Hossaini, R., Chipperfield, M. P., Montzka, S. A., Leeson, A. A., Dhomse, S., and Pyle, J. A. (2017) 'The increasing threat to stratospheric ozone from dichloromethane', *Nature Communications*. Nature Publishing Group, **8**(May), pp. 1–9. doi: 10.1038/ncomms15962.

Hourdin, F., Musat, I., Bony, S., Braconnot, P., Codron, F.Dufresne, J.-L., Fairhead, L., Filiberti, M.-A., Friedlingstein, P.Grandpeix, J.-Y., Krinner, G., LeVan, P., Li, Z.-X., and L.and F. (2006) 'The LMDZ4 general circulation model : climate performance and sensitivity to parametrized physics with emphasis on tropical convection', *Climate Dynamics*, **27**, pp. 787–813. doi: 10.1007/s00382-006-0158-0.

Hourdin, F., Grandpeix, J. Y., Rio, C., Bony, S., Jam, A., Cheruy, F., Rochetin, N., Fairhead, L., Idelkadi, A., Musat, I., Dufresne, J. L., Lahellec, A., Lefebvre, M. P., and Roehrig, R. (2013) 'LMDZ5B : the atmospheric component of the IPSL climate model with revisited parameterizations for clouds and convection', *Climate Dynamics*, **40**, pp. 2193–2222. doi: 10.1007/s00382-012-1343-y.

Huneeus, N., Schulz, M., Balkanski, Y., Griesfeller, J., Prospero, J., Kinne, S., Bauer, S., Boucher, O., Chin, M., Dentener, F., Diehl, T., Easter, R., Fillmore, D., Ghan, S., Ginoux,

P., Grini, A., Horowitz, L., Koch, D., Krol, M. C., Landing, W., Liu, X., Mahowald, N., Miller, R., Morcrette, J.-J, Myhre, G., Penner, J., Perlwitz, J., Stier, P., Takemura, T., and Zender, C. S. (2011) 'Global dust model intercomparison in AeroCom phase I', *Atmospheric Chemistry and Physics*, **11**(15), pp. 7781–7816. doi: 10.5194/acp-11-7781-2011.

Hung, C.-W., Liu, X., and Yanai, M. (2004) 'Symmetry and asymmetry of the Asian and Australian summer monsoons', *Journal of Climate*, **17**, pp. 2413–2426. doi: 10.1175/1520-0442(2004)017<2413:SAAOTA>2.0.CO;2.

Hurst, D. F., Oltmans, S. J., Vömel, H., Rosenlof, K. H., Davis, S. M., Ray, E. A., Hall, E. G., and Jordan, A. F. (2011) 'Stratospheric water vapor trends over Boulder, Colorado: Analysis of the 30 year Boulder record', *Journal of Geophysical Research Atmospheres*, **116**(2), pp. 1–12. doi: 10.1029/2010JD015065.

IPCC (2013) *Climate Change 2013: The Physical Science Basis. Contribution of Working Group I to the Fifth Assessment Report of the Intergovernmental Panel on Climate Change*, *the Fifth Assessment Report*. Cambridge, UK and New York, USA: Cambridge University Press.

Janicot, S., (2009) 'A comparison of Indian and African monsoon variability at different time scales'. *Comptes Rendus Geoscience*, **351**, pp. 575–590. doi:10.1016/j.crte.2009.02.002.

Janicot S., Caniaux, G., Chauvin, F., de Coëtlogon, G., Fontaine, B., Hall, N., Kiladis, G., Lafore, J. P., Lavaysse, C., Lavender, S. L., Leroux, S., Marteau, R., Mounier, F., Philippon, N., Roehrig, R., Sultan, B., and Taylor, C. M. (2011) 'Intraseasonal variability of the West African monsoon', *Atmospheric Science Letters*, **12**, pp. 58–66. doi: 10.1002/asl.280.

Jensen, E. J., Thornberry, T., D., Rollins, A. W., Ueyama, R., Pfister, L., Bui, T., Diskin G. S., Di Gangi, J. P., Hintsa, E., Gao, Ru-Shan, Woods, S., Lawson, R. P., and Pittman, J. (2017) 'Physical processes controlling the spatial distributions of relative humidity in the tropical tropopause layer over the Pacific', *Journal of Geophysical Research:*

Atmospheres, **122**, pp. 6094-61074003. doi: 10. 1002/2017JD026632.

Jöckel, P., von Kuhlmann, R., Lawrence, M. G., Steil, B., Bernninkmeijer, C. A. M., Crutzen, P. J., Rasch, P. J., and Eaton, B. (2001) 'On a fundamental problem in implementing flux-form advection schemes for tracer transport in 3-dimensional general circulation and chemistry transport models', *Quarterly Journal of the Royal Meteorological Society*, **127**, pp. 1035–1052. doi: 10.1002/qj.49712757318.

Jöckel, P., Tost, H., Pozzer, A., Brühl, C., Buchholz, J., G. L., Hoor, P., Kerkweg, A., Lawrence, M. G., Sander, R. S. B., Stiller, G., Tanarhte, M., Taraborrelli, D., van Aardenne, J., and Lelieveld, J. (2006) 'The atmospheric chemistry general circulation model ECHAM5 / MESSy1 : consistent simulation of ozone from the surface to the mesosphere', *Atmospheric Chemistry and Physics*, **6**, pp. 5067–5104. doi: 10.5194/acp-6-5067-2006.

Kaiser, J., Engel, A., and Borchers, R. (2006) 'Probing stratospheric transport and chemistry with new balloon and aircraft observations of the meridional and vertical N2 O isotope distribution', *Atmospheric Chemistry and Phyics*, **6**, pp. 3535–3556. doi: 10.5194/acp-6-3535-2006.

Keith, D. W., Parson, E., and Morgan, M. G. (2010) 'Research on global sun block needed now', *Nature*, **463**(7280), pp. 426–427. doi: 10.1038/463426a.

Kovács, T., Feng, W., Totterdill, A., Plane, J. M. C., Dhomse, S., Gómez-martín, J. C., Chipperfield, M. P. (2017) 'Determination of the atmospheric lifetime and global warming potential of sulfur hexafluoride using a three-dimensional model', *Atmospheric Chemistry and Physics*, **17**, pp. 883–898. doi: 10.5194/acp-17-883-2017.

Kripalani, R. H., Oh, J. H., Kulkarni, A., Sabade, S. S., and Chaudhari, H. S. (2007) 'South Asian summer monsoon precipitation variability: Coupled climate model simulations and projections under IPCC AR4', *Theoretical and Applied Climatology*, **90**(3–4), pp. 133–159. doi: 10.1007/s00704-006-0282-0.

Krol, M., Houweling, S., Bregman, B., Broek, M., Van Den Segers, A., Velthoven, P.

Van Peters, W., and Dentener, F. (2005) ‘The two-way nested global chemistry-transport zoom model TM5 : algorithm and applications’, *Atmospheric Chemistry and Physics*, **5**, pp. 417–432. doi: 10.5194/acp-5-417-2005.

Krol, M., De Bruine, M., Killaars, L., Ouwersloot, H., Pozzer, A., Yin, Y., Chevallier, F., Bousquet, P., Patra, P., Belikov, D., Maksyutov, S., Dhomse, S., Feng, W., and Chipperfield, M. P. (2018) ‘Age of air as a diagnostic for transport timescales in global models’, *Geoscientific Model Development*, **11**(8), pp. 3109–3130. doi: 10.5194/gmd-11-3109-2018.

Lal, M., Nozawa, T., Emori, S., Harasawa, H., Takahashi, K., Kimoto, M., Nakajima, T., Takemura, T., and Numaguti, A. (2001) ‘Future climate change : Implications for Indian summer monsoon and its variability’, *Current*, **81**(9), pp. 1196–1207.

Lambright, W. H., and Stanley, A. C. J. (1989) ‘Arresting Technology : Government , Scientists , and Weather Modification’, *Science, Tecnhology, & Human Values*, 14(4), pp. 340–359. Available at: http://www.jstor.org/stable/689681 (accessed 20 November 2019).

Leedham Elvidge, E. C., Oram, D. E., Laube, J. C., Baker, A. K., Montzka, S. A., Humphrey, S., O’Sullivan, D. A., and Brenninkmeijer, C. A. M. (2015) ‘Increasing concentrations of dichloromethane, CH_2Cl_2, inferred from CARIBIC air samples collected 1998-2012’, *Atmospheric Chemistry and Physics*, **15**(4), pp. 1939–1958. doi: 10.5194/acp-15-1939-2015.

Liu, F., Chai, J., Wang, B., Liu, J., Zhang, X., and Wang, Z. (2016) ‘Global monsoon precipitation responses to large volcanic eruptions’, *Scientific Reports*. Nature Publishing Group, **6**(1), p. 24331. doi: 10.1038/srep24331.

Louis, J. F. (1979) ‘A parametric model of vertical eddy fluxes in the atmosphere’, *Boundary-Layer Meteorology*, **17**(2), pp. 187–202.

MacKenzie, A. R., Schiller, C., Peter, T., Adriani, A., Beuermann, J., Bujok, O., Cairo, F., Corti, T., DiDonfrancesco, G., Gensch, I., Kiemle, C., Krämer, M., Kroger, C.,

Merkulov, S., Oulanovsky, A., Ravegnani, F., Rohs, S., Rudakov, V., Salter, P., Santacesaria V., Stefanutti, L., and Yushkov, V., 'Tropopause and hygropause variability over the equatorial Indian Ocean during February and March 1999', *Journal of Geophysical Research,* **111**, D18112. doi:10.1029/2005JD006639.

Matsumi, Y., Comes, F. J., Hancock, G., Hofzumahaus, A., Hynes, A. J., Kawasaki, M., and Ravishankara, A. R. (2002) ' Quantum yields for production of O(1D) in the ultraviolet photolysis of ozone: Recommendation based on evaluation of laboratory data', *Journal of Geophysical Research,* **107**(0), pp. 1-20. doi: 10.1029/2001JD000510.

McCormick, M. P., and Veiga, R. E. (1992) 'SAGE II measurements of early Pinatubo aerosols', *Geophysical Research Letters*, **19**(2), pp. 155–158. doi: 10.1029/91GL02790.

McCormick, M. P., Thomason, L. W., and Trepte, C. R. (1995) 'Atmospheric effects of the Mt Pinatubo eruption', *Nature*, **373**, pp. 399–404. doi: 10.1038/373399a0.

Mellouki, A.. Talukdar, R. K., Schmoltner, A.-M., Gierczak, T., Mills, M. J., Solomon, S, and Ravishankara, A. R. (1992) 'Atmospheric lifetimes and ozone depletion potentials of methyl bromide (CH_3Br) and dibromomethane (CH_2Br_2)', *Geophysical Research Letters,* **19**, pp. 2059-2062. doi: 10.1029/92GL01612.

Ming, T., De Richter, R., Liu, W., and Caillol, S. (2014) 'Fighting global warming by climate engineering: Is the Earth radiation management and the solar radiation management any option for fighting climate change', *Renewable and Sustainable Energy Reviews*, **31**, pp. 792–834. doi: 10.1016/j.rser.2013.12.032.

Molina, M. J., Molina, L. T., Zhang, R., Meads, R. F., and Spencer, D. D. (1997) 'The reaction of $ClONO_2$ with HCl on aluminum oxide', *Geophysical Research Letters*, **24**(13), pp. 1619–1622. doi: 10.1029/97GL01560.

Monks, S. A., Arnold, S. R., Hollaway, M. J., Pope, R. J., Wilson, C., Feng, W., Emmerson, K. M., Kerridge, B. J., Latter, B. L., Miles, G. M., Siddans, R., and Chipperfield, M. P. (2017) 'The TOMCAT global chemical transport model v1 . 6 : description of chemical mechanism and model evaluation', *Geoscientific Model*

Development, **10**, pp. 3025–3057. doi: 10.5194/gmd-10-3025-2017.

Montzka, S. A., Reimann, S., Engel, A., Kruger, K., O'Doherty, S., and Sturges, W.T., (2011) Ozone depleting substances (ODSs) and related chemicals in, *Scientific Assessment of Ozone Depletion: 2010, Global Ozone Research and Monitoring Project-Report No. 52*, Wordl Meteorological Organization, Geneva, Switzerland, pp. 1-112.

Moon, D. R., Taverna, G. S., Anduix-Canto, C., Ingham, T., Chipperfield, M. P., Seakins, P. W., Baeza-Romero, M.T., and Heard, D. E. (2018) 'Heterogeneous reaction of HO_2 with airborne TiO_2 particles and its implication for climate change mitigation strategies', *Atmospheric Chemistry and Physics*, **18**, pp. 327–338. doi: doi.org/10.5194/acp-18-327-2018.

Morgenstern, O., Braesicke, P., Connor, F. M. O., Bushell, A. C., Johnson, C. E., Osprey, S.M., and Pyle, J. A. (2009) 'Evaluation of the new UKCA climate-composition model – Part 1 : The stratosphere', *Geoscientific Model Development*, **2**, pp. 43–57.

Mote, P., W., Rosenlof, K. H., McIntyre, M. E., Carr, E. S., Gille, J. C., Holton, J. R., Kinnersley, J. S., Pumphrey, H. C., Russel, J. M. III, and Waters, J. W., (2006) 'An atmospheric tape recorder: The imprint of tropical tropopause temperatures on stratospheric water vapor', *Journal of Geophysical Research*, **101**, D2, pp. 3989-4006. doi: 10.1029/95JD03422

National Research Council, (1966) *Weather and Climate Modification: Problems and Prospects (2 Volumes)*. Washington: USA, National Academic Press.

National Science Foundation (1966) 'Weather and Climate Modification: Report on the Special Commision on Weather Modification, National Science Foundation, December 20, 1965', *Bulletin of the American Meteorological Society*, **47**(3), pp. 166–183.

Neumann, J. Von (1955) 'Can we surive technology?', *Fortune*, pp. 106–108.

Novelli, P. C., Masarie, K. A., Lang, P. M. (1998) 'Distributions and recent changes of carbon monoxide in the lower troposphere', *Journal of Geophysical Research*, **103**, D15, pp. 15–19. doi: 10.1029/98JD01366.

Numaguti, A., Takahashi, M., Nakajima, T., and Sumi, A. (1997) 'Study on the climate system and mass transport by a climate model (CGER--1025-97). Japan.

Nützel, M., Dameris, M., and Garny, H. (2016) 'Movement, drivers and bimodality of the South Asian High', *Atmospheric Chemistry and Physics*, **16**(22), pp. 14755–14774. doi: 10.5194/acp-16-14755-2016.

Pan, L. L., Honomichl, S. B., Kinnison, D. E., Abalos, M., Randel, W. J., Bergman, J. W., and Bian, J. (2016) 'Transport of chemical tracers from the boundary layer to stratosphere associated with the dynamics of the Asian summer monsoon', *Journal of Geophysical Research: Atmospheres*, **121**(23), pp. 14159-14174. doi: 10.1002/2016JD025616.

Park, M., Randel, W. J., Gettelman, A., Massie, S. T., and Jiang, J. H. (2007) 'Transport above the Asian summer monsoon anticyclone inferred from Aura Microwave Limb Sounder tracers', *Journal of Geophysical Research Atmospheres*, **112**(16), pp. 1–13. doi: 10.1029/2006JD008294.

Park, M., Randel, W. J., Emmons, L. K., Bernath, P. F., Walker, K. A., and Boone, C. D. (2008) 'Chemical isolation in the Asian monsoon anticyclone observed in Atmospheric Chemistry Experiment (ACE-FTS) data', *Atmospheric Chemistry and Physics*, **8**(3), pp. 757–764. doi: 10.5194/acp-8-757-2008.

Park, M., Randel, W. J., Emmons, L. K., and Livesey, N. J. (2009) 'Transport pathways of carbon monoxide in the Asian summer monsoon diagnosed from Model of Ozone and Related Tracers (MOZART)', *Journal of Geophysical Research Atmospheres*, **114**(8), pp. 1–11. doi: 10.1029/2008JD010621.

Park, M., Randel, W. J., Kinnison, D. E., Emmons, L. K., Bernath, P. F., Walker, K. A., Boone, C. D., and Livesey, N. J. (2013) 'Hydrocarbons in the upper troposphere and lower stratosphere observed from ACE-FTS and comparisons with WACCM', *Journal of Geophysical Research Atmospheres*, **118**(4), pp. 1964–1980. doi: 10.1029/2012JD018327.

Parthasarathy, B., Munot, A. A., and Kothawale, D. R. (1994) 'All-India monthly and seasonal rainfall series: 1871-1993', *Theoretical and Applied Climatology*, **49**(4), pp. 217–224. doi: 10.1007/BF00867461.

Petrenko, V. V., Martinerie, P., Novelli, P., Etheridge, D. M., Levin, I., Wang, Z., Blunier, T., Chappellaz, J., Kaiser, J., Lang, P., Steele, L. P., Hammer, S., Mak, J., Langenfelds, R. L., Schwander, J., Severinghaus, J. P., Witrant, E., Petron G., Battle, M. O., Forster, G., Sturges, W. T., Lamarque, J.-F., Steffen, K., and White, J. W. C. (2013) 'A 60 yr record of atmospheric carbon monoxide reconstructed from Greenland firn air', *Atmospheric Chemistry and Physics*, **13**(15), pp. 7567–7585. doi: 10.5194/acp-13-7567-2013.

Ploeger, F., Gottschling, C., Griessbach, S., Grooß, J. U., Guenther, G., Konopka, P., Muller, R., Riese, M., Stroh, F., Tao, M., Ungermann, J., Vogel, B., and Von Hobe, M. (2015) 'A potential vorticity-based determination of the transport barrier in the Asian summer monsoon anticyclone', *Atmospheric Chemistry and Physics*, **15**(22), pp. 13145–13159. doi: 10.5194/acp-15-13145-2015.

Ploeger, F., Konopka, P., Walker, K., and Riese, M. (2017) 'Quantifying pollution transport from the Asian monsoon anticyclone into the lower stratosphere', *Atmospheric Chemistry and Physics*, **17**(11), pp. 7055–7066. doi: 10.5194/acp-17-7055-2017.

Pope, F. D., Braesicke, P., Grainger, R. G., Kalberer, M., Watson, I. M., Davidson, P. J., and Cox, R. A. (2012) 'Stratospheric aerosol particles and solar-radiation management', *Nature Climate Change*. Nature Publishing Group, **2**(10), pp. 713–719. doi: 10.1038/nclimate1528.

Pope, R. J., Richards, Nigel, A. D., Chipperfield, M. P., Moore, D. P., Monks, S. A., Arnold, S. R., Glatthor, N., Kiefer, M., Breider, T. J., Harrison, J. J., Remedios, J. J., Warneke, C., Roberts, J. M., Diskin, G. S., Huey, L. G., Wisthaler, A., Apel, E. C., Bernath, P. F., and Feng, W. (2016) 'Intercomparison and evaluation of satellite peroxyacetyl nitrate observations in the upper troposphere-lower stratosphere', *Atmospheric Chemistry and Physics*, **16**(21), pp. 13541–13559. doi: 10.5194/acp-16-13541-2016.

Popovic, J. M., and Plumb, R. A. (2001) ‘Eddy Shedding from the Upper-Tropospheric Asian Monsoon Anticyclone’, *Journal of the Atmospheric Sciences*, **58**(1), pp. 93–104. doi: 10.1175/1520-0469(2001)058<0093:ESFTUT>2.0.CO;2.

Prather, M. J. (1986) ‘Numerical Advection by Conservation of Second-Order Moments’, *Journal of Geophysical Research*, **91**, pp. 6671–6681. doi: 10.1029/JD091iD06p06671.

Prather, M. J., McElroy, M., Wofsy, S., Russel, G., and Rind, D. (1987) ‘Chemistry of the Global Troposphere: Fluorocarbons as Tracers of Air Motion’, *Journal of Geophysical Research*, **92**, pp. 6579–6613. doi: 10.1029/JD092iD06p06579.

Randel, W. J., and Park, M. (2006) ‘Deep convective influence on the Asian summer monsoon anticyclone and associated tracer variability observed with Atmospheric Infrared Sounder (AIRS)’, *Journal of Geophysical Research Atmospheres*, **111**(12), pp. 1–13. doi: 10.1029/2005JD006490.

Randel, W. J., Park, M., Emmons, L., Kinnison, D., Bernath, P., Walker, K. A., Boone, C., and Pumphrey, H. (2010) ‘Asian monsoon transport of pollution to the stratosphere’, *Science*, **328**(5978), pp. 611–613. doi: 10.1126/science.1182274.

Robock, A. (2014) ‘Stratospheric aerosol geoengineering’, *Issues in Environmental Science and Technology*, **38**, pp. 162–185. doi: 10.1063/1.4916181.

Rolf, C., Vogel, B., Hoor, P., Afchine, A., Günther, G., Krämer, M., Müller, R., Müller, S., Spelten, N., and Riese, M. (2018) ‘Water vapor increase in the lower stratosphere of the Northern Hemisphere due to the Asian monsoon anticyclone observed during the TACTS / ESMVal campaigns’, *Atmospheric Chemistry and Physics*, **18**, pp. 2973–2983. doi: 10.5194/acp-18-2973-201.

Rosenlof, H., Tuck, A. F., Kelly, K. K., and Russell, J. M. (1997) ‘Hemispheric asymmetries in water vapor and inferences about transport in the lower stratosphere’, *Jornal of Geophysical Research*, **102**(Dll), pp. 13213-13234. doi: 10.1029/97JD00873.

Rotman, D. A., Atherton, C. S., Bergmann, D. J., Kinnison, D. E., Molenkamp, C. R., Proctor, D. D., and Tannahill, J. R. (2004) ‘IMPACT , the LLNL 3-D global atmospheric

chemical transport model for the combined troposphere and stratosphere : Model description and analysis of ozone and other trace gases', *Journal of Geophysical Research*, **109**(D04303), doi: 10.1029/2002JD003155.

Seinfeld, J.H., and Pandis, S. N. (2016) *Atmospheric Chemistry and Physics: From Air Pollution to Climate Change 3rd edtion*. New York, USA: John Wiley and Sons, Incorporated.

Sitnikov, N. M., Yushkov, V. A., Afchine, A. A. A., Korshunov, L. I., Astakhov, V.I., Ulanovskii, A. E., Kraemer, M., Mangold, A., Schiller, C., and Ravegnani, F. (2007) 'The FLASH Instrument for Water Vapor Measurements on Board the High-Altitude Airplane', *Physical Instruments for ecology, medicine and biology*, **50**(1), pp. 121–129. doi: 10.1134/S0020441207010174.

Solomon, S., Ivy, D. J., Kinnison, D., Mills, M. J., Neely, R. R., and Schmidt, A. (2016) 'Emergence of healing in the Antarctic ozone layer', *Science*, **15**, pp. 269-274, doi: 10.1126/science.aae0061.

SPARC, (2006): SPARC: Assessment of Stratospheric Aerosol Properties (ASAP). L Thomson and Th. Peter (Eds.), SPARC Report No. 4, WCRP-124, WMO/TD - No.1295 Available at: www.sparc-climate-org/publications/sparc-reports/ (visited on May 29th 2020).

Stefanutti, L., Sokolov, L., Balestri, S., MacKenzie, A. R., and Khattatov, V. (1999) 'The M-55 Geophysica as a Platform for the Airborne Polar Experiment', *Journal of Atmospheric and Oceanic Technology*, **16**(10), pp. 1303–1312. doi: 10.1175/1520-0426(1999)016<1303:TMGAAP>2.0.CO;2.

Stefanutti, L., Mackenzie, A. R., and Santacesaria, V. (2004) 'The APE-THESEO Tropical Campaign : An Overview', *Journal of Atmospheric Chemistry*, **48**, pp. 1–33.

Stockwell, D. Z. , and Chipperfield, M. P. (1999) 'A tropospheric chemical transport model: Development and validation of the model transport schemes', *Quarterly Journal of the Royal Meteorological Society*, **125**, pp. 1747–1783. doi: 10.1002/qj.49712555714.

Stull, R. B. (2011) *Meteorology for Scientists and Engineers 3rd edtion*. Vancouver, Canada: University of British Columbia.

Tang, M. J., Telford, P. J., Pope, F. D., Rkiouak, L., Abraham, N. L., Archibald, A. T., Braesicke, P., Pyle, J. A., McGregor, J., Watson, I. M., Cox, R. A., and Kalberer, M. (2014) 'Heterogeneous reaction of N_2O_5 with airborne TiO_2 particles and its implication for stratospheric particle injection', *Atmospheric Chemistry and Physics*, **14**(12), pp. 6035–6048. doi: 10.5194/acp-14-6035-2014.

Tang, M. J., Keeble, J., Telford, P. J., Pope, F. D., Braesicke, P., Griffiths, P. T., Abraham, N. L., McGregor, J., Watson, I. M., Cox, R. A., Pyle, J. A., and Kalberer, M. (2016) 'Heterogeneous reaction of $ClONO_2$ with TiO_2 and SiO_2 aerosol particles: implications for stratospheric particle injection for climate engineering', *Atmospheric Chemistry and Physics*, **16**, pp.15397-15412. doi: 10.5194/acp-16-15397-2016.

Textor, C., Schulz, M., Guibert, S., Kinne, S., Balkanski, Y., Bauer, S., Berntsen, T., Berglen, T., Boucher, O., Chin, M., Dentener, F., Diehl, T., Easter, R., Feichter, H., Fillmore, D., Ghan, S., Ginoux, P., Gong, S., Grini, A., Hendricks, J., Horowitz, L., Huang, P., Isaksen, I., Iversen, T., Kloster, S., Koch, D., Kirkevag, A., Kristjansson, J. E., Krol, M., Lauer, A., Lamarque, J. F., Liu, X., Montanaro, V., Myhre, G., Penner, J., Pitari, G., Reddy, S., Seland, Ø., Stier, P., Takemura, T., and Tie, X (2006) 'Analysis and quantification of the diversities of aerosol life cycles within AeroCom', *Atmospheric Chemistry and Physics*, **6**(7), pp. 1777–1813. doi: 10.5194/acp-6-1777-2006.

Thompson, D. W. J., Solomon, S, .Kushner, P. J., England, M. H., Grise, K. M., and Karoly, D. J. (2011) 'Signatures of the Antarctic ozone hole in Southern Hemisphere surface climate change', *Nature Geoscience*, **4**(11), pp. 741–749. doi: 10.1038/ngeo1296.

Thornton, J. A., Jaeglé, L., and McNeill, V. F. (2008) 'Assessing known pathways for HO_2 loss in aqueous atmospheric aerosols: Regional and global impacts on tropospheric oxidants', *Journal of Geophysical Research Atmospheres*, **113**(5), pp. 1–16. doi: 10.1029/2007JD009236.

Tiedtke, M. (1989) ‘A Comprehensive Mass Flux Scheme for Cumulus Parameterization in Large-Scale Models’, *Monthly Weather Review*, **117**, pp. 1779–1800. doi: 10.1175/1520-0493(1989)117%3C1779:ACMFSF%3E2.0.CO;2.

Tuck, A. F., Baumgardner, D., Chan, K. R., Dye, J. E., Elkins, J. W., Hovde, S. J., Kelly, K. K., Loewenstein, M., Margitan, J. J., May, R. D., Podolske, J. R., Proffitt, M. H., Rosenlof, K. H., Smith, W. L., Webster, C. R., and Wilson, J. C. (1997) ‘The Brewer-Dobson Circulation In the Light of High Altitude In Situ Aircraft Observations’, *Quarterly Journal of the Royal Meteorological Society*, **123**, pp. 1–69. doi: 10.1002/qj.49712353702.

Turner, A. G., and Annamalai, H. (2012) ‘Climate change and the South Asian summer monsoon’, *Nature Climate Change*, **2**(8), pp. 587–595. doi: 10.1038/nclimate1495.

Ulanovsky, A. E., Yushkov, V. A., Sitnikov, N. M., and Ravengnani, F. (2001) ‘The FOZAN-II Fast-Response Chemiluminescent Airborne Ozone Analyzer’, *Physical Instruments for Ecology, Medicine and Biology*, **44**(2), pp. 249–256.

Uma, K. N., Das, S. K., Das, S. S., (2014) ‘A climatological perspective of water vapor at the UTLS region over different global monsoon regions: observations inferred from the Aura-MLS and reanalysis data’, *Climate Dynamics*, **43**, pp.407-420. doi: 10.1007/s00382-014-2085-9.

Umezawa, T., Baker, A. K., Oram, D., Sauvage, C., O’Sullivan, D., Rauthe-Schöch, A., Montzka, S. A., Zahn, A., and Brenninkmeijer, C. A. M. (2014) ‘Methyl chloride in the upper troposphere observed by the CARIBIC passenger aircraft observatory: Large-scale distributions and Asian summer monsoon outflow’, *Journal of Geophysical Research*, **119**(9), pp. 5542–5558. doi: 10.1002/2013JD021396.

Usher, C. R., Michel, A. E., Stec, D., and Grassian, V. H. (2003) ‘Laboratory studies of ozone uptake on processed mineral dust’, *Atmospheric Environment*, **37**, pp. 5337–5347. doi: 10.1016/j.atmosenv.2003.09.014.

Vaughan, G., Schiller, C., MacKenzie, A. R., Bower, K., Peter, T., Schlager, H., Harris,

N. R. P., and May, P. T. (2008) 'SCOUT-03/ACTIVE: High-altitude aircraft measurements around deep tropical convection', *Bulletin of the American Meteorological Society*, **89**, pp. 647–662. doi: 10.1175/BAMS-89-5-647.

Vernier, J. P., Fairlie, T. D., Natarajan, M., Wienhold, F. G., Bian, J., Martinsson, B. G.Crumeyrolle, S., Thomason, L. W., and Bedka, K. M. (2015) 'Increase in upper tropospheric and lower stratospheric aerosol levels and its potential connection with Asian pollution', *Journal of Geophysical Research Atmospheres*, **120**(4), pp. 1608–1619. doi: 10.1002/2014JD022372.

Viciani, S, .Montori, A., Chiarugi, A., and Amato, F. D. (2018) 'A Portable Quantum Cascade Laser Spectrometer for Atmospheric Measurements of Carbon Monoxide', *Sensors*, **18**(2380), pp. 1–18. doi: 10.3390/s18072380.

Visioni, D., Pitari, G., and Aquila, V. (2017) 'Sulfate geoengineering: A review of the factors controlling the needed injection of sulfur dioxide', *Atmospheric Chemistry and Physics*, **17**(6), pp. 3879–3889. doi: 10.5194/acp-17-3879-2017.

Vogel, B., Günther, G., Müller, R., Groo, J. U., Hoor, P., Krämer, M., Müller, S., Zahn, A., and Riese, M. (2014) 'Fast transport from Southeast Asia boundary layer sources to northern Europe: Rapid uplift in typhoons and eastward eddy shedding of the Asian monsoon anticyclone', *Atmospheric Chemistry and Physics*, **14**(23), pp. 12745–12762. doi: 10.5194/acp-14-12745-2014.

Voigt, C., Schlager, H., and Luo, B. P. (2005) 'Nitric Acid Trihydrate (NAT) formation at low NAT supersaturation in Polar Stratospheric Clouds (PSCs)', *Atmospheric Chemistry and Physics*, **5**, pp. 1371–1380. doi:10.5194/acp-5-1371-2005.

Volk, C. M., Elkins, J. W., Fahey, D. W., Dutton, G. S., Gilligan, J. M., Loewenstein, M., Podolske J. R., Chan, K. R., and Gunson, M. R. (1997) 'Evaluation of source gas lifetimes from stratospheric observations', *Journal of Geophysical Research: Atmosphere*, **102**, pp. 25543-25564. doi: 10.1029/97JD02215.

Wang, K., Pyle, J. A.Sanderson, M. G., and Bridgeman, C. (1999) 'Implementation of a

convective atmospheric boundary layer scheme in a tropospheric chemistry transport model', *Journal of Geophysical Research*, **104**(D19), pp. 23729–23745. doi: 10.1029/1999JD900383.

Wang, B., and Fan, Z. (1999) 'Choice of south Asian summer monsoon indices', *Bulletin of the American Meteorological Society*, **80**(4), pp. 629–638. doi: 10.1175/1520-0477(1999)080<0629:COSASM>2.0.CO;2.

Wang, B. (2006) *The Asian Monsoon*. Berlin, Germany: Springer Praxis Books.

Waugh, D. W., Crotwell, A. M., Dlugokencky, E. J., Dutton, G. S., Elkins, J. W., Hall, B. D., Hintsa, E. J., Hurst, D. F., Montzka, S. A., Mondeel, D. J., Moore, F. L., Nance, J. D., Ray, E. A., Steenrod, S. D., Strahan, S. E., and Sweeney, C. (2013) 'Tropospheric SF6 : Age of air from the Northern Hemisphere midlatitude surface', *Journal of Geophysical Research: Atmosphere*, **118**(11), pp. 429–441. doi: 10.1002/jgrd.50848.

Webster, P. J. (1987) 'The elementary monsoon', in *Monsoons*, edited by J. S. Fein and P. L. Stephens, pp. 3–32., John Wiley, New York.

Webster, P. J., and Yang, S. (1992) 'Monsoon and ENSO:Selectively interactive systems', *Quarterly Journal of the Royal Meteoroogical. Sociery*, **118**(507), pp. 877–926. doi: 10.1002/qj.49711850705.

Webster, P. J., and Fasullo, J. (2003) 'Monsoon: Dynamical Theory' *Encyclopedia of Atmospheric Sciences*', pp. 1370–1386. doi: 10.1016/B0-12-227090-8/00236-0.

Werner, B., Stutz, J., Spolaor, M., Scalone, L., Raecke, R., Festa, J., Colosimo, S. F., Cheung, R., Tsai, C., Hossaini, R., Chipperfield, M. P., Taverna, G. S., Feng, W., Elkins, J. W., Fahey, D. W., Gao, Ru-Shan, Hintsa, E. J., Thornberry, T. D., Moore, F. L., Navarro, M. A., Atlas, E., Daube, B. C., Pittman, J., Wofsy, S., and Pfeilsticker, K. (2017) 'Probing the subtropical lowermost stratosphere and the tropical upper troposphere and tropopause layer for inorganic bromine', *Atmospheric Chemistry and Physics*, **17**(2), pp. 1161–1186. doi: 10.5194/acp-17-1161-2017.

WMO (2014) *Scientific Assessment of Ozone Depletion: 2014, World Meteorological*

Organization, Global Ozone Research and Monitoring Project - Report No. 55, pp. 1-416, Geneva, Switzerland.

Yan, X., Konopka, P., Ploeger, F., Tao, M., Müller, R., Santee, M. L., Bian, J., and Riese, M. (2018) 'El Niño Southern Oscillation influence on the Asian summer monsoon anticyclone', *Atmospheric Chemistry and Physics*, **18**, pp. 8079–8096. doi: 10.5194/acp-18-8079-2018.

Yin, Y., Wurzler, S., Levin, Z., and Reisin, T. G. (2002) 'Interactions of mineral dust particles and clouds: Effects on precipitation and cloud optical properties', *Journal of Geophysical Research.*, **107**(D23), pp. 4724, doi:10.1029/2001JD001544.

Yushkov, V., Oulanovsky, A., Lechenuk, N., Roudakov, I., Arshinov, K., Tikhonov, F., Stefanutti, L., Ravegnani, F., Bonafe., U., Georgiadis, T. (1999) 'A Chemiluminescent Analyzer for Stratospheric Measurements of the Ozone Concentration (FOZAN)', *Journal of Atmospheric and Oceanic Technology*, **16**, pp. 1345–1350. doi: 10.1175/1520-0426(1999)016<1345:ACAFSM>2.0.CO;2.

Zheng, B., Chevallier, F., Yin, Y., Ciais, P., Fortems-Cheiney, A., Deeter, M. N., Parker, R. J., Wang, Y., Worden, H. M., and Zhao, Y. (2019) 'Global atmospheric carbon monoxide budget 2000–2017 inferred from multi-species atmospheric inversions', *Earth System Science Data*, **11**, pp. 1411-1436. doi: 10.5194/essd-11-1411-2019.

Zoger, M., Afchine, A., Eicke, N., Gerhards, M. T., Klein, E., McKenna, D. S., Morschel, U., Schmidt, U., Tan, V., Tuitjer, F., Woyke, T., and Schiller, C. (1999) 'Fast in situ stratospheric hygrometers : A new family of balloon-borne and airborne Lyman alpha photofragment fluorescence hygrometers', *Journal of Geophysical Research,* **104**(D1), pp. 1807–1816. doi: 10.1029/1998JD100025.

9 Contribution to published papers

Paper #1: Probing the subtropical lowermost stratosphere and the tropical upper troposphere and tropopause layer for inorganic bromine, Werner *et al.*, 2017:

I compared the O_3 and other ATTREX data with corresponding TOMCAT/SLIMCAT results, which formed the basis for the plots which include ozone in the paper.

Paper #2: Heterogeneous reaction of HO2 with airborne TiO2 particles and its implication for climate change mitigation strategies, Moon *et al.*, 2018*:*

I ran the SLIMCAT simulations to include uptake of HO_2 and O_3 onto TiO_2 and produced the plots in Figures 8 and 9.